Nuclear Heat Transfer and Passive Cooling

Study D: **System Code and CFD Analysis for a Light Water Small Modular Reactor**

FRAZER-NASH CONSULTANCY

Introduction to the Technical Volumes and Case Studies

Convection, Radiation and Conjugate Heat Transfer

Natural Convection and Passive Cooling

Confidence and Uncertainty

Liquid Metal Thermal Hydraulics

Molten Salt Thermal Hydraulics

Liquid Metal CFD Modelling of the TALL-3D Test Facility

Fuel Assembly CFD and UQ for a Molten Salt Reactor

Reactor Scale CFD for Decay Heat Removal in a Lead-cooled Fast Reactor

System Code and CFD Analysis for a Light Water Small Modular Reactor

Study D

Authors:	Daniel Miles	Frazer-Nash Consultancy
	Lewis Farrimond	Frazer-Nash Consultancy
	Richard Underhill	Frazer-Nash Consultancy
Contributors:	Sukhbinder Singh	Frazer-Nash Consultancy
	Benjamin Bayliss	Frazer-Nash Consultancy
	Juan Uribe	EDF Energy R&D
	Steven Moor	Rolls-Royce
Case Studies Lead:	Graham Macpherson	Frazer-Nash Consultancy
Approver:	Graham Macpherson	Frazer-Nash Consultancy

Document Number: FNC 60148/50161R

Issue and Date: Issue 1, December 2021

Legal Statement

Preface

Nuclear thermal hydraulics is the application of thermofluid mechanics within the nuclear industry. Thermal hydraulic analysis is an important tool in addressing the global challenge to reduce the cost of advanced nuclear technologies. An improved predictive capability and understanding supports the development, optimisation and safety substantiation of nuclear power plants.

This document is part of *Nuclear Heat Transfer and Passive Cooling: Technical Volumes and Case Studies*, a set of six technical volumes and four case studies providing information and guidance on aspects of nuclear thermal hydraulic analysis. This document set has been delivered by Frazer-Nash Consultancy, with support from a number of academic and industrial partners, as part of the UK Government *Nuclear Innovation Programme: Advanced Reactor Design*, funded by the Department for Business, Energy and Industrial Strategy (BEIS).

Each technical volume outlines the technical challenges, latest analysis methods and future direction for a specific area of nuclear thermal hydraulics. The case studies illustrate the use of a subset of these methods in representative nuclear industry examples. The document set is designed for technical users with some prior knowledge of thermofluid mechanics, who wish to know more about nuclear thermal hydraulics.

The work promotes a consistent methodology for thermal hydraulic analysis of single-phase heat transfer and passive cooling, to inform the link between academic research and end-user needs, and to provide a high-quality, peer-reviewed document set suitable for use across the nuclear industry.

The document set is not intended to be exhaustive or provide a set of standard engineering ‘guidelines’ and it is strongly recommended that nuclear thermal hydraulic analyses are undertaken by Suitably Qualified and Experienced Personnel.

The first edition of this document set has been authored by Frazer-Nash Consultancy, with the support of the individuals and organisations noted in each. Please acknowledge these documents in any work where they are used:

> Frazer-Nash Consultancy (2021) Nuclear Heat Transfer and Passive Cooling,
> Study D: System Code and CFD Analysis for a Light Water Small Modular Reactor.

Contents

1 Introduction

During the development of a new Nuclear Power Plant (NPP), engineers are faced with a number of challenges that require the application of a chain of different analytical methods to achieve the results of interest. This case study focuses on a design problem where the eventual goal is to assess the structural integrity of primary circuit components in the event of a fault.

A progression of thermal hydraulic analysis methods are required to derive the inputs to the eventual mechanical assessment which informs the design. Extensive guidance exists within the public domain on how individual thermal hydraulic analyses can be effectively applied to reactor designs. However, guidance on the application of multiscale thermal hydraulic analysis methods with different levels of fidelity to the solution of single design problems is more limited.

This case study therefore considers the application of an analysis route utilising both system code and Computational Fluid Dynamics (CFD) methods to a reactor design scenario, where the application of a single method is not sufficient to achieve the required results. Although the case study considers a specific example where the end result is a structural integrity assessment, the scope is limited to the thermal hydraulic and Conjugate Heat Transfer (CHT) aspects of the analysis. The specific objectives of this case study are to demonstrate:

- How system code and CFD methods can be combined to gain a more detailed understanding of a complex thermal hydraulic phenomena occurring during an accident transient.
- The steps required to develop a system code model for a specific plant transient.
- The use of CFD in an application where it is important to correctly represent the influence of buoyancy and local mixing of fluids with substantial temperature differences.
- The application of CHT modelling to derive detailed component temperature time histories from a transient CFD analysis.
- The validation of thermal hydraulic analysis methods against experimental measurements.

As for all the case studies in this series, this analysis provides a ‘worked example’ of a specific modelling task to illustrate the modelling approaches described in the technical volumes. Therefore, it is recommended that this case study is read in conjunction with the following technical volumes:

Volume 1: Introduction to the Technical Volumes and Case Studies
Volume 2: Convection, Radiation and Conjugate Heat Transfer
Volume 3: Natural Convection and Passive Cooling
Volume 4: Confidence and Uncertainty

While the methods demonstrated by this case study are applied to a specific example of a Pressurised Thermal Shock (PTS) in a large Pressurised Water Reactor (PWR), this analysis approach

could equally be applied to Small Modular Reactor (SMR) design problems, which feature comparable physical behaviour, and different reactor designs.

1.1 Case Study Description

This case study relates to the injection of cold coolant ($\approx$ 310 K) from the Emergency Core Cooling System (ECCS) into the hot primary circuit ($\approx$ 560 K) during a Small Break Loss-Of-Coolant Accident (SBLOCA) in a PWR. It is focused on identifying and understanding the analysis sequence and validation of simulation results against test data from the OECD/NEA ROSA project (CSNI, 2013).

Thermal stratification of the ECCS flow within the cold leg and the upper sections of the downcomer occurs because of incomplete mixing of the injected ECCS coolant with the main loop flow (Figure 1.1), typically following the loss of forced or natural circulation in the loops. This localised flow of cold fluid induces thermal stresses on the cold leg and Reactor Pressure Vessel (RPV) components, which could lead to a more serious failure, particularly given the increased susceptibility to failure of these components caused by the effects of radiation. PTS and its structural implications are discussed in more detail in Section 1.2 and in Volume 2. The eventual aim of a

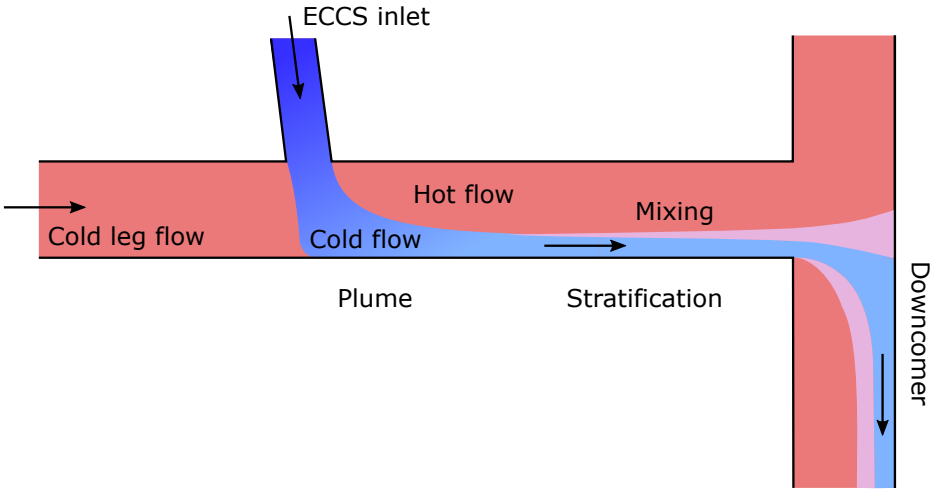

Figure 1.1: Flow phenomena during ECCS injection.

designer in this case is to assess the structural integrity of the cold leg and RPV components in the event of a SBLOCA. To perform this mechanical assessment, the local temperatures of the structural components are required as inputs, which are the result of heat transfer with the coolant. Whilst some conservative assumptions could be made regarding these inputs, this may result in an overly conservative mechanical assessment that constrains the design (increases RPV thickness or limits plant performance, for example), and does not provide insight into the phenomena. It is therefore desirable to complete a detailed thermal hydraulic assessment to derive these inputs.

The largest thermal shock typically occurs following a loss of flow in the primary loops which results in a rapid reduction in mixing of the cold injection flow. This loss of loop flow is a characteristic part of the whole plant response to the break. Considering both of these aspects, it is clear that it will not be possible to model both the whole plant response and the detailed local stratification behaviour using a single thermal hydraulic analysis method.

A sequence or hierarchy of analytical methods can be applied to gain more insight, where a system code is used to model the overall plant behaviour and progression of the accident transient, and CFD analyses used to model in finer detail the complex thermal hydraulic behaviour occurring in the cold leg and upper sections of the downcomer during the loss of loop flow. A high level introduction to the different thermal hydraulics analysis tools available and their applications can be found in Volume 1 (Section 4.1).

System codes are capable of modelling the entire primary and secondary circuit of a reactor, as well as the control and protection systems that are initiated in the event of a fault. However, for them to be able to represent the response of the entire system over long transient events, the level of fidelity used to represent individual reactor components must be simplified and approximated. In system codes, the thermal hydraulic equations are solved in one-dimensional, coarse grained volumes, and the heat, mass and momentum transport (including two-phase behaviour) is calculated mainly by empirical correlations determined from experimental test facilities over a range of scales.

Given the complex three-dimensional and locally heterogeneous thermal hydraulic phenomena in the cold leg and downcomer, CFD is the most appropriate analysis approach for this aspect of the analysis, although it is noted that some analytical/empirically based codes have been developed specifically for this application (e.g. REMIX). The additional benefit of using CFD in this application is that the model can be extended to include the solid components, the local convective heat transfer to them and the conductive heat transfer through them. Employing a CHT approach allows the temperature variation in the mechanical components to be directly derived from the CFD analysis, and at a higher level of detail than would be possible with a separate thermal structural model.

1.2 Pressurised Thermal Shock

PTS presents a significant issue in the design, operational surveillance and maintenance of large PWRs and SMRs. Reactor transients which subject the primary circuit to rapid temperature variations whilst under high pressure can lead to rapid propagation of structural defects and potentially challenge component integrity. The RPV and RPV nozzles are of particular concern due to localised embrittlement of the steel and welds by neutron radiation.

RPVs must therefore be designed, manufactured and tested to ensure that they have sufficient safety margins against structural failure, taking into account the normal operation and fault transients that could occur during the life of the plant. Subsequently, operating procedures, transient monitoring and In-Service Inspections (ISIs) have an important role in ensuring that these safety margins are retained despite the ageing of the plant.

The mechanical design of the primary circuit and RPV components must take into account all of the foreseeable loadings that they could be exposed to during the full life cycle of the NPP. One aspect of the supporting mechanical analysis is consideration of all pressure and temperature transients that the components could experience during normal operation, faults and accidents.

Detailed best practice guidance for deterministic assessment of the most significant PTS transients is available in IAEA (2010), which covers the whole analysis sequence and is summarised in Section 1.3. System codes are identified as the primary means of analysing the overall accident sequence with the aim of predicting the transient variation of the primary circuit pressure,

coolant temperature, loop mass flow rates and ECCS injection temperature and mass flow rate. IAEA (2010) recommends that more detailed 3D methods are used to assess the behaviour in the cold leg and downcomer where non-uniform mixing and buoyancy effects are significant.

In PWRs, LOCAs are one of the most significant transients contributing to the overall PTS risk. SBLOCAs tend to lead to less severe thermal shock but occur at higher primary system pressures, while Large Break Loss-Of-Coolant Accidents (LBLOCAs) lead to more severe thermal shock at lower primary system pressures.

In a typical SBLOCA sequence (described in further detail in Section 2.1), following the initial pressure drop due to the loss of 'inventory' (water in the primary circuit) at the break, the Main Coolant Pumps (MCPs) have tripped and natural circulation is occurring in the primary loops whilst the primary circuit continues to depressurise. The ECCS is initiated by the plant safety systems and the injected flow rate of cold water into the cold legs gradually increases as the primary pressure reduces.

Initially, whilst loop flows are sustained, mixing in the cold leg may prevent significant thermal stratification. As primary depressurisation continues, a number of different mechanisms can lead to the loss of loop flow. The most significant period of PTS typically occurs at this stage where cold ECCS flow is injected into a hot and stagnant cold leg which could be in either single-phase or two-phase conditions. Thermal stratification can then occur with a stripe of cold flow along the bottom of the cold leg and a cold plume in contact with the inner or outer wall of the RPV downcomer. The rapid and non-uniform cool-down of the cold leg and RPV while the primary circuit is still at a relatively high pressure induces significant thermal stresses in these components.

The mixing of cold ECCS injection into the hot, stagnant fluid in a cold leg has been the subject of significant international research, experiments and modelling efforts. A number of dedicated analysis codes, based on a combination of analytical methods and empirical data have been developed for assessing this behaviour (such as REMIX). However, there is an increasing focus on applying CFD methods to this analysis (Boyd, 2008). Recent examples of efforts to develop CFD methods for PTS modelling include Boumaza *et al.* (2014), Lai *et al.* (2020) and Angeli (2021). Each approach has its advantages and disadvantages.

- A dedicated code is likely to be simpler and quicker to use, because little model development is required and the physical domain and transport models are already configured for the specific application. The empirical data employed is able to provide a strong experimental basis for the validity of the models used. Caution is required regarding the extent of applicability of the models to geometries and flow conditions that are different to the ones that the models were derived from.
- In contrast, application of a general-purpose CFD code, capable of directly resolving the relevant physical phenomena, requires the development of a computational model specifically for the plant geometry. Once an appropriate methodology has been established, it is likely to be applicable to other similar geometries and flow conditions.

In either case, the onus is on the modelling engineer to ensure that the approach employed remains valid for each application. A significant further advantage of using a CFD code is that it can be extended to include the solid components of the cold leg and RPV in the model (CHT analysis).

Since the result of importance is the variation in the component temperatures, this is highly relevant because it allows the coupled effects of the conduction heat transfer in the solids, convective heat transfer from the flow and thermal mass of the solids to be captured with minimal simplification. Further information on CHT analysis is available in Volume 2.

This case study focuses on mixing under single-phase cold leg conditions in line with the scope of these technical volumes. However, it is worth noting that analyses are increasingly targeting two-phase flow assessments (CSNI, 2014) of ECCS injection into a partially or fully voided cold leg (e.g. Cremer *et al.*, 2019).

1.3 Typical Analysis Sequence

The analysis sequence for an assessment of PTS for a new NPP design (such as an SMR) is illustrated in Figure 1.2. This is an extensive process which would likely take a number of years to complete and requires input from a number of different technical disciplines. Whilst a large proportion of this work is clearly outside the scope of this limited thermal hydraulics case study, the intention is to demonstrate the scale of this process and identify where the aspects considered in the case study fit into it. The key steps identified in Figure 1.2 are:

Transient identification: Initially all of the potential plant transients that could lead to PTS need to be identified, considering normal operations, faults and accidents.

Down selection of the enveloping transients: The transients with the largest contribution to the overall PTS risk have to be identified, considering both the event frequency over the plant lifetime and the magnitude of the associated PTS. Preliminary system code analyses would likely be required to inform these judgements. Best practice guidance for PTS transient screening is available in IAEA (2010) and extensive work to identify the transients contributing the majority of the PTS risk has been performed for US PWRs (US NRC, 2007).

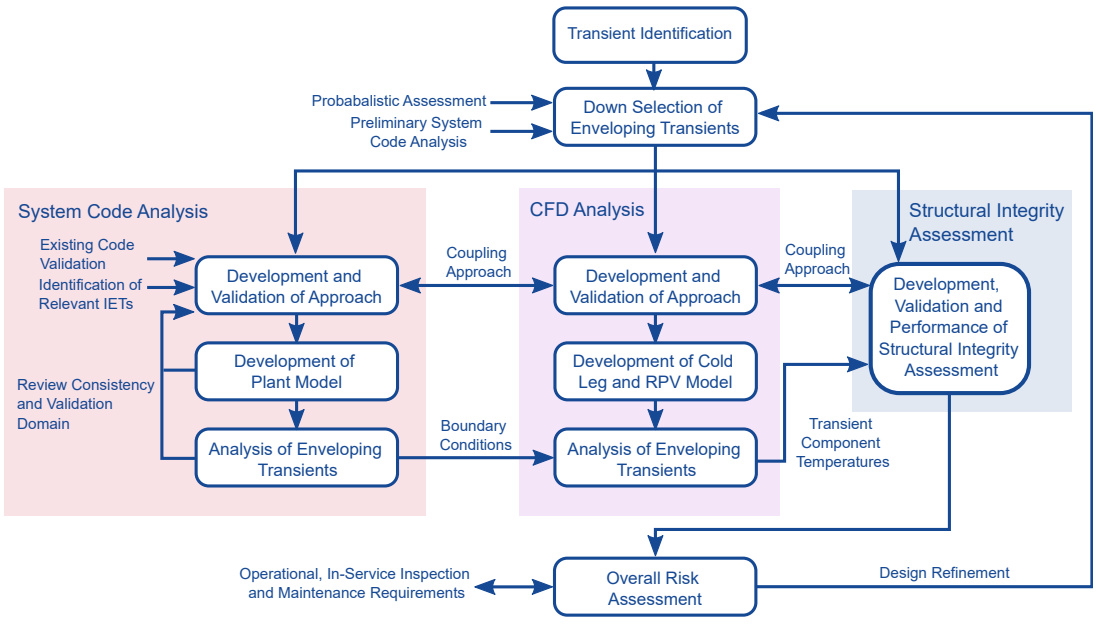

Figure 1.2: Illustrative analysis sequence for PTS.

Thermal hydraulic analysis: The identified enveloping transients need to be analysed in detail to determine the variation in the primary circuit component temperatures during the events. This analysis is a two-step process firstly using a system code to assess the overall plant behaviour and then performing a more detailed analysis of the flow behaviour and temperatures in the cold leg and RPV downcomer, in this case using CFD. Within each of these analysis strands a similar approach needs to be followed to first develop and validate a modelling approach before building a model of the actual plant and finally analysing the required transients.

The methodology development and validation is equally important for establishing the capability of the engineer or their organisation and of the selected codes and methods which may have existing relevant validation data available. Existing Separate Effect Test (SET) and Integral Effect Test (IET) data[1] relevant to the plant design and thermal hydraulic phenomena of interest should be identified if possible. In the absence of existing, relevant data it may be necessary to perform new tests to provide validation evidence. The methods for data transfer or coupling between the different analysis strands also need to be established.

For each transient, a number of sensitivity studies to key plant parameters (for example Loss-Of-Coolant Accident (LOCA) break size) would likely be performed to understand which configuration leads to the most severe PTS conditions. The actual plant model representation (volumes, heat structures), nodalisation and model settings should retain as closely as possible the approach that has been validated (Petruzzi and D'Auria, 2008). There is a feedback loop to ensure that the final analysis results remain within the validated domain of the codes and methods. For example, this case study only considers single-phase conditions in the CFD validation, but for broader analysis of PTS transients, further validation for two-phase conditions is likely to be necessary.

Structural integrity fracture mechanics analysis: The transient component temperature variations from the CFD analysis as well as the pressures from the system code analysis are used as inputs to the structural models which evaluate the stresses in the reactor components. The analysis aims to establish the probability that a defect initially present in the material will develop into a through-wall crack as a result of these stresses, taking into account radiation embrittlement effects. Analysis is typically performed using 3D Finite Element Analysis (FEA) methods. Similar development and validation exercises to the thermal hydraulics aspects would need to be performed for this part of the analysis. The process for data transfer between the CFD and FEA models would also need to be established.

Overall risk assessment: As a final step, the occurrence frequency of the enveloping transients and the probability of structural failure due to the stresses induced by the transients can be combined to assess the overall risk of failure. The proposed operational, ISI and maintenance requirements will also need to be considered and reviewed for consistency with any requirements resulting from the assessment. In the event that the overall failure risk is too high or the ISI or maintenance requirements are too onerous, refinement of the plant design may be required.

[1] SETs separate local phenomena in reactor components and sub-assemblies from the whole system response to develop and validate physical models, while IETs are intended to provide a similar thermal hydraulic dynamic system response to a postulated accident in a reference reactor. Further description is given in Volume 1, Section 4.6.

2 Problem Definition

A good understanding of why the analysis is being performed and what the results will be used for is vital to enable 'fit-for-purpose' decisions to be made throughout the model development. The problem definition and analysis planning steps are therefore essential to the success and efficiency of the thermal hydraulic analysis.

As discussed in Section 1.3, the full analysis sequence for the assessment of PTS is extensive. Only the initial methodology development and validation of the thermal hydraulic analysis are covered in this case study. A general introduction to Verification and Validation (V&V) and why they are important in nuclear thermal hydraulics analysis is available in Volume 1 (Section 4.3) and Volume 4 (Confidence and Uncertainty).

The OECD/NEA Rig-of-Safety Assessment (ROSA) project (CSNI, 2013) was performed to resolve key safety issues of Light Water Reactor (LWR) thermal hydraulics using the Japan Atomic Energy Agency (JAEA) Large Scale Test Facility (LSTF). This test programme has been selected as a suitable source of validation data for the system code and CFD analysis, as a number of SET and IET tests specifically designed for the study of PTS during an SBLOCA were performed during the 2005-2009 test programme (CSNI, 2013). A summary of the major outcomes from the experiments at this facility is given by Takeda *et al.* (2021). Detailed test rig geometry and results data are also readily available (Section 2.2). The identified ROSA tests therefore form the basis of the methodology development and validation considered in this case study:

- Section 3 describes the process which would be followed to build a system code model of the LSTF and validate the predicted plant response to a SBLOCA against the results of ROSA IET Test 1-2.
- Section 4 details the development and validation of the CFD analysis methodology based on the results of ROSA SET Test 1-1. The development of a CFD model and analysis of the Test 1-1 transient, including prediction of the solid component temperatures are described. Evidence to support the validation of the ability of the CFD model to predict the necessary phenomena is created by comparison of the modelling outputs to the test results.

The first step in any thermal hydraulic analysis is to understand which results are of importance and identify the processes and phenomena that have the most dominant influence on these results. The ability of the proposed analysis tools to model these phenomena can then be assessed. The Phenomena Identification and Ranking Table (PIRT) process described in Volume 1 (Section 4.2) is a formal and systematic means of completing this process.

A formal PIRT has not been completed as part of this case study, however these considerations remain important in the planning of the analysis, and a simplified process broadly aligned with the

main steps of a PIRT is demonstrated by this case study. Considering that the results of interest are different for the system code and CFD parts of the overall analysis sequence, these aspects have been described separately for each step in Section 3.1.1 and Section 4.1.2 respectively.

2.1 Typical Hot Leg SBLOCA Description

The progression of a SBLOCA transient is dependent on a large number of factors, including the size and location of the break, as well as the detailed plant design and safety systems (CSNI, 1989, US NRC, 1989). The key plant design features of importance are the elevation of the primary circuit components, the ECCS injection location and performance, the Steam Generator (SG) design and secondary cooldown strategy and the MCP trip strategy.

It is not possible to provide a single description of the typical system behaviour in a PWR during a SBLOCA which covers all break sizes, locations and plant designs, although the thermal hydraulic phenomena relevant to PTS remain similar. The description that follows is representative of a small hot leg break on a four-loop Westinghouse PWR, which is the design replicated by the LSTF. The description also focuses on a transient that is relevant for PTS, so the transient progression and thermal hydraulic phenomena of interest differ slightly from those which would typically be of most interest in a SBLOCA assessment of fuel temperatures.

Figure 2.1[1] provides a representative example of the evolution of the main system parameters during the transient and identifies the three main stages that are described below:

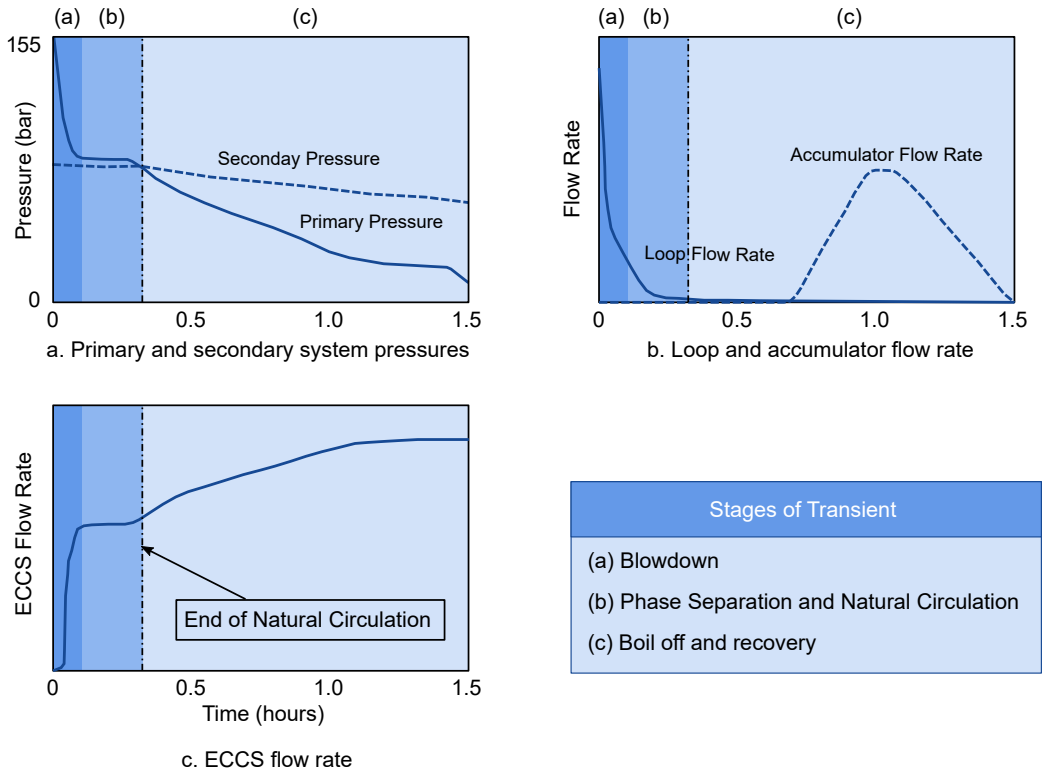

Figure 2.1: Typical variation in system parameters during an SBLOCA.

[1] The accumulator is a passive safety injection device for ECCS, which contains a large volume of water that is released into the primary circuit when the pressure drops below a set value.

Blowdown: Primary pressure rapidly falls to the saturation pressure at the core outlet temperature within the first few seconds of the break opening. The critical flow at the break is single phase liquid and the depressurisation rate is dependent on the break size. The pressuriser quickly empties, initiating the reactor scram signal shortly followed by the start of the ECCS systems and main steam and feedwater isolation on the secondary side. Once saturation conditions are reached, steam voids are formed in the hottest regions of the primary circuit; initially in the upper plenum and Pressure Vessel (PV) upper head followed by the hot legs (Figure 2.2). The steam production in the core due to the decay heat at the end of the blowdown stage is sufficient to reduce the rate of primary depressurisation (Figure 2.1).

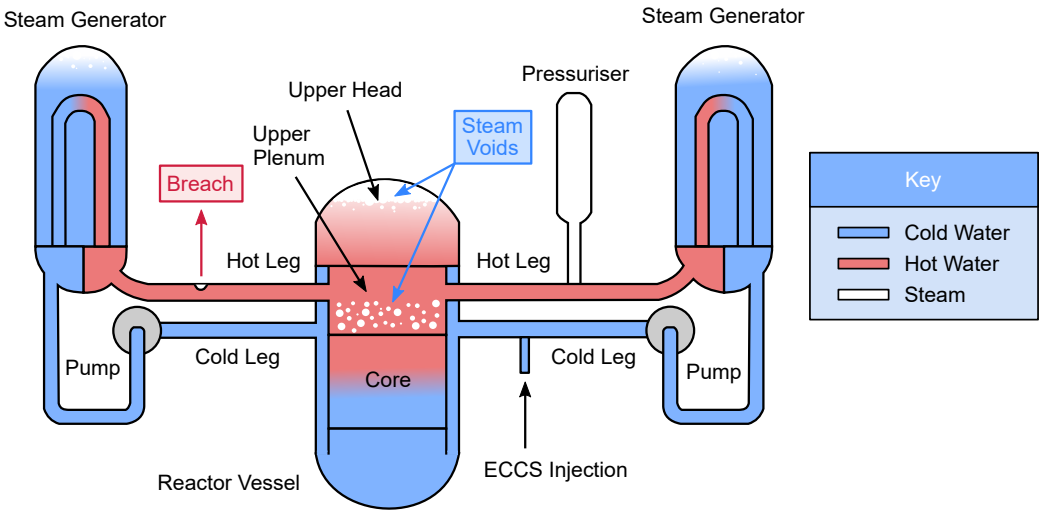

Figure 2.2: Blowdown stage of a hot leg SBLOCA in a PWR.

Phase separation and natural circulation: The MCPs are typically tripped either in the latter stages of the blowdown stage, when void formation occurs in the loop,s or early in this stage. Loop flows are maintained for a short period during pump coast down, followed by a transition to natural circulation conditions (Figure 2.3). The decay heat is removed both through the energy release at the break and via the natural circulation to the SGs.

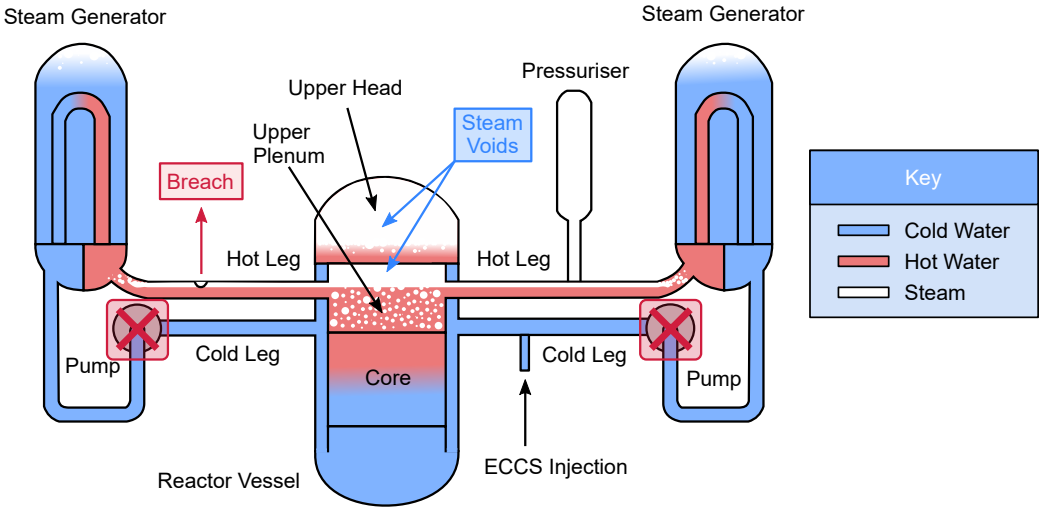

Figure 2.3: Natural circulation stage of a SBLOCA in a PWR.

End of natural circulation: This transition between stages is very significant for PTS analysis because the most onerous conditions typically occur at the point when the loop flow is lost. This leads to a sudden decrease in the mixing of the cold ECCS flow, allowing thermal stratification to occur in the cold leg. The time in the transient at which this occurs is also significant, if it happens earlier, when the primary pressure is still higher, then the induced stresses on the RPV components are greater. The progression of this stage of the transient depends on the break size:

1. If the energy lost via the break is greater than the decay heat, the primary depressurisation continues to be controlled by the break flow. The primary pressure will fall below that of the secondary side, and therefore so will its temperature because both are at saturation conditions. With the direction of heat exchange in the SG reversed, the driving forces for natural circulation in the loops no longer exist, loop flow ceases and void formation occurs in the upper portion of the SG.
2. If the energy lost via the break is not sufficient to match the decay heat, the primary system remains hotter than the secondary system and heat continues to be removed via the SGs. The primary depressurisation is controlled by the secondary side conditions and a controlled secondary cool down may be initiated to reduce the primary pressures to allow increased ECCS injection flow. This temporarily sustains the natural circulation in the loops, however a similar loss of natural circulation will occur when a liquid flow through the upper portion of the SG can no longer be maintained due to continuing inventory loss.

Alternatively, as primary inventory loss and void formation in the hot leg continues, the two-phase interface level will approach the level of the break. The break flow will transition from single-phase to increasingly high void fraction two-phase critical flow, which increases the rate of primary depressurisation. At this stage, the conditions will transfer to the first scenario described above and natural circulation will cease once the primary pressure drops below the secondary pressure. This is the case in the transient represented in Figure 2.1.

Boil off and recovery: In the later stages of the transient, the primary depressurisation continues due to the break flow and cooling provided by the cold ECCS injection. The two-phase interface level in the hot legs continues to reduce and void formation may also occur in the cold legs. Core uncovery[2] and reflood may also occur during this phase, but are not described in detail here as the focus is on PTS behaviour. As the primary pressure reduces, the flow rate that can be delivered by the ECCS increases, and once the set pressure of the accumulators is reached, a large volume of cold water is injected. There may be a temporary pause in the primary pressure reduction at this stage due to increased steam generation during recovery of core and hot leg water levels. Eventually a balance between the flow lost at the break and the ECCS injection is reached, the core inventory is recovered and a stable long term cooling regime is established.

It is worth noting that during this fault the steam exiting the break enters the reactor containment system, which involves a completely different set of the thermal hydraulic phenomena that need to be considered, such as steam injection and wall condensation (CSNI, 2007).

[2] Core uncovery begins when the fuel rods are no longer completely covered by coolant, which may lead to core melt if a sufficient level of cooling cannot be restored.

2.1.1 Important Thermal Hydraulic Phenomena

Extensive work to identify and rank the most important phenomena in general SBLOCA transients has been performed (for example Ortiz and Ghan, 1992, CSNI, 1996) and more specifically for PTS by Bessette *et al.* (2005). The information resulting from these formal PIRT processes has been compiled in Table 2.1 to provide a brief summary of the key phenomena associated with each phase of a hot leg SBLOCA as described in Section 2.1. A separate column is included for the most influential design parameters, to highlight the features that may lead to slightly different behaviour in different plant designs, or which could potentially be modified in a new NPP design.

Stage	Phenomena	Design Parameters
Blowdown	Single-phase liquid critical flow (at break) Phase separation without mixture level formation Single- and two-phase MCP behaviour Phase separation & heat transfer in vessel head	Core decay heat MCP trip timing MCP rundown characteristic Thermal mass of primary circuit components
Phase separation and natural circulation	Phase separation and mixture level formation Single- and two-phase natural circulation in loops Single- and two-phase critical flow (at break) SG heat transfer	Core decay heat ECCS injection pressure Secondary pressure control
End of natural circulation	Phase separation in upper portion of SG tubes ECCS mixing and condensation SG heat transfer	Secondary pressure control ECCS injection flow and temperature Primary circuit elevations
Boil off and recovery	Single-phase steam critical flow (at break) Core void and flow distribution Core heat transfer	Accumulator pressure, volume & temperature ECCS injection flow and temperature ECCS injection location

Table 2.1: Key thermal hydraulic phenomena and design parameters associated with each stage of a hot leg SBLOCA transient.

2.2 OECD/NEA ROSA Project

The OECD/NEA ROSA project (CSNI, 2013) focused on the validation of simulation models and methods for various complex phenomena that may occur during LWR accident transients, with the aim of increasing the level of detail and the accuracy of the analysis. In particular, the objective of Test 1[3] was to perform SET and IET experiments on thermal stratification and coolant mixing during ECCS injection.

Detailed information describing the LSTF geometry and ROSA project operating parameters is available because international benchmarking was a key focus of the project. Similarly, due to the targeted nature of the tests on particular phenomena, extensive instrumentation was installed providing a large amount of high quality data for validation purposes. Considering this, the results from the ROSA tests provide one of the most relevant, accessible and detailed validation cases for modelling PTS in PWRs. Development of an analysis methodology based on validation against this type of benchmark provides a good example of how confidence in an approach can be established

[3] In total, 12 experiments were performed for 6 types of subject from 2005 to 2009 (CSNI, 2013).

before going on to apply it to a real NPP design, and therefore provides an ideal basis for this case study.

The LSTF is an IET facility replicating the primary and secondary circuits of a four-loop Westinghouse-type PWR, including its control and protection systems. It is a full pressure, full-height, two-loop representation with a 1/48 volumetric scaling ratio. The layout of the LSTF is shown in Figure 2.4 and a detailed description of the facility is available in ROSA-V Group (2003).

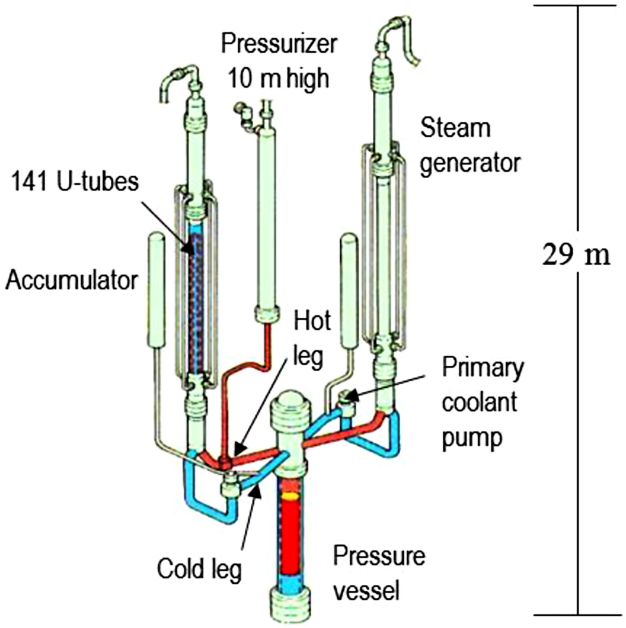

Figure 2.4: Schematic view of ROSA/LSTF from Takeda (2018).

During normal operation, the flow enters the PV via two cold legs and the bulk of the flow travels down the downcomer and into the lower plenum. The flow is then heated as it passes up through the core into the upper plenum and exits the PV via two hot legs (Figure 2.5).

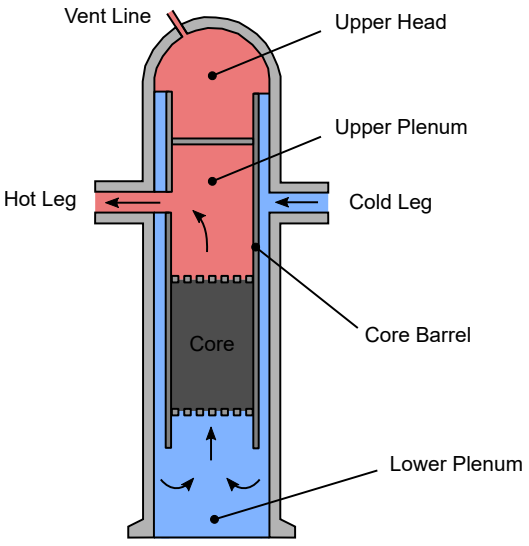

Figure 2.5: Coolant flow paths in PV during normal operation.

The LSTF primary coolant system consists of two similar loops: Loop A with the pressuriser and Loop B without (Figure 2.6). In each leg, the hot leg flow from the PV travels to the SG where it is cooled. It then passes through the crossover leg before entering the centrifugal MCP and into the cold leg to complete the circuit. The ECCS consists of a High Pressure Injection System (HPIS), Low Pressure Injection System (LPIS) and Accumulator Injection System (AIS).

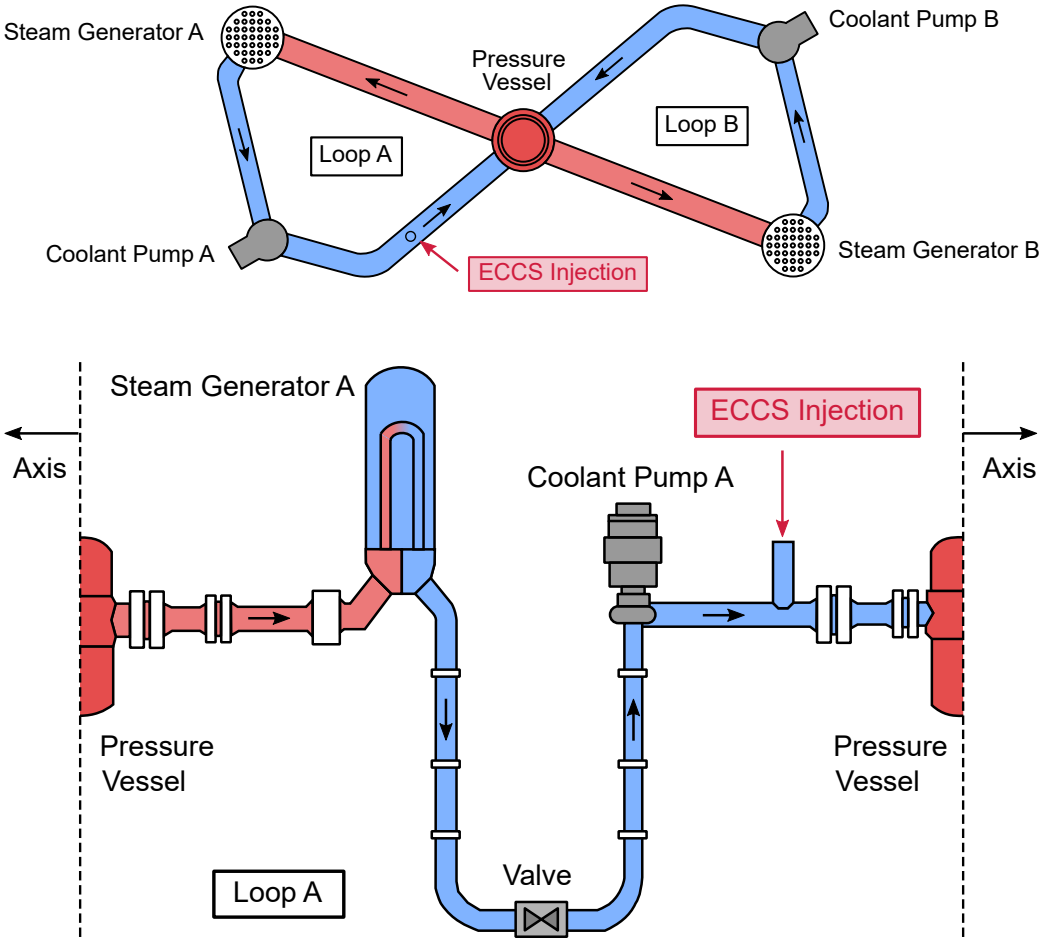

Figure 2.6: Plan view of coolant loops (top) and simplified view of Loop A (bottom).

2.3 ROSA Test 1 Program

For the OECD/NEA ROSA project, 144 additional thermocouples were installed in the cold legs and downcomer to allow detailed data to be captured for the validation of 3D models with a nominal accuracy of the thermocouple measurements of $\pm$ 2.75 K. Video probes were also installed in the cold legs to allow qualitative assessment of the flow behaviour. The tests included SETs with cold ECCS injection under controlled primary circuit conditions (single-phase and two-phase) as well as an IET simulating a SBLOCA fault sequence.

Separate tests have been selected for the system code and CFD model validation, as the system code simulates the whole plant response (IET), while the CFD analysis is focused on the thermal hydraulic phenomena in a specific region and so requires well defined boundary conditions (SET).

2.3.1 System Code Modelling

Test 1-2 (JAEA, 2008b) was identified for the system code model development and validation. It was conducted in May 2007, and is an IET simulating a 1 % hot leg SBLOCA on Loop B with automatic actuation of the HPIS and AIS through the ECCS injection nozzles of both cold legs. The transient is initiated from normal operating conditions with a primary circuit pressure of 155 bar, core power of 10 MW and both MCPs operating. The break occurs at t_0, the scram signal is issued when the primary circuit pressure reaches 130 bar (49 s) with core power following a decay curve and the coolant pumps coasting down.

The HPIS starts at 92 s after the primary pressure drops to 123 bar with single-phase conditions in the cold legs. The AIS starts at 2537 s (45 bar) once the cold leg conditions have transitioned to two-phase flow. In the initial period of ECCS injection, the flow rate in the primary coolant loops remains relatively high so mixing of the ECCS flow with the main coolant flow is relatively efficient and limited thermal stratification is observed. After around 300 s, once the MCPs have completely stopped, the loop flows are reduced and the flow becomes two-phase leading to much more significant thermal stratification, particularly when natural circulation flow ceases at around 450 s.

2.3.2 CFD Analysis

Test 1-1 (JAEA, 2008a) has been selected for the CFD methodology development and validation. It was conducted in October 2006, and is a SET with ECCS injection under steady-state natural circulation conditions.

The core power was set to 1.4 MW, which corresponds to 2 % of the scaled nominal power at 15.5 MPa with 100 % primary inventory. This generated a stable, single-phase natural circulation flow around the primary circuit with a nominal flow rate of 6 kg/s at a cold leg temperature of 555 K. The ECCS water was then injected separately into the cold legs of Loop A and Loop B for about 80 s using the charging pump (i.e. one cold leg injection at a time), with sufficient time between each ECCS injection to stabilise the natural circulation flow. During the test sequence, ECCS flow was injected into Cold Leg of Loop A (CL-A) at two different nominal flow rates, 0.225 kg/s and 0.980 kg/s.

The primary inventory was then reduced in steps to 80 %, 70 % and 50 % to achieve a range of two-phase natural circulation conditions in the loops. Alternating ECCS injection was repeated for each cold leg for each primary inventory level.

The CFD validation is focused on the first ECCS injection into Loop A, which provides a well defined single-phase test case. Once stable natural circulation conditions were established in the loop, a nominal ECCS flow of 0.225 kg/s was injected between 18 s and 100 s. In this test, the cold ECCS injection flow ramped up quickly and varied around the nominal value.

The thermocouples in the cold leg (Figure 2.7) provide good spatial and temporal measurements of the thermal stratification that occurs in the cold leg downstream of the ECCS nozzle. The plane locations are calculated based on the distance downstream of the ECCS injection point in terms of the cold leg diameter (D) of 207 mm[4].

[4] The additional thermocouples that were installed for the OECD/NEA ROSA project are located on Planes 1, 2 and 3.

The thermocouples attached to the PV wall in the downcomer (Figure 2.8) spread out circumferentially with distance from the cold leg in order to capture the expansion of the cold plume as it travels down the downcomer annulus. The plane locations are defined based on the LSTF elevations (EL values in mm on Figure 2.7)[5].

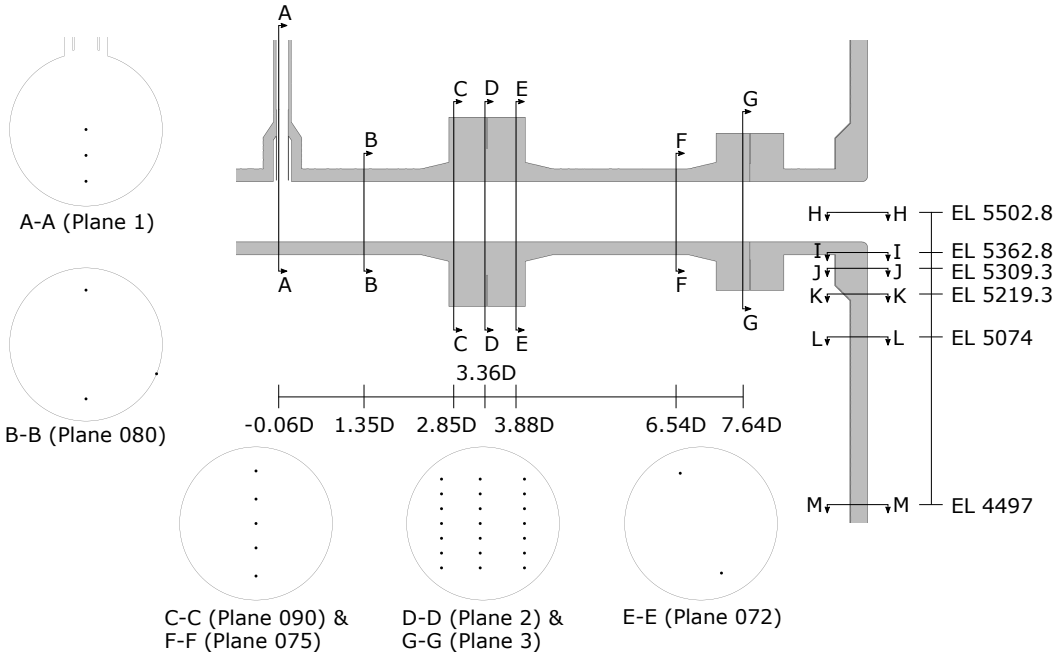

Figure 2.7: CL-A thermocouple planes with cross-sections viewed looking towards PV.

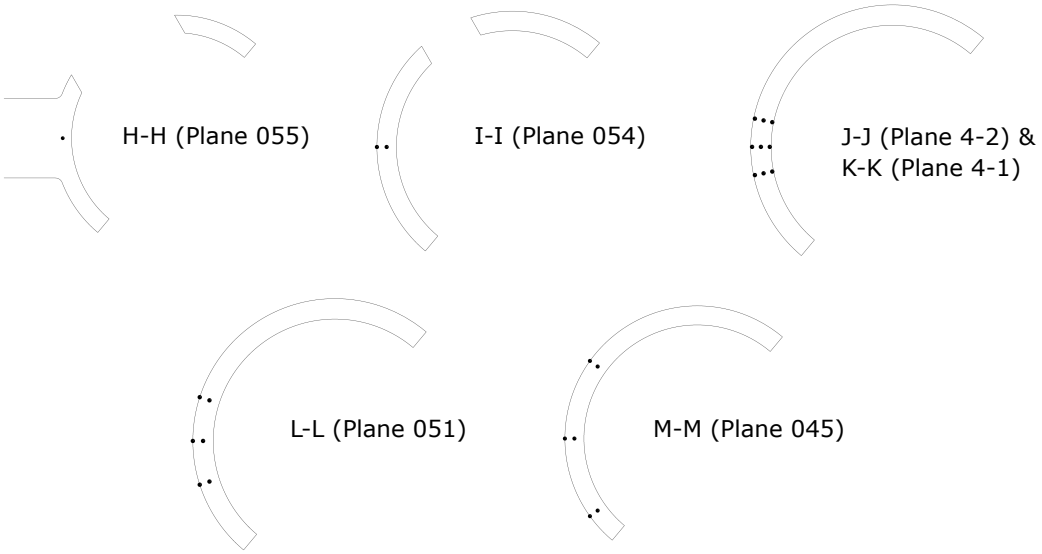

Figure 2.8: Downcomer thermocouple planes viewed looking down from above.

[5] The additional thermocouples that were installed for the OECD/NEA ROSA project are located on Planes 4-1 and 4-2.

3 System Code Analysis

3.1 Problem Definition

In the overall analysis sequence defined in Section 1.3 the role of the system code is to model the whole plant response to a number of transients that could result in PTS. The key results from the system code analysis are the primary circuit thermal hydraulic conditions at the time of interest in the transient which are an input to the CFD analysis.

ROSA SBLOCA Test 1-2 (Section 2.3.1) has been identified as a suitable IET for the development and validation of a system code methodology for assessing PTS transients. This section describes the approach that could be followed to develop a system code model of the ROSA/LSTF and validate it against the results of Test 1-2.

3.1.1 Results of Importance

The overall Figure of Merit (FOM) for PTS analysis is the probability of through-wall crack propagation in the primary circuit components. However, it is difficult to directly relate this to the system code analysis. Focusing more specifically on the thermal hydraulic component of the analysis sequence, the FOM could be the transient temperature variation in the cold leg and RPV components during a PTS transient. Again, as this is an output of the downstream CFD analysis it is not clear how to translate this into a set of requirements for the system code analysis.

Considering this, the FOM for the system code analysis should be considered to be the results that are required as input to the CFD analysis. These are the transient variation of the following parameters over the period of interest:

- Primary loop mass flow rates.
- Cold leg temperatures and liquid level (if in two-phase conditions).
- Primary system pressure.
- ECCS injection flow rate and temperature.

However, caution is required with this approach because the relationship between these results and the combination of them that will give the most onerous outputs in the downstream structural analysis is not immediately obvious. This is particularly true for complex results such as rate of temperature change and the 3D temperature distribution, both of which are likely to be significant. This highlights the importance of considering the full analysis sequence rather than just a part of it (US NRC, 2007).

A best estimate modelling approach is judged to be most appropriate for the system code aspects of the PTS modelling. The aim is therefore to develop and validate a model that can reliably represent the plant behaviour during the required transients, rather than specifically focusing on the

particular set of parameters which would result in the most onerous contribution to the overall PTS risk. A number of different transient analyses and sensitivity studies would likely be run within the full scope of the system code analysis to explore the parameter space and identify the sensitivity to the key plant design parameters (IAEA, 2008, CSNI, 2011a and CSNI, 2017).

Using the parameters identified above as validation comparisons is judged to be a suitable way to assess the adequacy of the model's performance in relation to the important thermal hydraulic phenomena for PTS. A number of additional results of interest have been identified that provide an indication of the model performance specifically for hot leg SBLOCA:

- Break mass flow rate and void fraction.
- Secondary system pressure.
- Pressuriser level.
- Secondary side (SG) feedwater and steam flow rates.
- Hot leg and core liquid levels.

Whilst these are not as directly relevant to the PTS behaviour, they provide additional confidence in the SBLOCA performance of the model and help to demonstrate its applicability to other transients involving similar thermal hydraulic phenomena. A notable absence from this list are any parameters relating to the fuel temperatures, which are often the FOM in LOCA analyses. As the intention is to assess PTS rather than the fuel integrity, the particular LOCA scenarios which are of interest are likely to be different, and there is not a requirement to represent the complex thermal hydraulic processes involved in the uncovery and re-flooding of the core in the same level of detail.

3.2 Planning the Analysis

3.2.1 Modelling Tool Selection

To fully represent the plant behaviour during an SBLOCA transient, the model needs to include the primary and secondary circuits and safety systems, as well as the response of the control systems. System codes are the obvious and only tractable choice of tool for this analysis. Extensive work has been completed to develop and validate system codes for PWR safety analysis, with some codes specifically targetting LOCA simulation. A general introduction to some of the principal system codes currently used in the nuclear industry worldwide is available in Volume 1 (Section 4.4.1).

It may occur to question why, given extensive existing validation of these codes for LOCA analysis, there is a need to perform additional validation for a specific use case. However, as highlighted previously, this process remains highly relevant for developing and demonstrating the capability of a user or an organisation in applying the selected code. User effects remain one of the primary drivers for uncertainty in system code analysis (CSNI, 1994, CSNI, 1998). This topic is discussed in more detail in Volume 4.

In the full scope of the PTS system code analysis for a new NPP design (Section 1.3) it would be necessary to analyse a large number of different accident scenarios, as well assessing the sensitivity of the results to the modelling assumptions and plant design parameters. This further supports the development of a general purpose system code model of the plant design as the most

appropriate way forwards. Once developed, the model could be adapted relatively easily to perform the numerous accident transients and sensitivity studies required.

A detailed system model of the ROSA/LSTF was developed by Queral *et al.* (2014) as part of the United States Nuclear Regulatory Commission (US NRC) Code Applications and Maintenance Program (CAMP) program which aims to further the V&V status of the US NRC thermal hydraulics codes. The model was developed in TRACE and was subsequently used to analyse all of the tests performed for the OECD/NEA ROSA project, including Test 1-1 (Julbe *et al.*, 2012) and Test 1-2 (Munoz-Cobo *et al.*, 2013). The TRACE model was adapted from an original TRAC-PF1 model of the ROSA facility developed by JAEA.

Given that these models originate from the owners of the LSTF there is a high degree of confidence in their representation of the plant, and it is sensible to utilise them as far as possible in the development of the approach in this case study. Further specifics on the modelling approach and input data applied in the TRACE model are available in Gallardo *et al.* (2012) and Queral *et al.* (2014). Further detailed information on the setup of the ROSA facility is available in ROSA-V Group (2003), and specific information on Test 1-2 conditions is available in JAEA, 2008b.

TRACE modelling of the ROSA/LSTF was also performed as part the more recent OECD/NEA ROSA-2 project (for example Takeda, 2018 and Gallardo *et al.*, 2019). Although this project did not include tests specific to PTS, these modelling efforts still provide useful information on how to effectively model the LSTF in TRACE.

The system code used should be selected based on a user or an organisational capability with a particular code and access to licenses are also important considerations, as well as the suitability for the particular application. For this case study, TRACE is considered the most appropriate, primarily because of the extensive international validation effort to demonstrate the suitability of TRACE for LOCA transients (Bajorek *et al.*, 2015) and the existing ROSA/LSTF modelling. Significant insight can be taken from this existing body of work in the development of the modelling approach.

3.2.2 Modelling Strategy

Planning of the model development is focused on the identification of the key model components by representing them appropriately, so that the important thermal hydraulic phenomena occurring within them during the transient can be captured. It should be noted that the development of a TRACE model specifically for application to the ROSA Test 1-2 transient is considered here, so some modelling choices would likely differ if the aim was to develop a system code model for more general application.

The effort required to develop a single system code model that reliably simulates all of the required plant transients is significant. It is almost inevitable when developing a model for a new NPP design that ‘fine-tuning’ some of the most relevant model features would be required as the design develops or new transients are analysed. The key model components for this case study are highlighted and discussed below.

RPV: The RPV consists of the downcomer, lower plenum, core, upper plenum and upper head along with cold leg and hot leg inlets/outlets. The key thermal hydraulic phenomena asso-

ciated with the vessel are the transfer of the core decay heat to the coolant, the formation of a void in the RPV head during depressurisation and the associated tracking of the liquid level. The flow path within the RPV is complex and three-dimensional so consideration needs to be given to the importance of the three-dimensional behaviour and the modelling approach chosen accordingly. For the system code part of the analysis the focus is on the overall behaviour of the primary circuit and not the detailed flow within the core or the LOCA consequences in terms of the fuel temperatures. It is therefore reasonable to simplify the geometrical representation of the RPV and the transfer of the decay heat to the coolant.

Pressuriser: The behaviour within the pressuriser is only relevant for a short period in the blowdown stage of the transient. Once it empties and voidage occurs in other parts of the system, it no longer retains the ability to regulate the primary pressure through the action of the heaters and sprays. Although the proportional and base heaters in the pressuriser were activated during the blowdown phase of Test 1-2, the impact on the overall transient progression is judged to be negligible and it is therefore not necessary to include the heaters in the model for this specific transient. The key parameters to be captured within the pressuriser model are therefore the geometry and the initial water level.

ECCS: Both the flow rate and temperature of the ECCS injection are key parameters at all stages of the transient and are particularly relevant to the PTS behaviour. The ECCS flow is delivered by a centrifugal pump, so the flow rate is dependent on the pump performance curve, the primary pressure at the injection nozzle and the injection system pressure losses. The injection temperature is primarily dependent on the temperature in the supply tank but also to a lesser extent the heat input from the pump. For a typical system code model it may be necessary to model the ECCS system in a relatively high level of detail to ensure that any interaction between the transient and the system are captured (e.g. the influence of containment heating on the supply tank temperature). However, in this case, because the injection temperature was kept constant during the test, the modelling can be simplified with a flow rate calculated from the primary pressure and the pump performance curve.

Steam Generators: The primary-to-secondary heat transfer is important during all stages of the transient. The phase separation and voidage in the upper part of the primary side of the SG tubes is typically important for determining the time at which full loop natural circulation breaks down, which is also the time at which the most onerous PTS usually occurs.

In ROSA Test 1-2 the MCPs maintain a flow in the primary loops during rundown until after voiding in the loops has started to occur. As a result, there is a very limited natural circulation phase, and the loop flow is already close to zero when the pumps stop rotating. The detailed two-phase flow behaviour in the SG tubes is therefore less important, which allows some simplification of the model. The Queral *et al.* (2014) ROSA/LSTF model originally used a single U-tube representation of the SG and was later extended to include multiple U-tube groups of different lengths. For ROSA Test 1-2 a single U-tube representation is judged to be sufficient, but this approach would likely be a limitation for more general application of the model.

Both the main steam isolation valve and the SG feedwater are isolated during the initial stage of the transient following reactor trip. After isolation the SG pressure is regulated through repeat lifting of a relief valve once the secondary pressure reaches a threshold value.

Main Coolant Pumps: The MCPs are tripped following reactor trip during the initial stage of the transient. They coast down gradually, still generating a flow within the loops until around 300 s. Correct modelling of the generated loop flow rates during this coast down period will have a significant impact on the whole plant behaviour. The pump rotational speed was recorded during the test, so this data can be used directly in combination with the pump performance curve to simplify this aspect of the model. This approach is consistent with the one taken by Munoz-Cobo *et al.* (2013).

Break model: The break flow rate is a key parameter at all stages of the transient because it is strongly coupled with the primary side pressure. The void fraction at the break is also a key parameter as the change from single-phase liquid to two-phase and then single-phase steam discharge has a strong influence on the rate of primary system depressurisation.

3.2.3 Model Development Process

Due to the large number of components and systems that need to be taken into account in a system code model, its development is a complex process which can be further broken down into a number of steps:

- Development of a baseline set of inputs for the ROSA/LSTF.
- Establishing a well converged steady-state solution, consistent with the initial conditions of ROSA Test 1-2.
- Further development of the inputs allowing the response of all of the required systems activated during the Test 1-2 transient to be captured.
- Establishing a transient solution consistent with the ROSA Test 1-2 results.
- Assessment of further SBLOCA transients using the established ROSA/LSTF model to ensure its applicability beyond the transient used for its development and testing.

This type of structured approach allows for incremental development and testing of the model, ensuring the correct functionality of each individual component at each stage before adding further complexity. This is established best practice for system code model development (Petruzzi and D'Auria, 2008, INL, 2018) due to the large number of components and physical phenomena represented by the model, as well as the complex interactions between them.

Developing an organisational system code modelling capability and a set of validated system code models for application to a new NPP design is a significant undertaking that is likely to take a number of years. The steps outlined in this case study to establish the requirements, develop an initial model and validate it against experimental data, such as that from ROSA/LSTF are a good starting point for this larger process. Knowledge and confidence gained through these initial activities would then be applied to the development of a model for the new NPP design, for which less specifically relevant experimental data is likely to be available.

3.2.4 Model Testing

This section describes the process that would be used to test and refine a system code model once the main inputs have been defined, and builds on the high level model development process described above.

Steady-State Analysis: When setting up a model to replicate a plant state, the initial conditions should represent a point in time where reactor conditions are not changing (i.e. a steady-state). System codes include the functionality to confirm whether or not the model is stable based on the boundary conditions and model set up. Typically, convergence within the model is based on a number of parameters, such as pressure, to determine whether the model is stable. The convergence criteria are defined by the user.

System codes also have the functionality to modify a boundary condition to ensure a certain plant parameter is achieved during steady-state. For the ROSA model, steady-state could be established by allowing the code to modify the pump speed to achieve the desired flow rate in the cold leg exit region, i.e. the steady-state conditions established before the LOCA was initiated in Test 1-2 (JAEA, 2008b).

Once the model satisfies the user defined convergence criteria, this provides the plant parameters and boundary conditions for the initialisation of subsequent simulations.

Null transient: Once a converged steady-state solution has been achieved, it is recommended that the user confirm that this steady plant condition can be maintained with the specific code features designed to identify and enforce that stable state switched off. The typical method used to carry out this check is to run a null transient. This is a transient simulation initialised from the established steady-state conditions with the same steady boundary conditions imposed. A satisfactory result is achieved if no significant change in plant conditions is observed from the initial conditions. A similar test can be achieved by running a transient simulation with a delay before the initiating event is applied in the model.

Transient Runs: The next step in testing the model would be definition of the time varying inputs required to model the full Test 1-2 transient. In this case, the key input is the definition of the break opening, because the remainder of the transient behaviour is driven by the corresponding variation in the primary parameters and the automatic actions of the safety systems at the defined thresholds.

It is unlikely that a transient simulation with good replication of the experimental data would be achieved on the first attempt. A number of iterations and some refinement of the model are likely to be required in order to achieve a satisfactory result, and some discrepancies will likely always remain due to the inherent limitations of the system code modelling approach.

During this refinement process it is important to maintain a focus on the required outcomes of the analysis, recalling the results of importance defined at the planning stage (Section 3.1.1). For example, in a LOCA the most onerous PTS occurs relatively early in the transient so fine tuning the model to achieve good performance in the long term phase of the transient may not be required. Similarly, the key inputs to the CFD analysis are related to the cold leg and RPV, so small deviations in the secondary side behaviour may not be significant provided they do not impact the overall transient progression.

As highlighted in Section 3.2.2, successfully performing the Test 1-2 transient with good

agreement of the main system parameters would form the first step in establishing a validated system code analysis methodology which could then be applied to a new NPP design.

In the full scope of the PTS analysis it should be expected to be necessary to simulate transients other than SBLOCA, so further validation of the model for other scenarios may be required. In each case, some refinement of the model may be necessary to address the prevalent thermal hydraulic phenomena of the particular transient. Selecting an IET facility, such as the ROSA LSTF, for these validation exercises presents a significant advantage because a large number of different transients have been performed, potentially allowing all of the required model validation to be achieved using a single system code model.

3.2.5 Extending the Model

The selection of an IET for this case study presents an opportunity in terms of model simplification which would not be available when generating a more general system code model for a new NPP design. A number of key parameters such as the pump rotational speed and ECCS injection temperature are available from the test data and can therefore be input directly into the model, avoiding the need for more sophisticated models of these components.

This approach enables the model to be tailored specifically to the requirements of the present analysis, so that it can be focused on the primary circuit with limited representation of the secondary circuit and safety systems required. Modelling of the control systems can be limited to the reactor trip based on the signal of low pressuriser pressure. All of the other control and safety system actions initiated during the transient can be linked to the reactor trip signal with an associated delay.

This provides a way to test and validate the main components of the system code model before extending it to include more detailed representation of the secondary circuit, safety and control systems. These developments to the model could then validated using test data from other ROSA transients. In each case a similar process could be followed, first highlighting the key thermal hydraulic phenomena and then defining an appropriate modelling strategy and model extent to capture them in the level of detail required for the transient.

3.2.6 Quality Assurance

Quality assurance is a key aspect of thermal hydraulic analysis for nuclear applications, and a planned approach to quality assurance is recommended in order to identify problems early and minimise the amount of re-work or the chance of introducing latent errors.

As mentioned in Section 3.2.1, user effects are one of the primary drivers for uncertainty and error in system code analysis (CSNI, 1994), so detailed documentation, a clear verification plan and self-checking are essential.

Most system code models are based on a text based input file, which means that it is easy to make certain kinds of mistake in the model setup, nodal connections and options selected within the code. Therefore, the model originator needs to:

- Clearly justify and document all decisions and assumptions that have been made for each component in the model and the connections between them.

- Ensure that the input file is well organised and comments are used throughout to highlight the components within the model and options selected.
- Use a version control process to clearly document changes and developments of the model.
- Self-check all aspects of the model setup and solution because the model originator is best placed to identify issues early.

A suitably qualified and experienced person should be selected to lead the model verification, who is sufficiently independent from the originator. The verification process should check all aspects of the model, including:

- Overall approach and key modelling assumptions.
- Geometry, nodalisation and connections within the system code model.
- Individual component boundary conditions, correlations and options that have been used, as well as the justification for them.
- Initial and transient boundary conditions for the system and the control systems that have been implemented.
- That appropriate sensitivity studies have been undertaken to demonstrate that the nodalisation, time step, etc. are appropriate.
- The convergence of the solution, whether the results are physically reasonable and if they show the expected flow phenomena and trends.

4 CFD Analysis

The 3D nature of the flow field local to the region of ECCS injection and its subsequent mixing and propagation downstream lends itself to analysis using CFD techniques.

This CFD analysis is focused on the initial methodology development, validation of the local thermal stratification and plume behaviour during ECCS injection and the subsequent prediction of reactor structural component temperatures. It is intended to provide a practical example of an appropriate approach to planning and executing a CFD analysis of PTS.

4.1 Problem Definition

The aim of the CFD analysis is to undertake the validation step of the PTS analysis sequence (Figure 1.2). This has been achieved by simulating the cold ECCS injection into CL-A for Test 1-1 of the OECD/NEA ROSA project (Section 2.3.2), and comparing the flow and temperature predictions against the measured test data.

In addition, the heat transfer from the coolant to, and within, the solid components of the CL-A and PV is included to predict the solid temperatures, which would be used in a structural integrity assessment to analyse the impact of PTS.

The overall objective of the analysis sequence is to undertake an assessment of the risk of PTS for a new NPP design, and this will involve multiple long transient simulations. A Reynolds-Averaged Navier-Stokes (RANS) turbulence modelling approach (as described in Volume 3, Section 3.2) has been selected, as the preferred modelling option a Large Eddy Simulation (LES) method is considered too computationally expensive. Therefore, a key aspect of this validation exercise is to assess whether a RANS turbulence modelling approach is appropriate.

4.1.1 Important Thermal Hydraulic Phenomena

A schematic representation of the ECCS injection is shown in Figure 1.1, which shows the expected buoyant flow pattern due to the difference in fluid density between the cold ECCS injection flow and hot primary CL-A flow.

Since system codes are 1D they are unable to resolve the spatial variation (temperature and velocity) in the cold leg. This is because system codes use bulk flow properties (i.e. a single value across each pipe), and the temperature downstream of the injection is calculated using the mass weighted average of the two flows with no dependence on the local velocity gradients and geometry.

The most significant thermal hydraulic phenomena associated with this flow structure are:

- A jet in crossflow.

- A negatively buoyant plume at the site of the ECCS injection and in the downcomer.
- Thermal stratification and mixing downstream in the cold leg and downcomer.

A clear comparison can be drawn against some of the buoyancy affected flow phenomena described in Volume 3 (Section 2.1). Of particular interest is the prediction of the thermal stratification in the cold leg and the size of the cold plume in the downcomer, which drives the heat transfer to the walls, thermal gradient through the solid and subsequent PTS.

4.1.2 Results of Importance

The main output from the CFD analysis is the temperature variation through the cold leg and PV components over the course of the transient. The transient solid temperature variation would then be used as an input to the structural integrity assessment.

Although some wall temperature measurements are available in the LSTF, the level of confidence in the solid temperature predictions will be enhanced by demonstrating that the following flow behaviour are appropriately captured in the model:

- The heat transfer from the solid to the fluid due to the thermal stratification in the pipe and subsequent transient variation in the metal temperature.
- The level of mixing in CL-A as a function of time and distance from the ECCS injection location.
- The size and shape of the cold ECCS plume as it travels along CL-A and then down the downcomer annulus.

4.2 Planning the Analysis

4.2.1 Existing Work

PTS is a key reactor safety issue that has been investigated extensively (e.g. Scheuerer and Weis, 2012, Tunstall *et al.*, 2016b and Cremer *et al.*, 2019), and was the subject of the most recent Committee on the Safety of Nuclear Installations (CSNI) CFD benchmark with uncertainty quantification on cold leg mixing (Orea *et al.*, 2020). This provided detailed validation data for the mixing at the interface of a buoyancy driven, stratified flow; at the time of writing, the final report has not been released by the CSNI.

Thermal fatigue in T-junctions is also relevant to ECCS injection, and has received significant interest (e.g. Tunstall *et al.*, 2016b) following the incident at the Civaux-1 plant in France in 1998. In particular, the CSNI Vattenfall T-Junction benchmark (CSNI, 2011b) investigated the ability of CFD to predict the mixing in a T-junction and amplitude and frequency of the thermal fluctuations. This showed that the k-ω Shear Stress Transport (SST) turbulence model outperformed other RANS approaches, but also highlighted the superiority of LES methods over RANS models. Other studies have shown the advantages of using Reynolds Stress Models (RSMs) in T-junctions (e.g. Tunstall *et al.*, 2016a).

The availability of detailed geometry and test data for ROSA Test 1-1 means that many of the concerns when planning a CFD analysis (e.g. definition of inlet boundary conditions and quality of

measurement data for validation) are reduced. In addition, a number of CFD analyses of this test case have been published previously:

- Farkas and Tóth (2010) conducted a CFD analysis of Test 1-1 using ANSYS Fluent without the solid components included. The results showed that an RSM performed better than the standard k-ε and realizable k-ε turbulence models. The results demonstrated that the temperature distribution in the downcomer is strongly influenced by the geometry of the cold leg-downcomer junction.
- A later study by Scheuerer and Weis (2012) using ANSYS CFX, included the cold leg-downcomer junction radius and full length and circumference of the downcomer without the solid components. The temperature stratification was well predicted along the cold leg and in the downcomer. This demonstrated that the k-ω SST turbulence model predicted similar results to the BSL RSM model at reduced computational expense.
- A smaller study by Lee (2018) finds similar levels of agreement using ANSYS CFX with the BSL RSM turbulence model. Here again, the measured inlet conditions are applied to a fluid domain with adiabatic walls.

Overall, the previous work demonstrated that the BSL RSM and k-ω SST turbulence models both provided similar levels of agreement to the test data. The presence of the 19 mm radius fillet at the cold leg-downcomer junction, which is not clearly defined in the ROSA LSTF drawings, was shown to have a significant influence on whether the cold plume flows down the inner surface of the PV or outer surface of the core barrel. This highlights the importance of small geometrical details in CFD models, such as fillets, which can often be ignored or simplified.

The main difference between the previous work and the current case study is that the previous studies were focused on the fluid dynamic mixing and did not include the solid components. The prediction of thermal gradients and transient temperatures within the solid components is a key part of this validation exercise.

4.2.2 Extent of Domain

The results of interest identified in Section 4.1.2 occur in the region downstream of the ECCS injection location and predominantly before the flow turns the corner into the downcomer, with some important phenomena extending down into the downcomer itself.

The guidance in Volume 1 (Section 4.5.2) has been applied to determine the extent of the computational domain (Figure 4.1) as follows:

Inlet boundary: Figure 2.6 shows that after flowing through the pumps, the flow in CL-A travels through a length of pipework and a bend before reaching the ECCS injection nozzle. The pipe flow development, and the influence of the bend, could impact the flow structure at the point of injection. Therefore, the inlet boundary for CL-A has been extended six duct diameters (6D) upstream of the bend to allow the pipe flow to develop and interact at the bend. The same is true for the ECCS injection pipework, which has been extended 14D upstream to allow the ECCS flow to develop.

Outlet boundary: As one aim of the analysis is to predict the temperature distribution in the CL-A and RPV structure, and previous published work (Section 4.2.1) shows that the cold plume

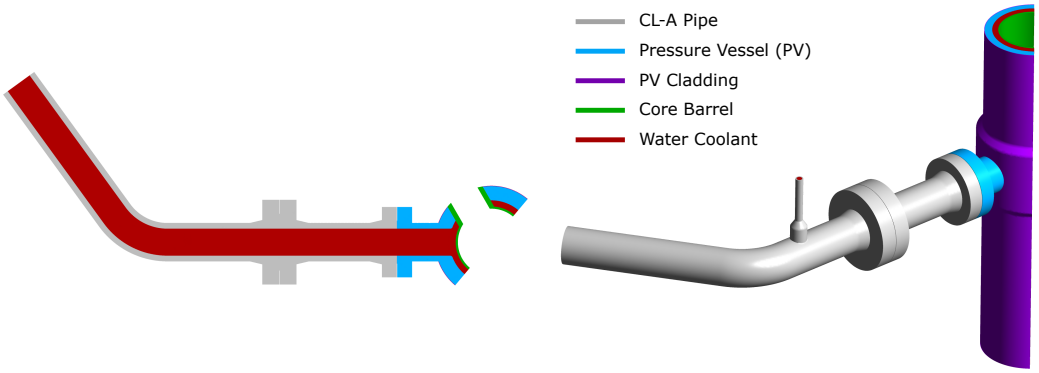

Figure 4.1: Extent of computational domain: Plan view (left), isometric view (right).

continues some way into the downcomer, the downcomer outlets have been extended vertically up and down from the cold leg-downcomer centreline by 1.12 m and 1.65 m respectively (compared to downcomer width of 0.046 m and D_h = 0.092 m). Although this does not represent the full height of the downcomer, it is expected to be far enough that the CL-A and downcomer flow profile are not affected.

Downcomer circumferential extent: Figure 2.6 shows that the layout of the RPV with regard to the hot and cold legs of Loop A and B is rotationally symmetrical. Volume 1 (Section 4.5.2) highlights the fact that where a geometry is periodic, care should be taken to ensure that the flow structure is also periodic. The flow through Cold Leg of Loop B (CL-B) is equivalent to CL-A, but without the ECCS injection. Therefore, the CL-B downcomer flow profile is likely to be similar to CL-A, without any temperature variation. Although the flow in the downcomer is not truly periodic, the benefit gained by reducing the extent of the domain (half model size) is considered to outweigh the effect on solution accuracy as the ratio of ECCS to CL-A flow rates is small. Therefore, half of the PV downcomer has been modelled with rotational periodicity and the boundary located midway between the hot and cold legs.

Hot leg: The flow exits the upper plenum through the hot leg, which passes through the downcomer annulus at the same height as the cold leg. This blockage in the downcomer annulus close to the cold leg entrance could impact the flow and should be included in the model. The hot leg junction is assembled using a bellows and sleeve arrangement, but this detailed geometry is not considered important to the CL-A flow.

Because the key purpose of this case study is to predict the transient variation of the solid component temperatures, it is important to include all corresponding solid geometry adjacent to the CFD domain (e.g. CL-A pipework flanges, PV, cladding and core barrel).

Thermal insulation is used to reduce the heat loss from the PV, primary and secondary circuit components. The effectiveness of the insulation and temperature drop through the CL-A pipe will determine the impact on the pipe temperatures and whether it should be explicitly included in the model. The thermal gradient through the CL-A pipework can be calculated by summing the thermal resistances of each heat transfer component, as detailed in Volume 2 (Section 2.1.2.4).

$$\frac{1}{h_{eff,os}} = R_{th,os}A_{os} = \frac{r_{os}}{r_{is}h_{water}} + \frac{r_{os}\ln(r_{os}/r_{is})}{k_{steel}} + \frac{r_{os}\ln(r_{oi}/r_{os})}{k_{ins}} + \frac{r_{os}}{r_{oi}h_{air}}$$

Where r_{is}, r_{os} and r_{oi} are the radii of the steel inner surface, steel outer surface and insulation outer surface respectively. Based on an air temperature of 306 K and 125 mm of Rockwool insulation with a natural convection Heat Transfer Coefficient (HTC) to the air of about 5 $W/m^2 K$, this gives an effective HTC of 0.6 $W/m^2 K$ that is dominated by the insulation with a heat flux of 149 W/m^2 ($q = h_{eff,os}(T_{water} - T_{air})$). The calculated temperature on the steel outer surface is 553.4 K and the temperature difference across the steel pipe is 0.4 K, which can be compared against the measured values.

Due to the large thermal mass (mc_p) of the solid steel, the temperature of the steel outer surface is not expected to change significantly and will be dominated by the thermal resistance through the insulation. Therefore, it is not considered necessary to include the 125 mm of insulation in the mesh, especially as the detailed geometry of the insulation is not known. The insulation will, therefore, be represented in the model by an effective external HTC and ambient air temperature applied to the outside.

4.2.3 Flow Characterisation

Before starting to develop the CFD model, it is useful to assess the flow and characterise the thermal hydraulic phenomena identified in Section 4.1.1. The measured CL-A and ECCS flow rates and temperatures vary during Test 1-1 as the ECCS injection is initiated and take around 50 s to develop into a relatively constant ECCS injection flow (Figure 4.2).

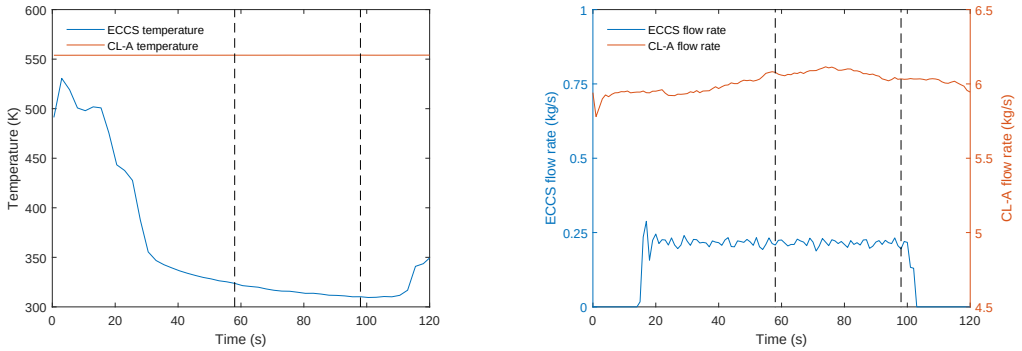

Figure 4.2: Measured temperatures and flow rates for Test 1-1 (JAEA, 2008a).

Therefore, the main flow parameters (discussed in Volumes 2 and 3) have been calculated (Table 4.1) by averaging the measured values between 58 s and 98 s. The HTC at the wall has been estimated using the Dittus-Boelter equation for turbulent flow ($Nu_D = 0.023 Re_D^{4/5} Pr^n$, where n = 0.4 for the fluid being heated). The Biot number, Bi, has been calculated based on the full thickness of the wall as the heat transfer is just on the inner surface.

This demonstrates that the flow is fully turbulent within the cold leg and ECCS injection pipe, so the heat transfer to the solid will be primarily by forced convection. The high Biot number in the CL-A and downcomer solid components means that convection heat transfer is expected to be substantial compared to conduction, and so a thermal gradient is expected through the wall thickness as the solid is cooled over the Test 1-1 transient. The thin wall of the ECCS injection pipe means that the solid temperature is effectively uniform.

Test 1-1 (58 s to 98 s average)	ECCS	CL-A	Downcomer
Mass flow rate (kg/s)	0.215	6.07	6.29
Temperature (K)	315.4	554.0	547.2
Velocity (m/s)	0.182	0.237	0.190
Density (kg/m^3)	998	760	774
Hydraulic diameter (m)	0.0387	0.207	0.092
Reynolds number, *Re*	11×10^3	389×10^3	136×10^3
Surface HTC ($W/m^2\,K$)	1,200	1,800	1,800
Biot number, *Bi*	0.7	4.6	6.3

Table 4.1: Flow characteristics and non-dimensional parameters for Test 1-1.

The Atwood number $((\rho_1 - \rho_2)/(\rho_1 + \rho_2)$ = 0.13 for the ECCS and CL-A flows. This is useful in characterising the stability of stratified flows and comparing between different injection temperatures and fluids (Orea *et al.*, 2020).

The ECCS injection is perpendicular to the CL-A flow, and so represents a jet in crossflow (Zhang and Yang, 2017), where the downstream jet structure is characterised by a pair of counter-rotating vortices due to the interaction of the crossflow with the jet shear layer. Hosseini *et al.* (2008) categorised the behaviour of a turbulent jet in a T-junction area based on the momentum ratio (M_R) into four types: wall jet, re-attached jet, turning jet, and impinging jet.

$$M_R = \frac{\rho_m U_m^2 \, (D_m \times D_b)}{\rho_b U_b^2 \, \pi \, (D_b/2)^2}$$

The subscript m relates to the main pipe (CL-A) and b relates to the branch pipe (ECCS). In this case, M_R = 8.7, which represents a wall jet (i.e. $M_R > 4$), characterised by a higher main flow and lower branch flow. A wall jet is not expected to separate from the main pipe wall with local velocity and temperature fluctuations.

If the jet momentum is neglected, there are two forces on the cold ECCS fluid; a vertical buoyancy force (F_b) due to the difference in density compared to the hot CL-A fluid and a horizontal force (F_d) due to the main CL-A pipe flow, which is equivalent to a drag force on the ECCS fluid. The ratio of these forces (on a small vertical section, dz, of a cylinder of diameter D_b) has been used to estimate the relative significance of the buoyancy effects on the cold ECCS flow[1].

$$\frac{F_b}{F_d} = \frac{g(\rho_b - \rho_m)(\pi D_b^2/4)dz}{0.5 C_d \rho_m U_m^2 D_b dz} = \frac{g(\rho_b - \rho_m)}{\rho_m} \frac{\pi}{2} \frac{D_b}{U_m^2} = 3.3$$

This assumes that $C_d \approx 1$, which is approximately true for flow around a cylinder. Therefore, the ECCS injection flow is expected to turn quickly on entering the CL-A and stay close to the top wall until the effect of buoyancy forces cause the cool ECCS fluid to drop to the bottom of the CL-A pipe where it becomes a cold stratified layer. As it travels along the CL-A it will gradually mix with the hot CL-A fluid and then flow into the downcomer.

[1] This expression has the form of an inverse densimetric (or internal) Froude number squared, since $Fr = U/\sqrt{g'D}$, where $g' = g(\rho_b - \rho_m)/\rho_m$, known as reduced gravity (Turner, 1973).

4.2.4 Modelling Tool Selection

Volume 1 (Section 4.5.4) gives an overview of some CFD codes that have been used for Nuclear Thermal Hydraulics (NTH) analyses and could be used for this case study. All of these codes have been successfully validated for a range of use cases and offer the required physical models (CHT, steady/unsteady solvers, turbulence models, etc.). The selection of a particular CFD code for a NTH analysis will depend on a number of factors, such as:

- Is there evidence that the tool has been validated for this particular application?
- Does the tool have a particular physical model or option that provides a significant benefit to the analysis?
- Does the modelling engineer have experience using the tool?
- Does the code meet the required quality assurance criteria for the specific application in the context of a graded approach (e.g. ASME NQA-1)?

ANSYS CFX has been chosen for this case study primarily because the modelling engineer is familiar with CFX, has access to a license (this being a preferred tool of their organisation), and there is existing available evidence that it is able to successfully model this type of flow.

In addition, the development of CFX satisfies ASME NQA-1, and the IAPWS-IF97 model (Wagner *et al.*, 2000) for water/steam is implemented in the code as standard. This is important as the accurate prediction of buoyancy driven behaviour is driven by the significant variation of density with temperature.

The ANSYS DesignModeler package has been selected for geometry creation and ICEM HEXA for mesh generation, as they are part of the ANSYS toolset and so enable an efficient workflow.

4.2.5 Modelling Strategy

This section discusses the selection and justification for the mesh generation strategy and the physical and numerical modelling approach.

4.2.5.1 Mesh Generation

Guidance on mesh generation considerations are given in Volume 1 (Section 4.5.2). The first task is to select the type of mesh that should be used in each region of the domain (i.e. structured hexahedral, unstructured tetrahedral/hexahedral/polyhedral, near-wall prismatic or hybrid mesh). It is worth noting that CFX is currently limited to hexahedral, tetrahedral, pyramids and prisms, and does not allow polyhedrals.

For the fluid domain, the following benefits of a structured hexahedral mesh outweigh the potential time saving of an unstructured mesh type in this case:

- Since Test 1-1 is a transient test case, the computational cost of the solution is likely to be significant. Therefore, it is beneficial to minimise the cell count and control the local cell size (to reduce time step limitations) to reduce the solution time. Structured grids aligned with the flow can provide higher quality solutions (reduced numerical diffusion) with fewer cells than unstructured grids.

- The geometry of the computational domain is relatively simple and made up of pipes, intersections and annuli. There are recognised suitable approaches for structured multi-block meshes for these configurations of geometry.
- The important thermal hydraulic phenomena are generally aligned with the geometry. However, at the ECCS injection location two orthogonal flow directions meet, which may lead to flow across high aspect ratio cells, if this is not meshed appropriately.
- It is important to ensure that the buoyancy driven mixing is properly resolved, and numerical diffusion is minimised in this region. This is likely to be well captured by a structured mesh, and should be checked with a mesh sensitivity study.

For the solid domain, a different set of considerations is necessary:

- The solid geometry is more complicated than the fluid domain as flanges and thin walled structures (insulation, heat shields and core barrel) may cause difficulties generating a structured mesh.
- Guidance for CHT analysis in Volume 2 (Section 3.4.2) suggests that an inflation layer mesh with a small first cell height next to the fluid-solid interface is required to capture the temperature variation in the solid due to fluctuating fluid temperatures.
- Software specific advice regarding solid-fluid interfaces should be followed for mesh generation. In the case of CFX (ANSYS, 2020), a general grid interface can be used for the fluid-solid interface meaning there is no requirement for a conformal mesh.

Therefore, an unstructured tetrahedral mesh will be generated for the solid domain with an inflation layer grown from the inner solid surface. This simplifies the meshing approach, while enabling the time-varying thermal gradient at the inner solid surface to be appropriately resolved. Although a non-conformal fluid-solid interface will be used, it is important that the fluid-facing surface of the solid mesh is appropriately resolved to allow heat transfer to be interpolated correctly at the interface.

A number of methods for deciding appropriate mesh resolution of flow features and boundary layers are available, which are discussed in Section 4.3.2. In addition, a mesh sensitivity study has been undertaken (Section 4.4.2) as recommended in Volume 1 (Section 4.5.2).

4.2.5.2 Physical and Numerical Models

The physical and numerical models that are required for the CFD solution are based on the thermal hydraulic phenomena that have been identified and characterised.

Energy: To predict the thermal mixing in CL-A and the heat transfer to the pipework, it is necessary to solve the energy equation. The total energy equation option in CFX, which includes both mechanical and thermal energy, is required when the IAPWS-IF97 material properties are used.

Buoyancy: The mixing of the cold ECCS injection and formation of thermal stratification in CL-A are driven by buoyancy effects. Therefore, the full buoyancy model (rather than the Boussinesq approximation) has been selected in CFX with gravity applied in the vertical direction. This uses a source term derived from the difference in local fluid density to reference density, which is added to the momentum equation.

Conjugate heat transfer: CHT is enabled for the interfaces between the fluid and solid domains. This is necessary to ensure heat transfer across the interface and predict the thermal gradients in the solid domains.

Turbulence: As discussed in Section 4.1, although LES is likely to offer advantages for this type of flow (Section 4.2.1), a RANS modelling approach has been selected for this case study. Since the overall objective of the analysis sequence is to undertake an assessment of the risk of PTS for a new NPP design, this will involve multiple long transient simulations, which are currently considered impractical using LES.

Benchmarking and existing analyses have found that the k-ω SST turbulence model provides reasonable results for the expected phenomena, and therefore it was selected as the first choice. This is consistent with the need to resolve the viscous sublayer (Volume 2, Section 3.4.2.5) using a wall resolving 'low-Re' method (ideally $y^+ \approx 1$) in order to predict the surface heat transfer. However, the sensitivity of the solution to a range of RANS turbulence models has also been assessed as part of this case study (Section 4.4.3).

Steady or Unsteady: Since the ECCS injection varies with time, the results will have large-scale unsteady motion caused by this externally varying boundary condition, and as such, an unsteady (transient) approach must be taken. In addition, jets in crossflow are inherently unsteady and would be expected to fluctuate even under steady boundary conditions.

Spatial discretisation: A high order scheme (Volume 3, Section 3.2.4) is required in this case to minimise numerical diffusion, as the mixing of the hot and cold flows relative to the CL-A pipework is important in determining the effect of PTS. Therefore, the high resolution scheme in CFX (ANSYS, 2020) has been chosen for this analysis.

Temporal discretisation: A high order scheme is required for mixing transport because a first-order scheme may smooth out or suppress some of the motion. Therefore, the second-order backward Euler scheme in CFX has been selected.

4.2.6 Solution Strategy

Once the modelling approach has been defined, it is worthwhile planning the approach used to solve the model and case selection in order to maximise the benefit from each solution.

Before undertaking the full Test 1-1 transient simulation, it is necessary to assess and confirm the suitability of the mesh and turbulence model that has been selected. This can be best achieved by:

- Solving an initial steady-state solution with constant ECCS injection flow rate.
- Switching simulation to be transient and solving for a short period of time until a statistically averageable state is reached, ideally twice the length of time it takes a fluid particle to pass through the domain assuming that it is travelling at the bulk flow velocity.
- Starting to sample the data to compute mean and Root Mean Square (RMS) values for the flow and temperature fields, and solving until the time-averaged temperatures have converged.

This approach enables time-averaged data to be generated and compared between cases, and the simulations to be solved at a significantly lower computational expense than running the full Test 1-1 transient. Since the flow conditions are nominally constant during the test, the fluid thermocouple

temperatures can be averaged over the last 40 s, as they are unlikely to be significantly affected by the slow variation in metal temperature. The following cases should be run in order to finalise the modelling approach:

- A baseline case to confirm that the thermal hydraulic phenomena are captured and the mesh is refined in the appropriate places. This provides an initial comparison and assessment against the averaged thermocouple measurements.
- The mesh sensitivity study can then be completed by solving a coarse and refined mesh. The differences between the meshes can then be quantified using the time-averaged values at the thermocouple locations.
- Finally, the turbulence model sensitivity can be performed. The time-averaged results can then be compared against the averaged thermocouple measurements to assess which turbulence model is most appropriate in this case.

This solution approach enables the impact of the mesh and turbulence model on the temperature predictions to be assessed and confirm that it is appropriate. The final solution of the Test 1-1 transient can then be solved by first running a steady-state solution with no ECCS flow, and then applying the measured time-varying flow rate and temperature profiles to the CL-A and ECCS inlets over the 120 s transient.

Monitors should be included at all of the thermocouple locations (Section 2.3.2), particularly the wall temperature locations (Planes 080, 054, 051 and 045), in order to predict the time-varying temperatures in the fluid and solid over the course of the transient.

4.2.7 Quality Assurance

A planned approach to quality assurance is recommended by Volume 1 (Section 4.5.1) in order to identify problems early and minimise the amount of re-work. An overview of the quality assurance plan for this case study is given below:

- A suitably qualified and experienced person was selected to lead the verification of the case study, independent from the originator.
- Details of the geometry from ROSA-V Group (2003) were passed with a 3D Computer Aided Design (CAD) file to the verifier to perform spot checks on the geometry (e.g. CL-A and ECCS pipe radii and lengths, bend details, flanges, radii of the PV, clad and core barrel and locations of thermocouple measurements).
- The verifier checked the generation of the mesh for calculated sizing and quality and that it was refined sufficiently to resolve the expected flow features.
- The settings for the physical and numerical models were checked to make sure they were correctly applied in accordance with the analysis software recommendations and best practice (Volumes 1, 2 and 3).
- When results were available, the verifier checked the convergence and an overview of the solution behaviour to confirm that the expected flow phenomena were adequately modelled and resolved.

4.3 Performing the Analysis

4.3.1 Geometry Creation

In Section 4.2.2 the extent of the analysis domain was planned, taking into account recommendations for extending the inlet and outlet boundaries away from the region of interest, and using a rotational periodic boundary condition to reduce the computational expense.

The first task when performing the analysis was to generate a CAD geometry suitable for the CFD model. The system description document (ROSA-V Group, 2003) provides detailed drawings which were used to create the geometry using the ANSYS DesignModeler package. The full geometry comprises the fluid domain and four separate solid bodies, which are colour coded in Figure 4.3; PV and first flange, CL-A and ECCS pipework, core barrel and 3 mm PV cladding.

The overall CAD model is shown in Figure 4.1, while details of the ECCS injection nozzle and cold leg-downcomer junction are shown in Figure 4.3. This shows the detailed geometry of the ECCS injection nozzle with thermal sleeve (the thin walled tube extending into the expanded area at the ECCS injection location) that has been included in the model (Figure 2-3 of JAEA, 2008a). The thermal sleeve is designed to reduce the thermal fatigue at the ECCS nozzle, and was included in the model because it could affect the cold ECCS jet development and subsequent mixing.

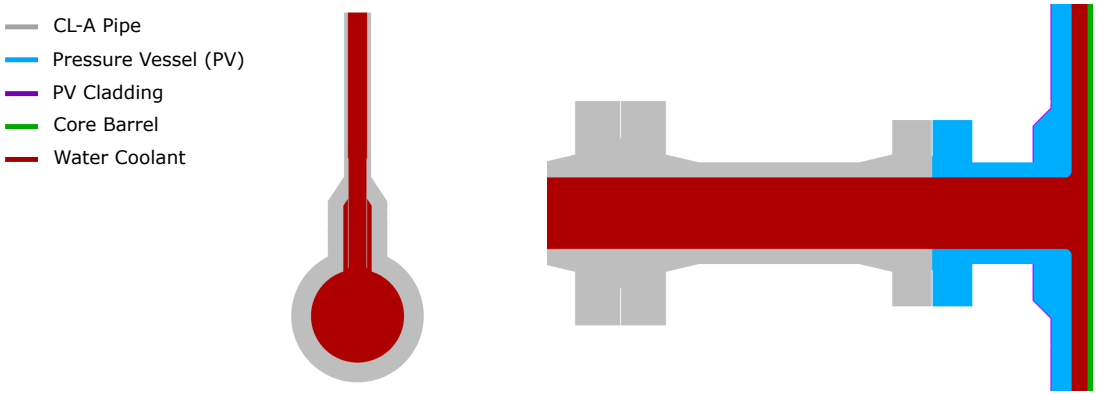

a: ECCS injection nozzle b: Cold leg-downcomer junction

Figure 4.3: CAD geometry of CFD model.

In addition, the 19 mm radius fillet at the cold leg-downcomer junction (Farkas and Tóth, 2010) has been included, as previous work (Section 4.2.1) has shown that this has an important effect on the downcomer flow profile. The following simplifications have been made to the geometry to remove unnecessary detail from the model and reduce the mesh size:

- The thermocouple wiring and support structure (Figures 2-16 and Fig 2-17 of JAEA, 2008a) has been neglected. This represents a reasonable blockage to any circumferential flow in the bottom of the CL-A pipe and the narrow downcomer annulus. Assessing the effect of excluding this geometry is one of the follow-on tasks recommended once the results have been reviewed at the end of the analysis.
- The ECCS injection nozzle that enters the downcomer at an elevation of 4.27 m has been neglected, as it is below the lowest thermocouple location.

- The check valve simulation nozzle that enters the downcomer at an elevation of 6.087 m has been neglected, as it is above the cold leg injection.
- The bellows arrangement at the hot leg penetration has been removed. This prevents any leakage from the downcomer into the hot leg. The amount of flow leakage is unknown, but the impact on the cold leg flow is expected to be negligible.
- The 5.5 mm fluid gap between the core barrel and core barrel cover has been neglected and is assumed to be solid, as the temperatures on the inside surface of the downcomer are not of interest in this case study.

Particular attention is given to the interfaces between each domain, as it is important that the CAD representation on either side of a CHT boundary is identical, otherwise the interpolation can introduce numerical error. Every face of each body is also assigned an appropriate tag (Named Selections in ANSYS), for easy identification and application of mesh and CFD controls.

4.3.2 Mesh Generation

Care must be taken to adequately resolve key flow and geometric features, and Volume 1 (Section 4.5.2) provides further detail on the importance of mesh generation. Poor mesh quality is a common source of solution stability problems, and deficiencies in accuracy in CFD simulations, so this section details the method used to generate the mesh step-by-step.

4.3.2.1 Fluid Domain

A structured hexahedral meshing approach has been selected for the fluid domain (Section 4.2.5.1), which is more 'labour intensive' to create than an unstructured mesh, but ensures that the flow is aligned with the mesh and can significantly reduce the number of cells required. This involves decomposing the domain into a number of structured regions or 'blocks', into which a structured mesh can be transformed, and can be done using a 'top-down' or 'bottom-up' approach.

High Level Blocking: For this case study, a 'top-down' blocking approach was used, and the entire domain was initially contained within a single bounding box. The bounding box was then split across the three orthogonal planes to subdivide it into more blocks to represent the CL-A and downcomer (Figure 4.4a). The superfluous blocks resulting from the initial splits were then deleted, leaving only the blocks that represent the CL-A and downcomer (Figure 4.4b).

The block and underlying CAD geometry are separate from each other at this stage, and so an association process was required to match the blocks to the geometry, based on vertices, edges and faces. The faces of the blocks were projected onto the geometry and used to define the transformation of the structured mesh. Associating the blocks with the geometry at this stage helped with subsequent meshing steps as the blocks were located and orientated correctly, which simplified the additional splits needed to control the projection in regions of high curvature (Figure 4.4c).

ECCS Injection Region: The high level blocking shown in Figure 4.4c does not have any blocks for the ECCS injection nozzle. Blocking must be created so that the orthogonal flow in the small bore injection pipe is combined with the CL-A pipe in a structured manner.

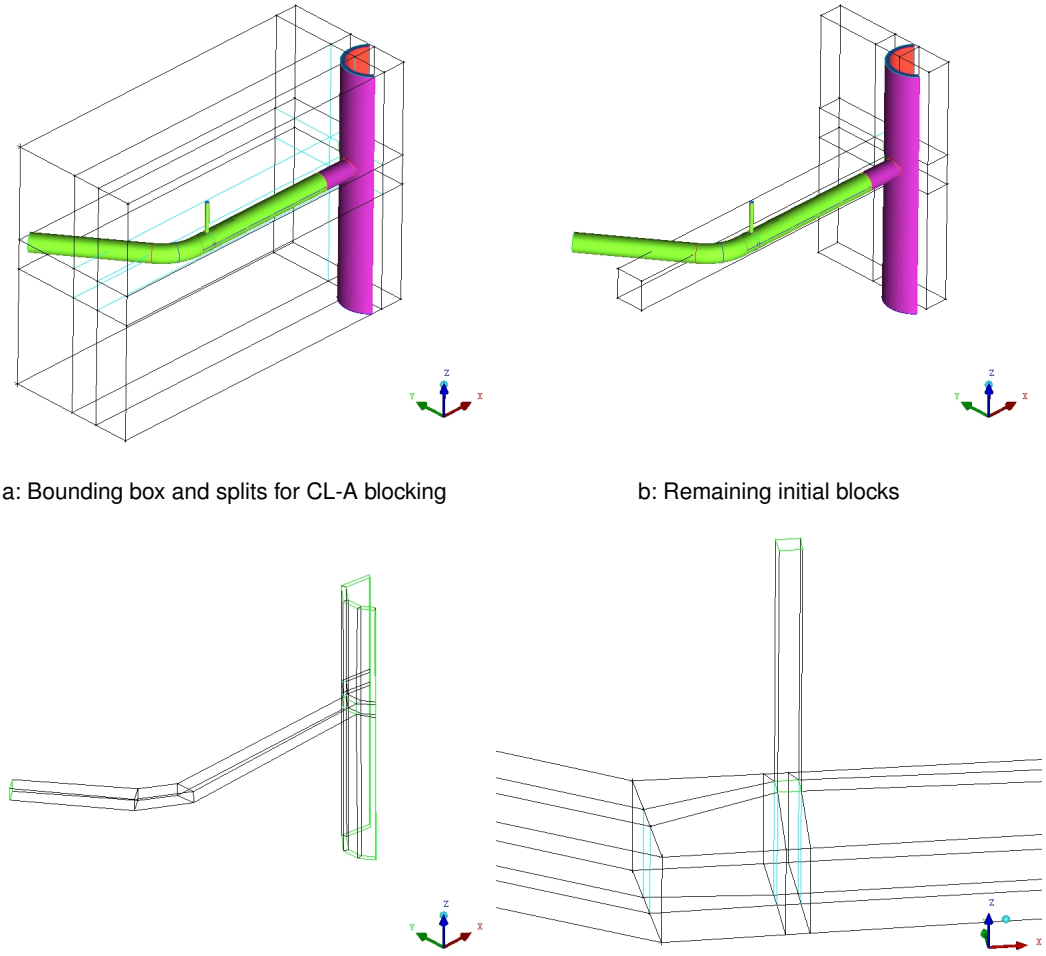

a: Bounding box and splits for CL-A blocking

b: Remaining initial blocks

c: Associated blocking with additional splits

d: ECCS injection blocking with extrusion

Figure 4.4: Blocking approach for fluid domain.

Splits were added in the XZ and XY planes to isolate the ECCS injection pipe, which could then be associated to the geometry. The face of the block at which the pipe enters was now extruded up to create the block for the ECCS injection pipe (Figure 4.4d). Further splits to the blocking structure around the ECCS inlet were then needed in order to resolve the thermal sleeve geometry.

O-Grids: With the blocking mostly complete for the CL-A and ECCS pipework, the analyst must now think ahead to the required mesh structure because some blocking features are required at this stage to ensure good quality.

If a single block face is projected to a circle, the resulting mesh transformation generates highly skewed cells at the corner of each block, and a continuous boundary layer mesh is not possible. Therefore, an ‘O-grid’ blocking sub-structure was used to reduce the skewness and generate a good quality boundary layer mesh. ‘O-grids’ were applied to both the CL-A and ECCS pipework

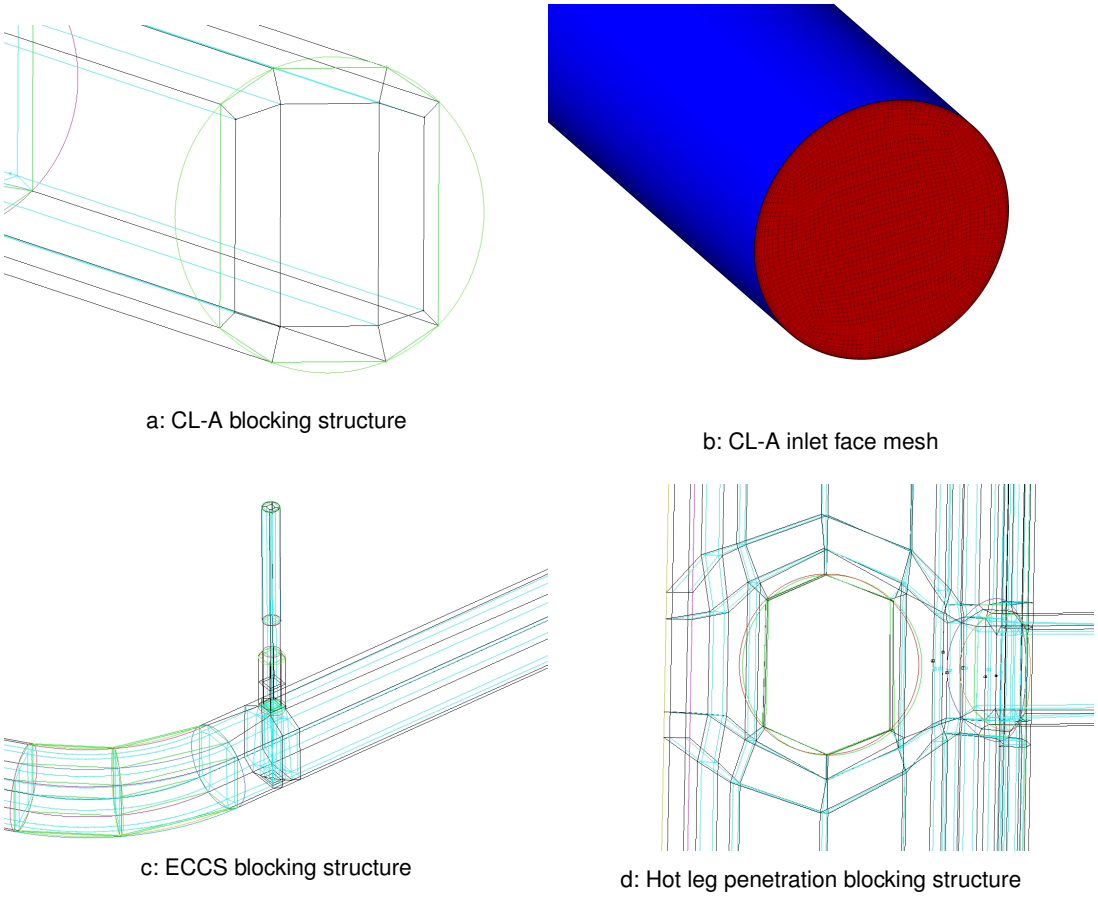

a: CL-A blocking structure

b: CL-A inlet face mesh

c: ECCS blocking structure

d: Hot leg penetration blocking structure

Figure 4.5: 'O-Grid' blocking and mesh.

to achieve the desired mesh resolution and quality. The resulting blocking structure and mesh is shown in Figure 4.5.

An 'O-grid' was also applied around the hot leg penetration. Whereas previously the 'O-grid' was used to mesh inside a circular domain, in the case of the hot leg penetration it was used to mesh around one by removing the central block (Figure 4.5d). 'O-grids' are a common and adaptable technique for structured meshing of irregularly shaped internal and external flows. Their use is much wider than presented in this case study, which demonstrates only simple examples.

A similar 'O-grid' blocking structure was applied to the cold leg-downcomer junction with the corner of the block at the top of the 'O-grid' attached to the mid-point of the 19 mm radius fillet. This created a good quality, regular, flow aligned mesh at this junction. However, the resulting blocking structure is difficult to view and so can be best visualised in the final mesh (Section 4.3.2.4).

4.3.2.2 Fluid Domain Mesh

Once the blocking structure is complete and capable of providing high quality cells for all expected flow phenomena, the process of meshing can take place. During this stage, small iterative changes were made to the blocking and sizing functions, with the aim of increasing the resolution of the captured flow phenomena to the required level.

Boundary Layer Refinement: Volume 2 (Section 3.4.2) provides information on the appropriate methodology to generate a boundary layer mesh. It recommends that the boundary layer mesh should accommodate the full thickness of the boundary layer with at least 10 to 20 cells across its thickness. A key aspect of this is the choice of First Cell Height (FCH), which was estimated to achieve a target y^+ of 1.

As the flow in this case study is internal pipe flow, the friction factor (f) was used to estimate the local skin friction coefficient (C_f'). Assuming a surface roughness of 0.01 mm and using the Swamee-Jain equation for turbulent flow (Volume 2, Section 3.4.2.5), the calculated FCHs are listed in Table 4.2 with the other boundary layer mesh parameters.

Location	Friction factor	FCH (mm)	Growth rate	Number of layers
CL-A	0.015	0.0125	1.8	10
ECCS	0.031	0.058	1.3	10
Downcomer	0.018	0.014	1.6	10

Table 4.2: Boundary layer mesh parameters.

Radial and Circumferential Refinement: Due to the use of an 'O-grid' blocking structure, the radial and circumferential refinement are closely linked. There are three phenomena that need to be resolved in the CL-A pipe:

- The pipe flow velocity profile.
- The shear layer and turning associated with the ECCS jet.
- The stratification layer.

The velocity profile for turbulent flow in a pipe is well understood, and is effectively resolved using a good quality boundary layer mesh, as discussed above. The number of cells required to resolve the shear layer and thermal stratification is less straightforward, and so a mesh sensitivity study is required to demonstrate that the solution is independent of the mesh density.

The baseline mesh comprises 76 cells around the circumference of the ECCS pipe and 160 cells around the CL-A pipe. Circumferential refinement was also required around the downcomer, however as the radius is significantly larger than CL-A more cells were required in order to keep the expansion ratio reasonable. In total 148 cells are used around the circumference of the downcomer, which are concentrated around CL-A and the hot leg penetration, with fewer towards the periodic boundary conditions. There are 50 cells across the downcomer annulus. Around the hot leg penetration, 140 cells are used circumferentially. This provided sufficiently detailed resolution of the geometry, and maintained cell quality.

Axial Refinement: There is a trade-off required in choosing an axial refinement between computational cost and mesh quality. Where the flow is aligned with the axial direction of the pipe, higher aspect ratio cells (with the long axis in the axial direction) are acceptable and will provide a reduction in computational expense. Although this comes at the potential cost of missing smaller features in the flow.

At the ECCS injection and cold leg-downcomer junction the flow direction is not necessarily aligned with the axial direction of the pipework, and so the level of axial refinement needs to be increased

to achieve a reasonable aspect ratio. Therefore, the mesh was refined in these regions and the cell size grows when moving away from them in the axial direction.

To generate the mesh, periodic constraints were applied to the symmetry planes identified in Section 4.2.2. The surface mesh was generated on the blocks and then converted to a full volume mesh ready for export to CFX. The fluid domain mesh consists of 5,183,340 structured hexahedral cells, and details of the mesh on key planes in the model are shown in Figure 4.6[2].

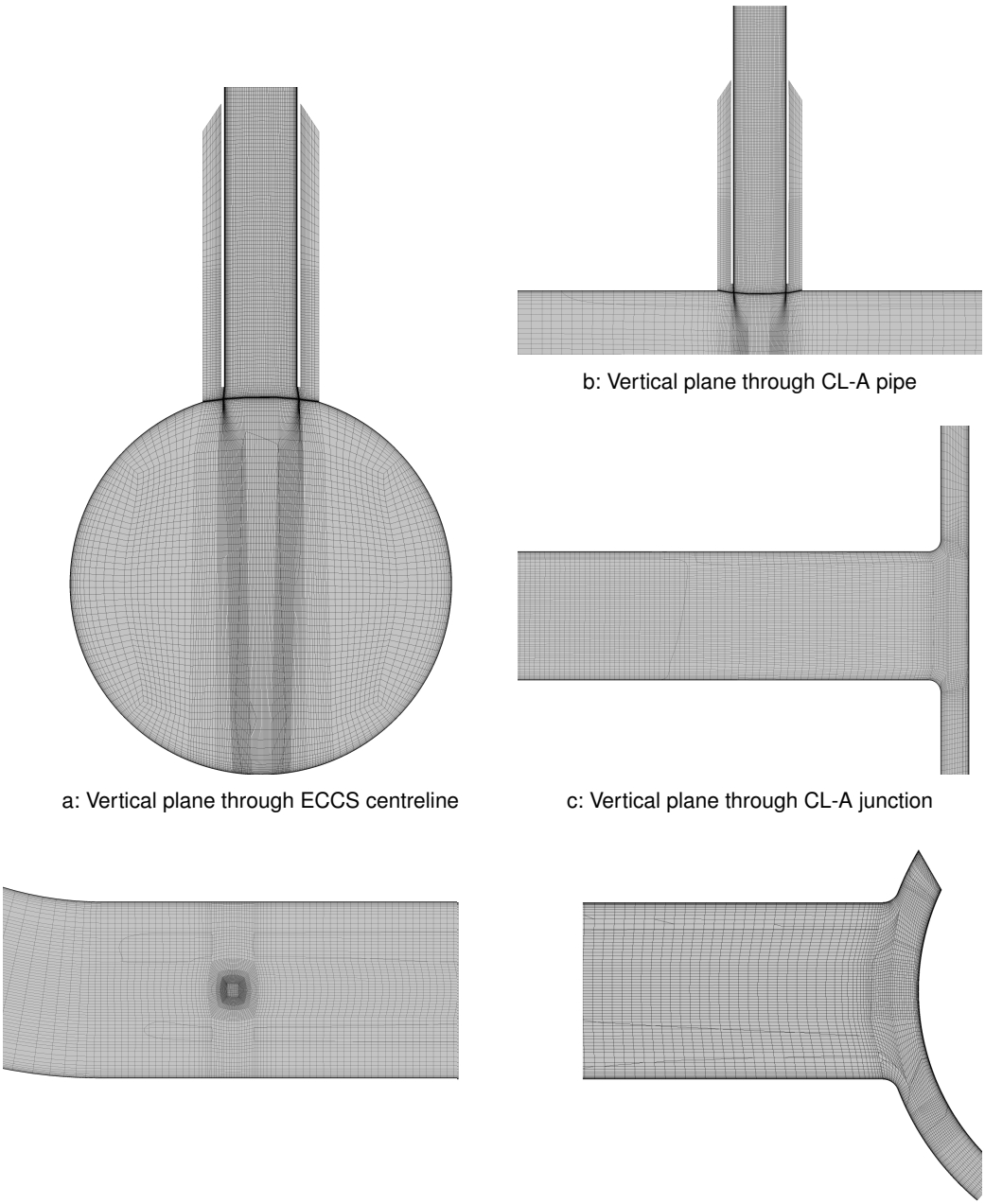

a: Vertical plane through ECCS centreline

b: Vertical plane through CL-A pipe

c: Vertical plane through CL-A junction

d: Horizontal plane through CL-A centreline

Figure 4.6: Fluid domain mesh.

[2] The spurious lines on the figure are not real and merely a visualisation artefact.

4.3.2.3 Solid Mesh Generation

The chosen approach was to generate an unstructured tetrahedral mesh for the solid domains of the CL-A and ECCS pipework, PV and core barrel with prismatic inflation layers grown from the inner solid surface. In a similar way to choosing ICEM for the fluid mesh, ANSYS meshing was chosen to generate the solid mesh as it is an industry standard approach compatible with the proposed analysis software.

ANSYS meshing has a variety of settings that can be controlled by the user. This generates a tetrahedral mesh that respects the geometry faces and grows with high quality cells into the volume. Surface controls can be applied to achieve the required size distribution. The following settings have been used to generate an acceptable quality solid mesh:

- A prismatic mesh was applied to the inner surface of all solids with a FCH of 0.4 mm, growth rate of 1.2 and 10 layers.
- A tetrahedral unstructured mesh was applied to all solid domains.
- General sizing settings were applied to all domains setting the cell size to 0.02 m. This size ensures that there are at least 2 cells between the top of the prismatic layer and outer surface of the solid, and is consistent with the circumferential fluid mesh resolution.
- A local face size of 0.005 m was applied to the ECCS pipework to ensure that the circumferential resolution of the pipe was captured, and approximately matches the fluid mesh resolution.

The resulting solid domain mesh comprises 6,966,691 cells, and details of the mesh on key planes in the model are shown in Figure 4.7.

4.3.2.4 Quality

Three measures of mesh quality are used in ANSYS CFX to determine the suitability of a mesh:

- Mesh Orthogonality measures skewness in the mesh between adjacent cells. An orthogonality angle of $> 20^{\circ}$ is recommended.
- Expansion factor measures the rate of change of adjacent cell volumes. An expansion factor below 20 is recommended.
- Aspect ratio measures the proportion of the longest to shortest dimensions of elements. A value below 1,000 is recommended.

Fluid Domain: The minimum orthogonal angle is 16.5° with 154 elements that fail to meet the recommended criterion for orthogonal angle. These elements are located in the sharply changing region at the cold leg-downcomer junction, all close to the wall. There is expected to be some local inaccuracy in these cells, and non-orthogonal cells can also cause solution stability problems. If solution difficulties had occurred, revision of these cells to improve their quality would have been one of the first actions taken.

The maximum expansion factor in the mesh is 13 and all elements are below the recommended expansion factor of 20.

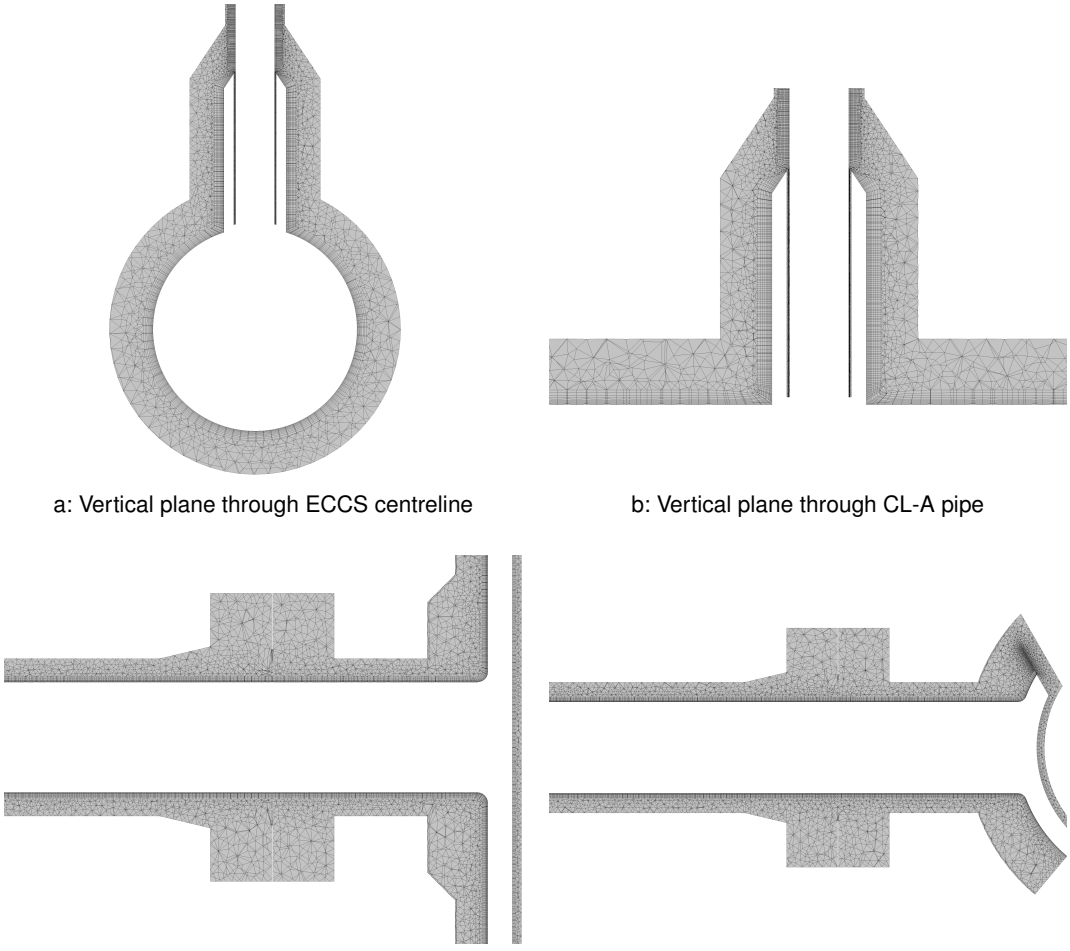

a: Vertical plane through ECCS centreline

b: Vertical plane through CL-A pipe

c: Vertical plane through CL-A junction

d: Horizontal plane through CL-A centreline

Figure 4.7: Solid domain mesh.

150,786 elements fail to meet the recommended aspect ratio criteria of 1,000 with a maximum aspect ratio of 6,747. However, no elements exceed the 10,000 criterion used in the CFX preprocessor. All 150,786 are found in the boundary layer next to the walls, where the flow direction is well defined and high aspect ratios are not expect to affect numerical accuracy. High aspect ratio cells in boundary layers often occur in CHT problems where wall $y^+ = 1$ is targeted and complex shapes are required to be meshed with varying resolutions.

The mesh quality metrics are considered acceptable for the case study, as in the region of interest all metrics are within the recommended values and only a small proportion of the domain exceeds those values.

Solid Domains: The quality requirements given above are also applicable to the solid domains, however they are less important than for the fluid domain because only the conduction equations are solved, rather than the Navier Stokes equations.

As recommended in Volume 2 (Section 3.4.2), the mesh should be suitable for resolving through-wall gradients. If the features are small, and especially if they are far away from the fluid, then they will make little difference to the thermal mass that gets calculated during the transient.

Less than 1% of the elements fail to meet one of the CFX quality checks in the solid domain, exhibiting a maximum aspect ratio of 276. The maximum expansion ratio of 159 and minimum orthogonal angle of 8.5° are for cells that are all located at the small face between pipe flanges, and represent a small proportion of the domain.

A more instructive impression of the quality of the solid domain mesh can be gained by looking at cross-sections in the regions of interest, as shown in Figure 4.7. From this, it can be seen that the prismatic layer and solid mesh refinement is expected to be suitable to capture through wall gradients that might occur and influence the PTS assessment.

Additionally, a superposition of the fluid and solid domain meshes at their interface is shown in Figure 4.8. The two meshes are of a similar refinement at the surface, as is required to achieve accurate interpolation for heat transfer at the fluid-solid interface.

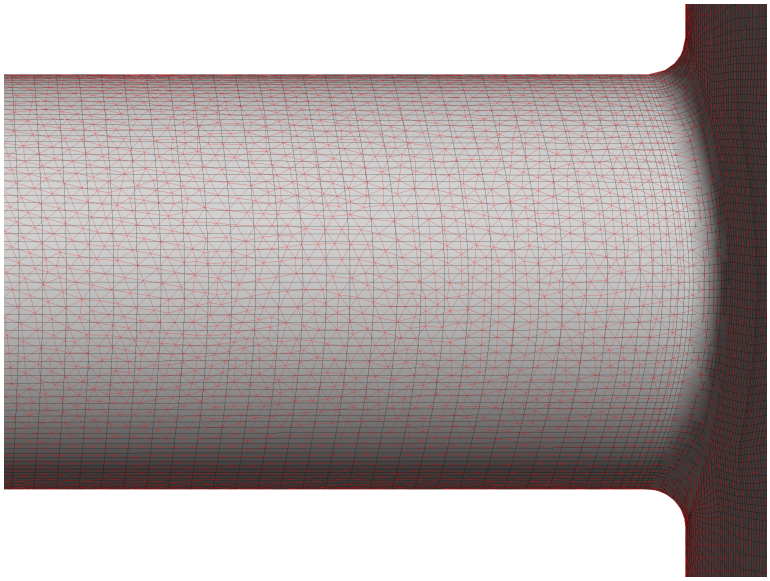

Figure 4.8: Solid to fluid mesh interface.

4.3.3 Modelling Approach

Once the meshing approach has been successfully designed and implemented, it is necessary to define the inlet and boundary conditions, material properties, solution settings, monitors and convergence parameters. It is important to independently verify that these inputs are correctly specified, so that the simulation matches the test as closely as possible, following the guidance described in Volume 3 (Section 3.2.4).

4.3.3.1 Inlet and Boundary Conditions

As part of the overall analysis sequence (Section 1.3), boundary conditions would normally be provided from a system code. However, since this is a validation exercise for the CFD analysis, it is more appropriate to use the reported test results. Therefore, the boundary conditions for this analysis have been taken from the intended and measured test conditions for Test 1-1 (JAEA, 2008a). Engineering judgement and empirical calculations have been used where data are not available, such as the external HTC between the air and the insulation.

The reference pressure for the domain is set to the pressurizer pressure of 15.26 MPa as described by the intended test conditions (JAEA, 2008a). Ideally, the intermediate downcomer pressure would be used as it is closer to the model outlet, but this was not available. The pressure drop through the model is expected to be small, and the impact on material properties is expected to be negligible. The reference density is set to the density at the CL-A inlet using the IAPWS-IF97 model (Wagner *et al.*, 2000).

The locations of all boundary conditions are shown in Figure 4.9.

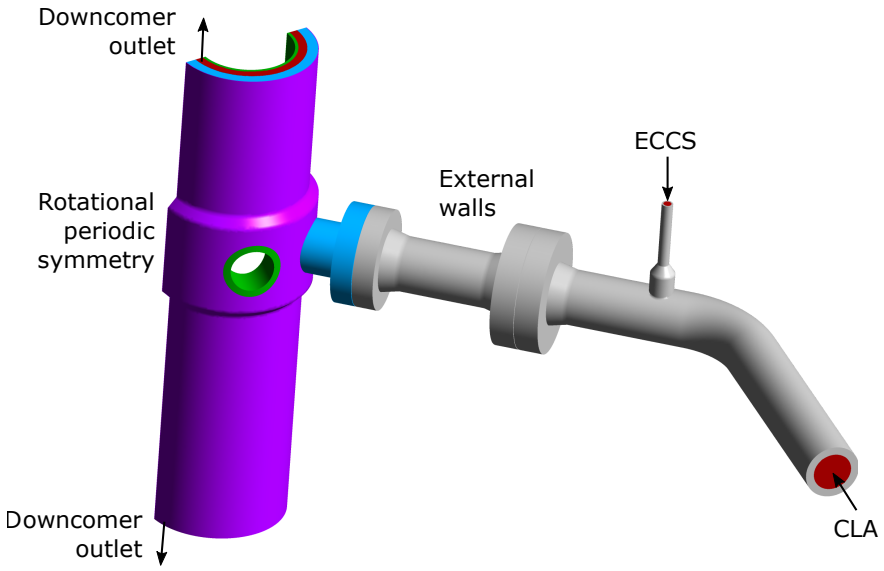

Figure 4.9: Location of boundary conditions.

CL-A and ECCS Inlet: The inlet boundary conditions for the initial transient solution with fixed boundary conditions (Section 4.2.6) have been calculated by averaging the last 40 seconds of measured test data (Table 4.1). The inlet conditions for the full transient simulation use the measured mass flow rate and temperature data with linear interpolation between the available data points.

The flow direction is set to be normal to the inlet face, i.e. in direction of pipe flow. The inlet turbulence has been specified based on a turbulence intensity and length scale. The turbulence intensity (I) is calculated based on the following equation (Basse, 2019), where f is the pipe ('Darcy' or 'Moody') friction factor described in Volume 2 (Section 3.4.2.5):

$$I = 0.0276 \times \log(f) + 0.1794$$

The turbulence length scale is set according to the CFX modelling guide (ANSYS, 2020) to be 30 % of D_h. The values calculated for the initial transient solution are shown in Table 4.3.

Location	Intensity	Length scale (m)
CL-A	0.06255	0.0621
ECCS	0.08379	0.0123

Table 4.3: CL-A and ECCS inlet turbulence parameters.

Downcomer Outlet: The downcomer outlet boundary condition is specified relative to the reference pressure as a static pressure of 0 Pa. This ensures that the pressure is set to an appropriate value for the entire domain. In addition, it is important to set an appropriate reference density as this enables the hydrostatic pressure difference between the top and bottom of the downcomer to be implemented correctly.

External Walls: The external surfaces of the pipes and PV cladding have a constant HTC and ambient temperature applied. This is considered appropriate as the heat loss is dominated by the insulation and details of the external air flow are not available. The effective HTC can be calculated using a thermal resistance approach (Section 4.2.2), which includes 125 mm thick Rockwool insulation using the properties detailed in ROSA-V Group (2003) and an external HTC of 5 $W/m^2 K$, which can be estimated using a correlation (Volume 2, Section 2.1.2.3) to represent natural convective cooling. The ambient temperature is set to 306 K.

Core Barrel Internal Wall: The internal wall of the core barrel is exposed to the core flow. Comparison of thermocouple locations TE-SP055F (core fluid temperature) and TW-S060E (core barrel internal wall temperature) show little difference during the test period (JAEA, 2008a). Therefore, a fluid temperature of 576 K was initially used with a high HTC (1,000 $W/m^2 K$). This was subsequently changed to an adiabatic boundary for the final validation case (Section 4.5) because the downcomer thermocouple locations predicted unrealistic increases in temperature during the transient when using a heat transfer boundary condition.

4.3.3.2 Material Properties

The ROSA LSTF test rig uses water/steam as the primary circuit working fluid. As discussed in Section 4.2.4, the International Association for the Properties of Water and Steam (IAPWS)-IF97 model for water/steam properties is available in CFX, and the 'look-up' mode has been selected to reduce the number of calls to the more complex IF97 routine.

The CFX solver calculates a table of values with a user specified temperature resolution (spacing) at the start of the solution and then interpolates the properties at each solution iteration. Tables are generated for liquid water (fluid remains single phase in this test) between 273 K and 600 K, and 14.5 MPa to 16 MPa, with 150 intermediate points.

Material properties for the solid components are given in ROSA-V Group (2003), and are implemented as a function of temperature with linear interpolation in-between. These include:

- Pressure vessel: Carbon Steel SB49.
- ECCS pipework and PV cladding: Stainless Steel SUS316LTP-S.
- Primary loop pipework: Stainless Steel SCS13A.

ROSA-V Group (2003) does not give properties for the SCS13A stainless steel. Therefore, the properties of SUS316LTP-S have been used as they are assumed to be sufficiently similar.

4.3.3.3 Model Settings

The appropriate physical and numerical models need to be applied to the CFD solver to simulate the flow, heat transfer, buoyancy and turbulent mixing within the model (Section 4.2.5.2). The model has been solved using double precision numerics with gravity applied vertically downwards. The high resolution scheme (second-order accurate) has been used for all equations (pressure, velocity, turbulence and energy), while the implicit second-order backward Euler scheme has been used for the transient with a time step of 0.01 s. The default under-relaxation settings were used in the model and no stability issues occurred during the solution.

The solution strategy is detailed in Section 4.2.6, which includes solving an initial steady RANS solution before switching the solution to an unsteady RANS simulation. The final Test 1-1 transient simulation took 54 hours to solve on 128 cores.

4.3.3.4 Monitor Locations

ROSA-V Group (2003) gives detailed information about the location of instrumentation in LSTF, and JAEA (2008a) provides details of the additional thermocouples installed for the OECD/NEA ROSA project. Volume 1 (Section 4.5.1) recommends that solution monitors should be identified and positioned in order to demonstrate convergence in the parameters of interest.

Since the ECCS flow is inherently transient, the primary aim of monitors is to provide detailed transient data at specific points in the model to allow comparison against the measured thermocouple data. Therefore, monitor locations were set up for all thermocouple locations in the domain extent, as shown in Figures 2.7 and 2.8. These locations capture regions of interest, such as:

- Thermocouple rakes along CL-A showing development of the stratification region.
- Thermocouple arrays in the downcomer spreading out from the cold leg-downcomer junction to measure the cold plume location and mixing process.
- Thermocouples on the inner surface of the CL-A pipework and PV to measure the metal cooling during the transient.

4.3.3.5 Checking Convergence

CFD models are solved over a number of iterations until the flow field is considered converged. The process of judging convergence is case specific, but generally a combination of flow monitors and residuals should be considered. In order to properly assess convergence for this case study, the following checks have been conducted:

- Using the monitors placed at the locations of all thermocouple measurements in the domain. These were compared under steady inlet conditions to ensure that no unphysical behaviour is observed and that quantities have reached a statistically steady value.
- Residuals of velocity, momentum, energy and turbulence equations were assessed for the steady-state to ensure they are appropriately reduced and no further iteration is required. When the transient case was run, the residuals at each time step were compared to ensure that they converged each time step.
- Imbalances in the mass, momentum and energy conservation were checked to ensure that they are close to zero.

4.4 Baseline Results

The baseline results use the solution strategy defined in Section 4.2.6 in order to demonstrate the suitability of the mesh and turbulence model. This has been achieved by running a transient simulation with constant boundary conditions. This solution approach allows the following aspects to be assessed by comparing the time-averaged temperature predictions to the equivalent measured data:

- The level of unsteadiness in the flow and the differences between the steady RANS, instantaneous and time-averaged Unsteady Reynolds-Averaged Navier-Stokes (URANS) temperature predictions.
- Independence of the results to mesh resolution.
- Most appropriate RANS turbulence model.

4.4.1 Steady vs Unsteady RANS

As discussed in Section 4.2.6, a steady-state model has been run to provide a starting condition for subsequently performing a transient analysis during the injection period. This approach is recommended for unsteady phenomena such as the mixing of the ECCS injection plume into the CL-A, despite the boundary conditions for the injection remaining steady.

4.4.1.1 Flow Phenomena

Figure 4.10 shows contours of velocity magnitude on a vertical plane through the CL-A centreline and at four CL-A measurement planes downstream of the ECCS injection for the steady RANS and instantaneous values at the end of the URANS solution. These results can be compared to the expected flow phenomena shown in Figure 1.1 and characterised in Section 4.2.3.

The simulations show that the negatively buoyant plume leaves the ECCS and turns sharply due to the CL-A crossflow, but then sinks to the bottom of the CL-A pipe due to buoyancy. At the first measurement plane (Plane 080), the cold ECCS jet is still clearly visible and shows the expected horseshoe vortex for a jet in crossflow. Subsequently, the jet structure becomes less noticeable as the cold ECCS flow mixes with the hot CL-A flow.

The instantaneous URANS predictions highlight the fluctuating velocities in the ECCS jet as it enters the CL-A pipe, and the expected unsteady nature of the flow. By comparison, the steady RANS simulation predicts a smooth jet profile with increased mixing in the downstream section.

4.4.1.2 Temperatures

The equivalent contours of temperature for the steady RANS, final instantaneous URANS and time-averaged URANS results are shown in Figure 4.11.

The instantaneous URANS temperature predictions follow the flow distribution and highlight the fluctuating cold ECCS flow as it enters the CL-A pipe and sinks to the bottom, which creates a transient stratified flow in the downstream section of the CL-A pipe.

When this unsteady jet motion is averaged over time to form the time-averaged URANS results, the jet profile, mixing and subsequent stratification appear smooth and uniform with little variation

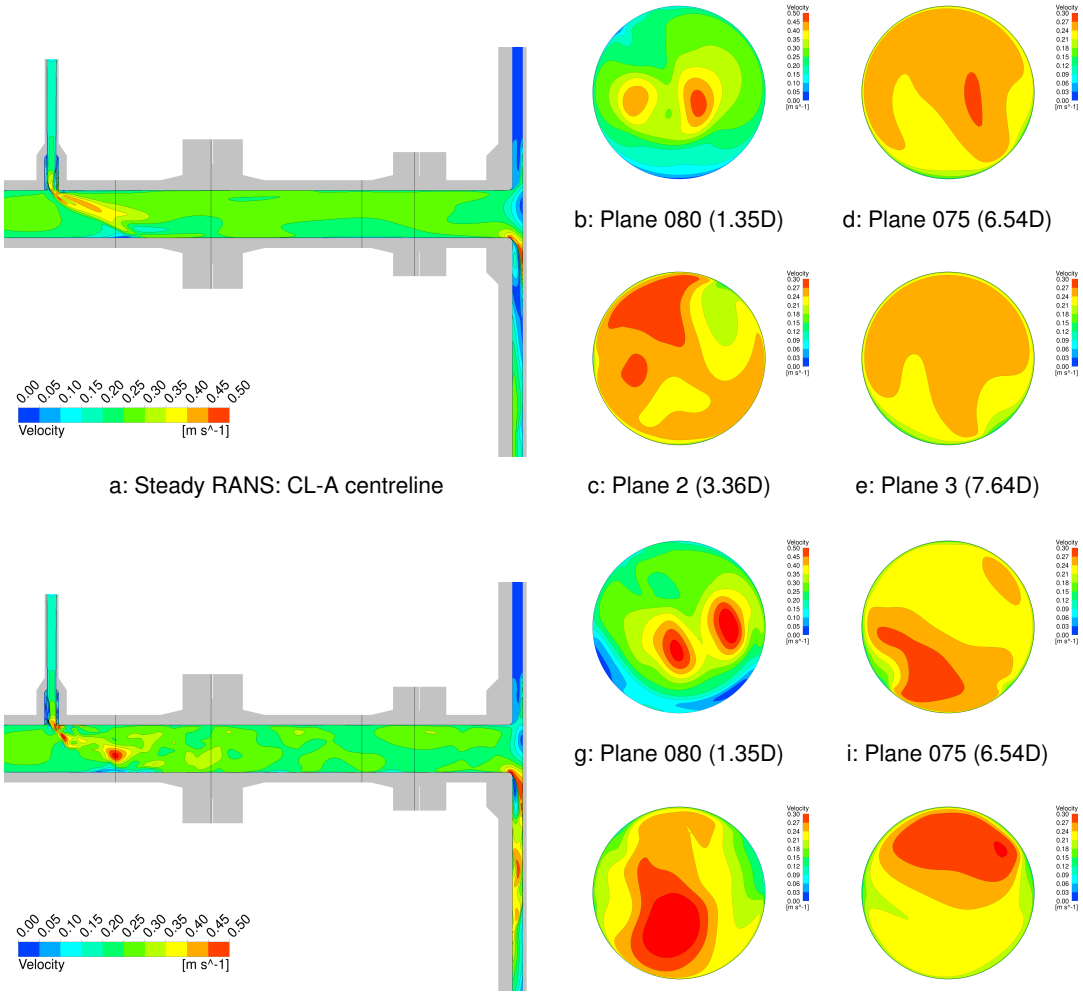

a: Steady RANS: CL-A centreline

b: Plane 080 (1.35D)

d: Plane 075 (6.54D)

c: Plane 2 (3.36D)

e: Plane 3 (7.64D)

f: Instantaneous URANS: CL-A centreline

g: Plane 080 (1.35D)

i: Plane 075 (6.54D)

h: Plane 2 (3.36D)

j: Plane 3 (7.64D)

Figure 4.10: Steady RANS and instantaneous URANS velocity predictions.

across the pipe (Plane 3) before the flow enters the downcomer. This is consistent with the time-averaged measured data.

In contrast, the steady RANS solution predicts a single jet, which is maintained along the CL-A pipe with increased mixing between the ECCS and CL-A pipe flow. This significantly reduces the vertical temperature variation in the pipe at Plane 3, and demonstrates that a steady RANS approach is not appropriate for this type of flow.

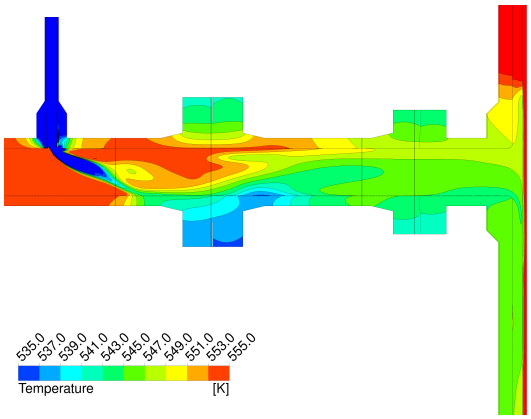

a: Steady RANS: CL-A centreline

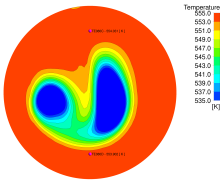

b: Plane 080 (1.35D)

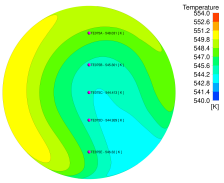

d: Plane 075 (6.54D)

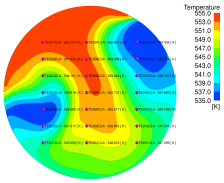

c: Plane 2 (3.36D)

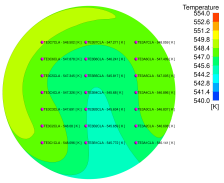

e: Plane 3 (7.64D)

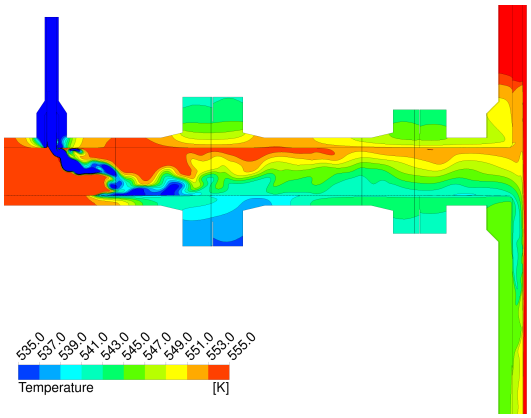

f: Instantaneous URANS: CL-A centreline

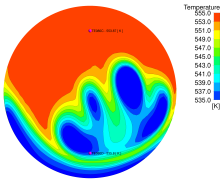

g: Plane 080 (1.35D)

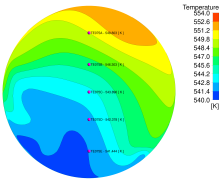

i: Plane 075 (6.54D)

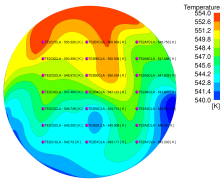

h: Plane 2 (3.36D)

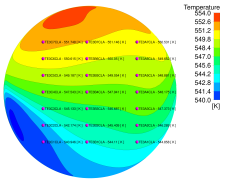

j: Plane 3 (7.64D)

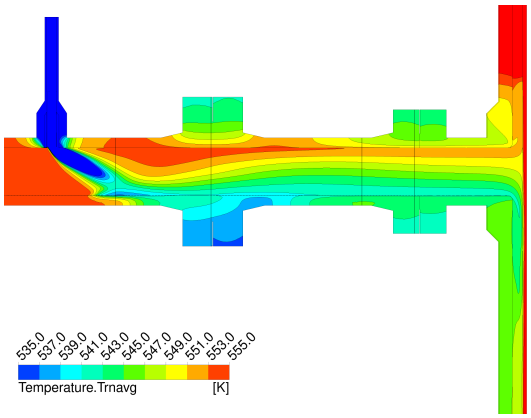

k: Time-averaged URANS: CL-A centreline

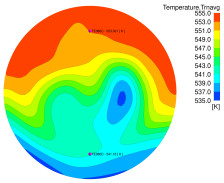

l: Plane 080 (1.35D)

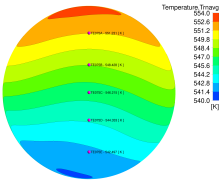

n: Plane 075 (6.54D)

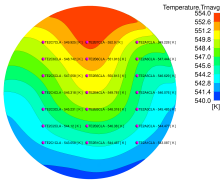

m: Plane 2 (3.36D)

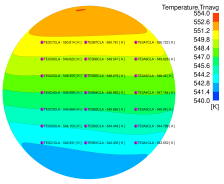

o: Plane 3 (7.64D)

Figure 4.11: Steady RANS and URANS temperature predictions.

4.4.2 Mesh Sensitivity Study

As described in Section 4.2.5.1 and Section 4.3.2, the spatial discretisation (mesh) within the fluid and solid domains must be:

- Sufficiently well resolved to capture the required flow phenomena.
- Suitable for capturing the detailed behaviour of the boundary layer, with a y^+ of approximately 1 and sufficient resolution in the boundary layer.

Figure 4.12 shows the contours of y^+ on the fluid side of the fluid-solid interface. This confirms that the FCH (Section 4.3.2.2) is appropriate to resolve the viscous sublayer in the CL-A and downcomer with a $y^+ < 5$.

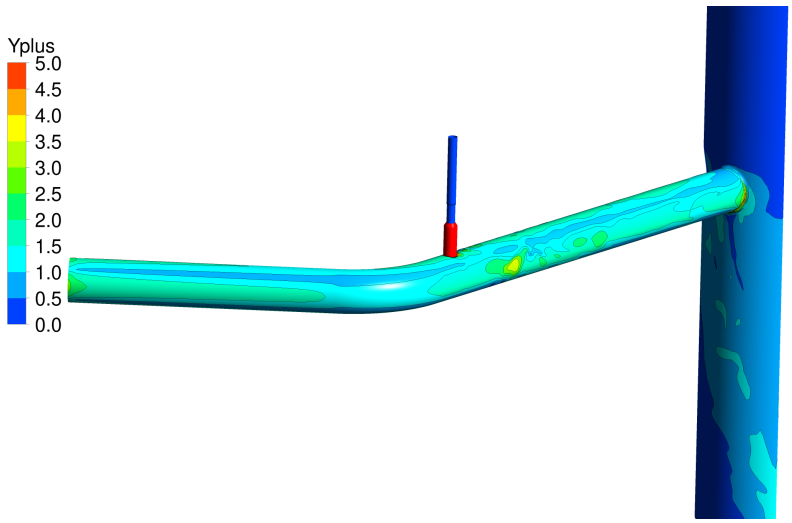

Figure 4.12: Contours of y^+ on fluid side of fluid-solid interface.

A mesh sensitivity study has been conducted to determine whether the spatial discretisation is appropriate for resolving the flow features of interest. The coarser and finer meshes were generated by specifying a mesh spacing factor in ICEM. This applies a global decrease/increase to each edge spacing, while maintaining the same FCH and adjusting the boundary layer growth accordingly. Due to the size of the mesh, using a mesh spacing factor of two on the baseline mesh was not practical within the budget and time constraints of this case study.

The cases were run with the time step adjusted to ensure that the domain Courant-Friedrichs Lewy (CFL) numbers remained approximately comparable between each case. The CFL number in the baseline model is below 1 for most of the domain with localised high values at the ECCS inlet due to the flow through the inflation layer mesh in that region, and so is considered an appropriate and unavoidable compromise between having sufficient spatial resolution and acceptable computational cost. The metrics for the baseline and coarser/finer meshes are detailed in Table 4.4.

Case	Coarsest	Coarse	Baseline	Fine
Mesh spacing factor	0.7	0.85	1.0	1.18
Fluid and solid mesh (cells)	2,352,050	7,865,615	12,150,031	18,032,243

Table 4.4: Mesh metrics for mesh sensitivity study.

Each case was solved transiently with the same conditions as the baseline model (Section 4.4.1). Since the flow varies with time, it is necessary to compare the time-averaged temperature predictions at the thermocouple locations, rather than consider the instantaneous results. This has been achieved by comparing the time-averaged CFD predictions to the measured data for each fluid thermocouple location and calculating the RMS temperature difference ($\sqrt{\overline{(T_{cfd} - T_{meas})^2}}$) for each measurement plane. The sensitivity study results are plotted in Figure 4.13 and listed in Table 4.5.

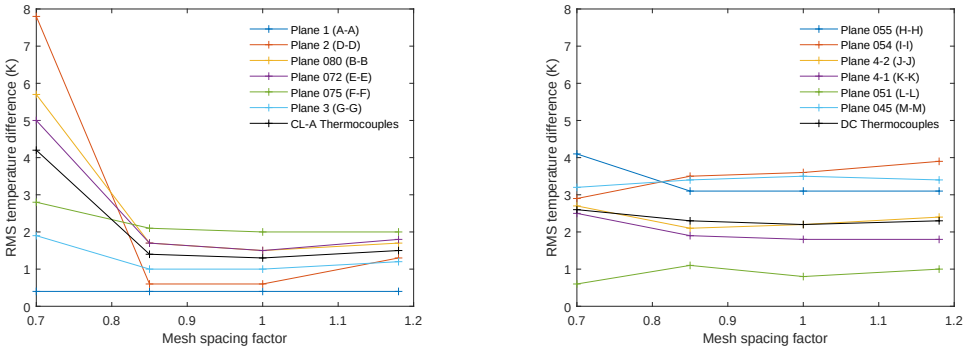

Figure 4.13: Time-averaged mesh sensitivity results (RMS temperature difference).

Case	Coarsest	Coarse	Baseline	Fine
Plane 1 (A-A) (°C)	0.4	0.4	0.4	0.4
Plane 080 (B-B) (°C)	7.8	0.6	0.6	1.3
Plane 2 (D-D) (°C)	5.7	1.7	1.5	1.7
Plane 072 (E-E) (°C)	5.0	1.7	1.5	1.8
Plane 075 (F-F) (°C)	2.8	2.1	2.0	2.0
Plane 3 (G-G) (°C)	1.9	1.0	1.0	1.2
Plane 055 (H-H) (°C)	4.1	3.1	3.1	3.1
Plane 054 (I-I) (°C)	2.9	3.5	3.6	3.9
Plane 4-2 (J-J) (°C)	2.7	2.1	2.2	2.4
Plane 4-1 (K-K) (°C)	2.5	1.9	1.8	1.8
Plane 051 (L-L) (°C)	0.6	1.1	0.8	1.0
Plane 045 (M-M) (°C)	3.2	3.4	3.5	3.4
CL-A thermocouples (°C)	4.2	1.4	1.3	1.5
Downcomer thermocouples (°C)	2.6	2.3	2.2	2.3
All thermocouples (°C)	3.8	1.7	1.7	1.8

Table 4.5: Time-averaged mesh sensitivity results (RMS temperature difference).

The mesh sensitivity study results demonstrate that there is little difference in the time-averaged temperature predictions for the coarse, baseline and fine meshes. The temperature differences increase substantially for the coarsest mesh, which confirms that the baseline mesh is appropriate and the results can be considered mesh independent. It is also worth noting that the baseline time-averaged CFD predictions are generally in good agreement (within 2 °C) of the time-averaged measurements.

4.4.3 Turbulence Model Comparison

As an alternative to the k - ω SST turbulence model used in the baseline model, simulations have been run with the standard k - ε and BSL RSM turbulence models in CFX. The time-averaged temperature contours are shown on Planes 2 and 3 for each turbulence model in Figure 4.14, and the RMS temperature differences are listed in Table 4.6.

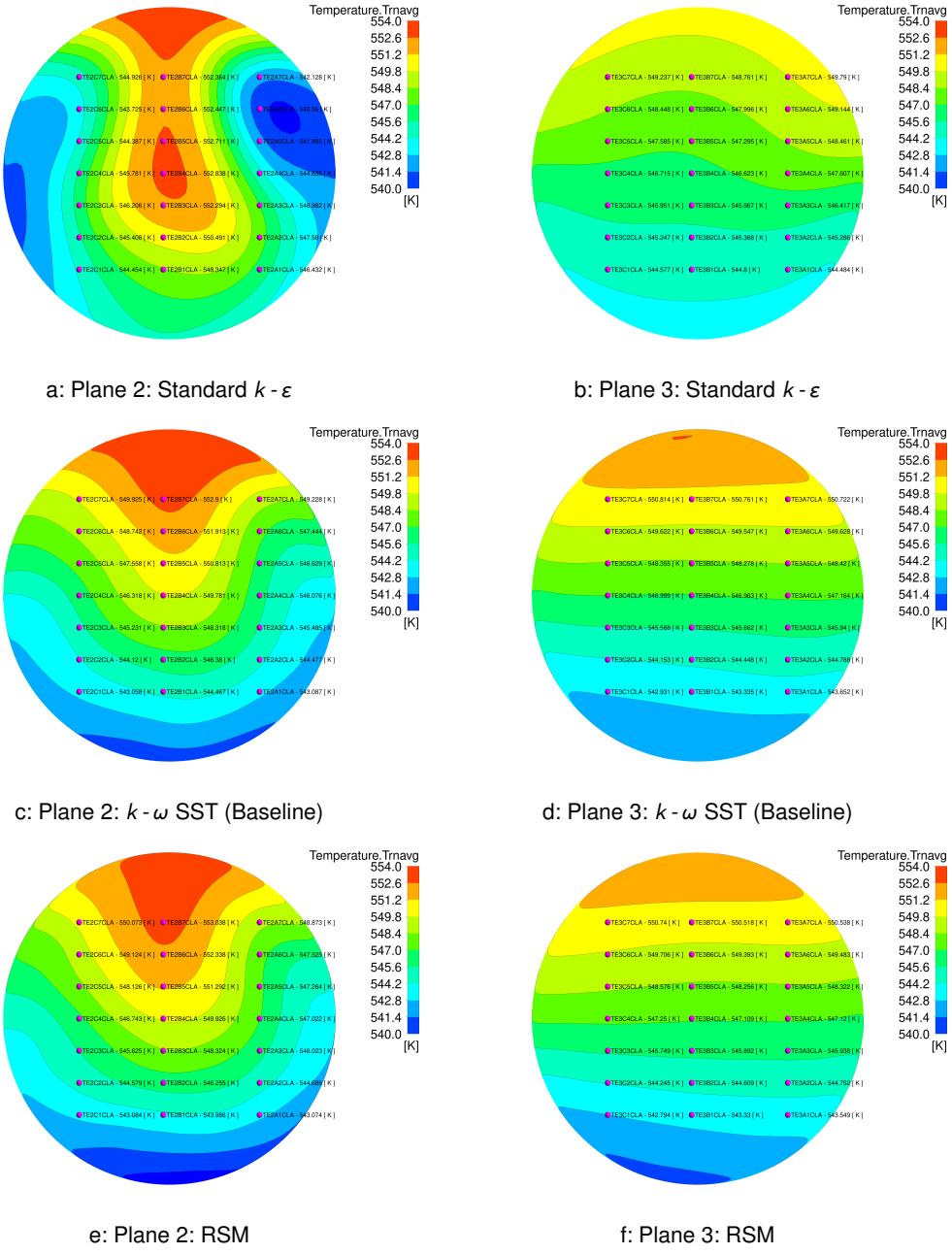

a: Plane 2: Standard k - ε

b: Plane 3: Standard k - ε

c: Plane 2: k - ω SST (Baseline)

d: Plane 3: k - ω SST (Baseline)

e: Plane 2: RSM

f: Plane 3: RSM

Figure 4.14: Time-averaged temperature contours for different turbulence models.

A comparison of the different turbulence model results shows that the time-averaged k - ω SST and RSM predictions are consistent with each other, while the standard k - ε turbulence model results show significant differences compared to the time-averaged measured data and level of mixing and

Model	k - ε	k - ω SST	RSM
Plane 1 (A-A) (°C)	0.4	0.4	0.4
Plane 080 (B-B) (°C)	8.7	0.6	1.7
Plane 2 (D-D) (°C)	4.2	1.5	1.6
Plane 072 (E-E) (°C)	3.3	1.5	1.4
Plane 075 (F-F) (°C)	2.7	2.0	2.0
Plane 3 (G-G) (°C)	1.3	1.0	1.1
Plane 055 (H-H) (°C)	3.8	3.1	3.1
Plane 054 (I-I) (°C)	0.9	3.6	3.2
Plane 4-2 (J-J) (°C)	2.4	2.2	1.9
Plane 4-1 (K-K) (°C)	2.1	1.8	1.4
Plane 051 (L-L) (°C)	0.9	0.8	1.1
Plane 045 (M-M) (°C)	3.0	3.5	3.6
CL-A thermocouples (°C)	3.4	1.3	1.4
Downcomer thermocouples (°C)	2.3	2.2	2.0
All thermocouples (°C)	3.0	1.7	1.6

Table 4.6: Time-averaged results for turbulent model comparison (RMS temperature difference).

stratification in the CL-A pipe. This is consistent with the conclusions from the previous published results for this case study (Section 4.2.1) and discussed in Volume 3 (Section 3.2.6).

Since the time-averaged k - ω SST and RSM results are similar to each other, particularly in the CL-A pipe, the k - ω SST turbulence model has been selected for the final validation case as it is less computationally expensive and so is considered more appropriate within an iterative design process.

4.5 Validation Results

The OECD/NEA ROSA tests provided a significant number of thermocouples for the purpose of validating the fluid and solid temperature predictions. The Test 1-1 transient represents a stable, single-phase natural circulation flow around the primary circuit with ECCS water injected for about 80 s. The Test 1-1 transient simulation was solved by running an initial steady-state solution with no ECCS flow, and then applying the measured time-varying flow rate and temperature profiles to the CL-A and ECCS inlets over a 120 s transient.

The time-varying fluid and solid temperature contours at 15 s time intervals (Figures 4.15 and 4.16) show the transient progression of the jet flow and asymmetric cooling of the upper and lower surfaces due to the cold ECCS injection and stratified temperature variation in the CL-A pipe.

Prior to the ECCS injection, the CL-A pipe and downcomer are all 'soaked' to the CL-A inlet temperature with minimal through-wall temperature gradient, except at the flange locations. As the ECCS flow begins, a large thermal gradient is predicted in the solid at the fluid-solid interface, which gradually extends into the pipe wall over time. The change in thermal gradient between the CL-A (stainless steel) and PV (carbon steel) components that can be seen at the flange joint closest to the PV is due to the increased thermal conductivity of the carbon steel. The thermal gradient in the CL-A and downcomer material is well resolved by the inflation layer mesh, and so could be used to support a structural integrity assessment.

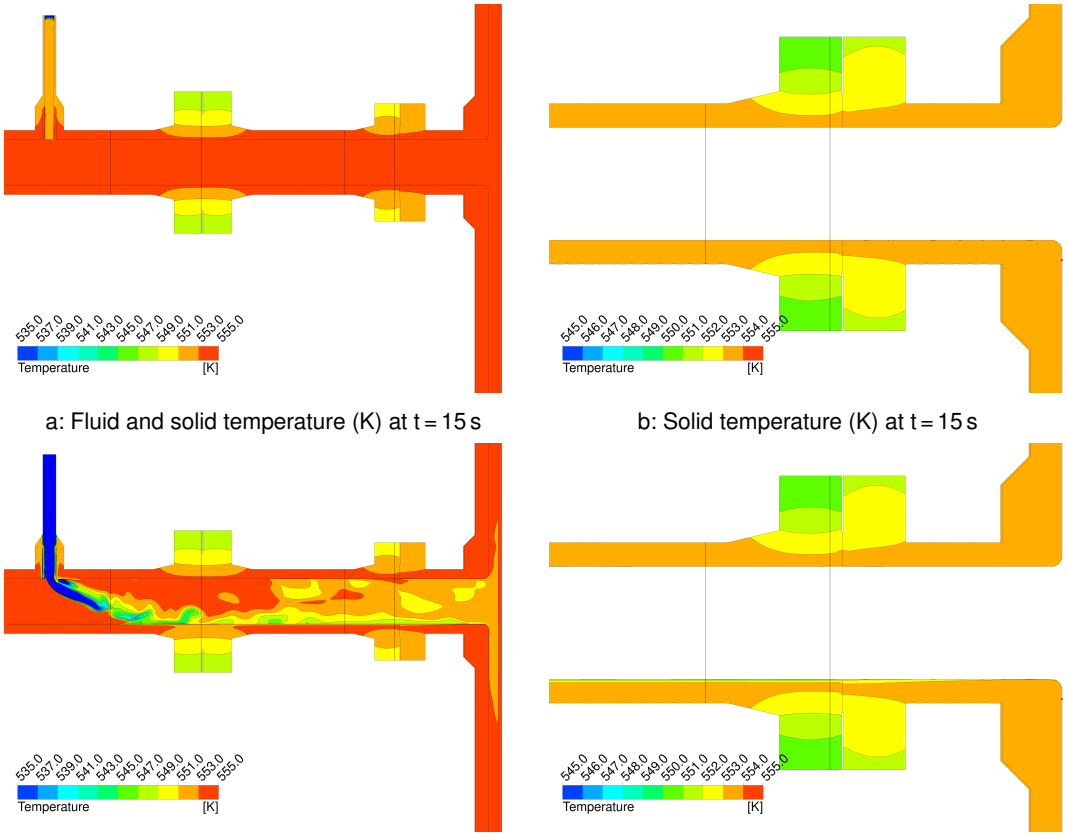

a: Fluid and solid temperature (K) at t = 15 s

b: Solid temperature (K) at t = 15 s

c: Fluid and solid temperature (K) at t = 30 s

d: Solid temperature (K) at t = 30 s

Figure 4.15: Transient temperature variation on vertical centre plane.

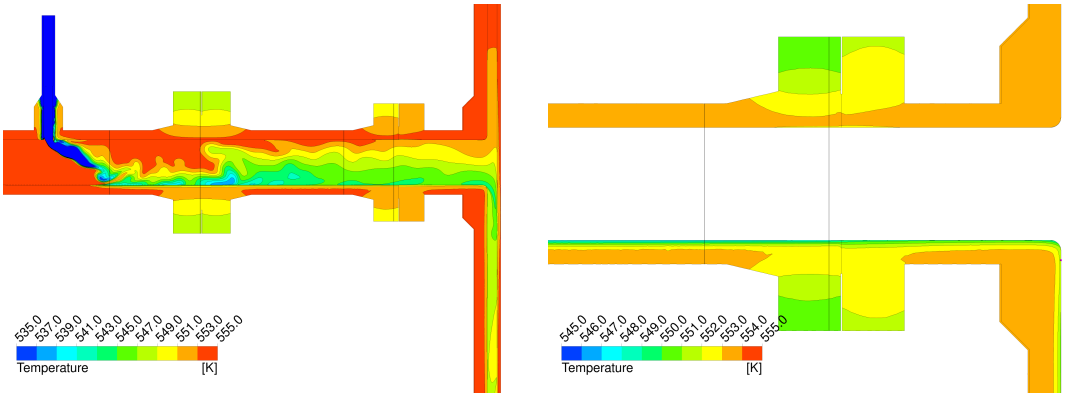

a: Fluid and solid temperature (K) at t = 45 s

b: Solid temperature (K) at t = 45 s

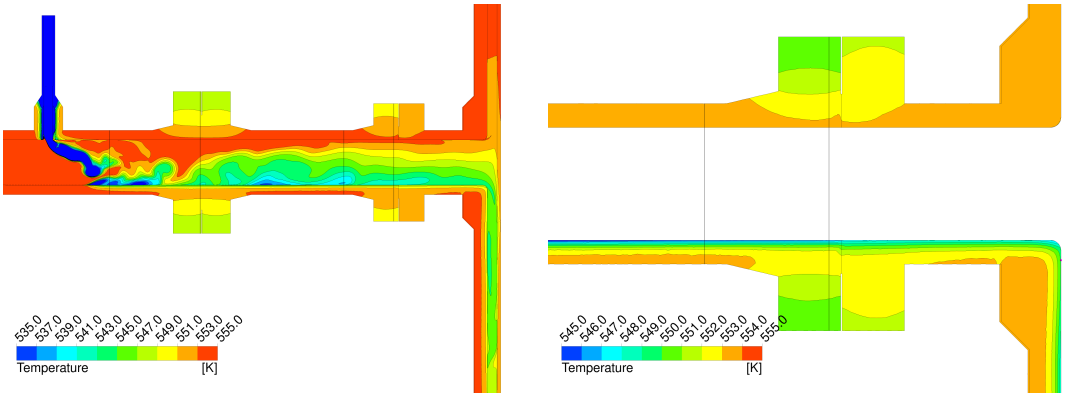

c: Fluid and solid temperature (K) at t = 60 s

d: Solid temperature (K) at t = 60 s

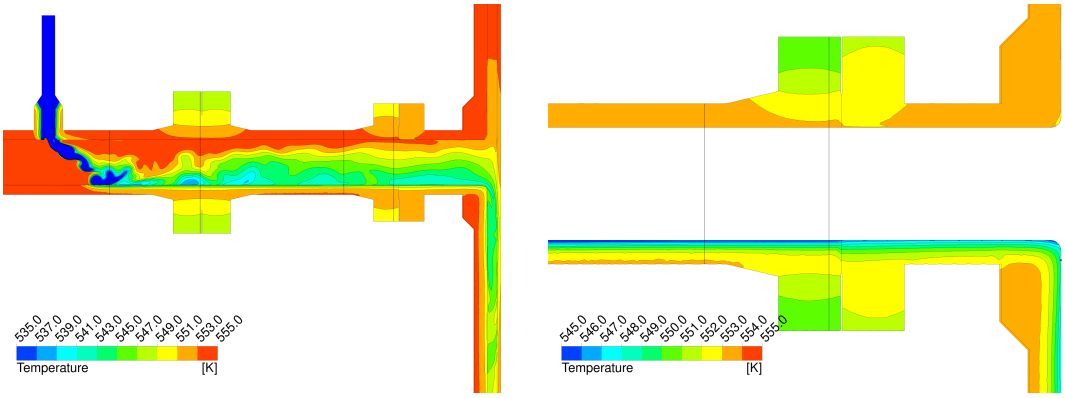

e: Fluid and solid temperature (K) at t = 75 s

f: Solid temperature (K) at t = 75 s

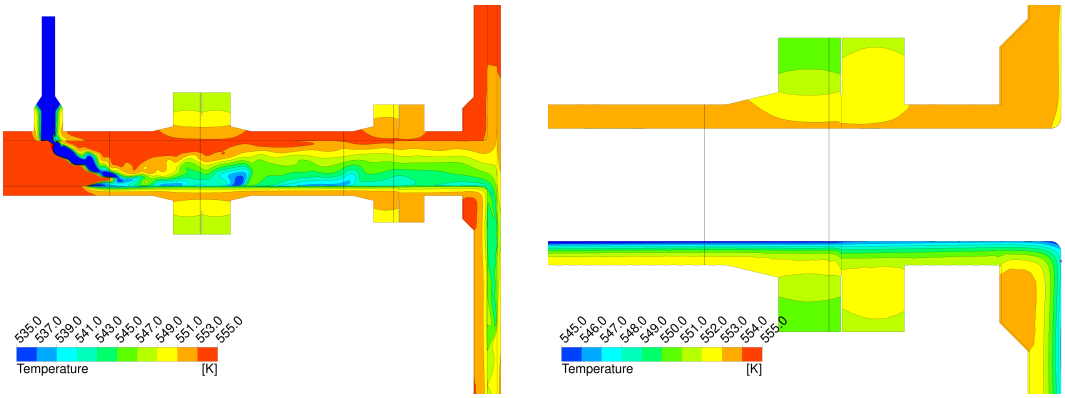

g: Fluid and solid temperature (K) at t = 90 s

h: Solid temperature (K) at t = 90 s

Figure 4.16: Transient temperature variation on vertical centre plane.

In order to better visualise the ECCS flow and temperature variation within the fluid and solid regions, temperature contours have been plotted on the CL-A (Figure 4.17) and downcomer (Figure 4.18) measurement planes at a single time point near the end of the ECCS injection (t = 90 s).

Figure 4.17 shows the progression of the cold ECCS flow along the CL-A pipe with the cooling in the lower section creating a thermal gradient through the thickness of the CL-A pipe wall. This also highlights the variation in pipe cooling around the CL-A pipe circumference with little cooling at the top centre location. As the flow travels along the pipe, the cold ECCS flow gradually mixes with the hot CL-A pipe flow and creates a stratified flow in the CL-A pipe as it enters the CL-A / downcomer junction. The internal wall temperature (Figure 4.18a) shows that the cooler flow in the bottom of the CL-A pipe cools the downcomer inner surface below the junction.

The flow is predicted to separate (Figure 4.10) as it accelerates and turns into the downcomer which creates a small recirculating region below the junction, although the size of this region is reduced by the presence of the 19 mm fillet. The extent of this separation is consistent across all RANS turbulence models investigated.

The shape of the separation region can be seen in Figure 4.18b, which is the measurement plane just below the downcomer junction. This cold stripe then propagates down the downcomer and gradually mixes with the surrounding fluid. This highlights the increased cooling at the CL-A pipe location and thermal gradient through the PV wall.

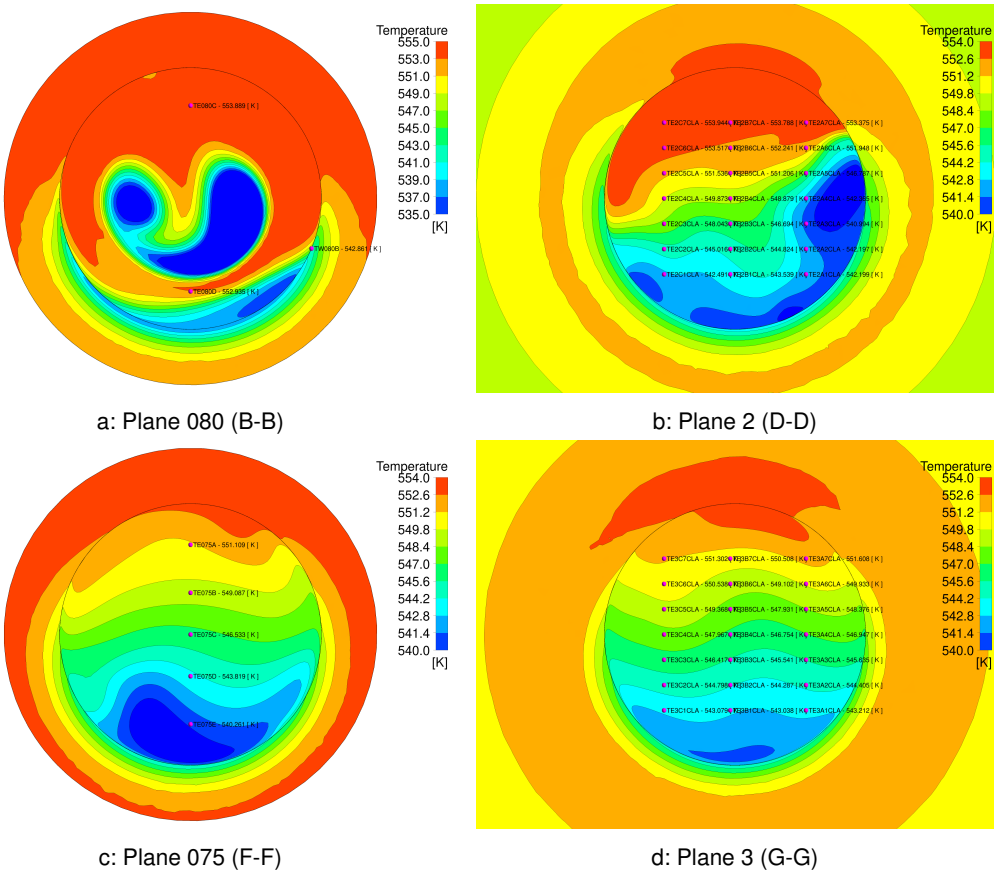

a: Plane 080 (B-B)

b: Plane 2 (D-D)

c: Plane 075 (F-F)

d: Plane 3 (G-G)

Figure 4.17: Temperature (K) contours at t = 90 s on the CL-A planes identified in Figure 2.7.

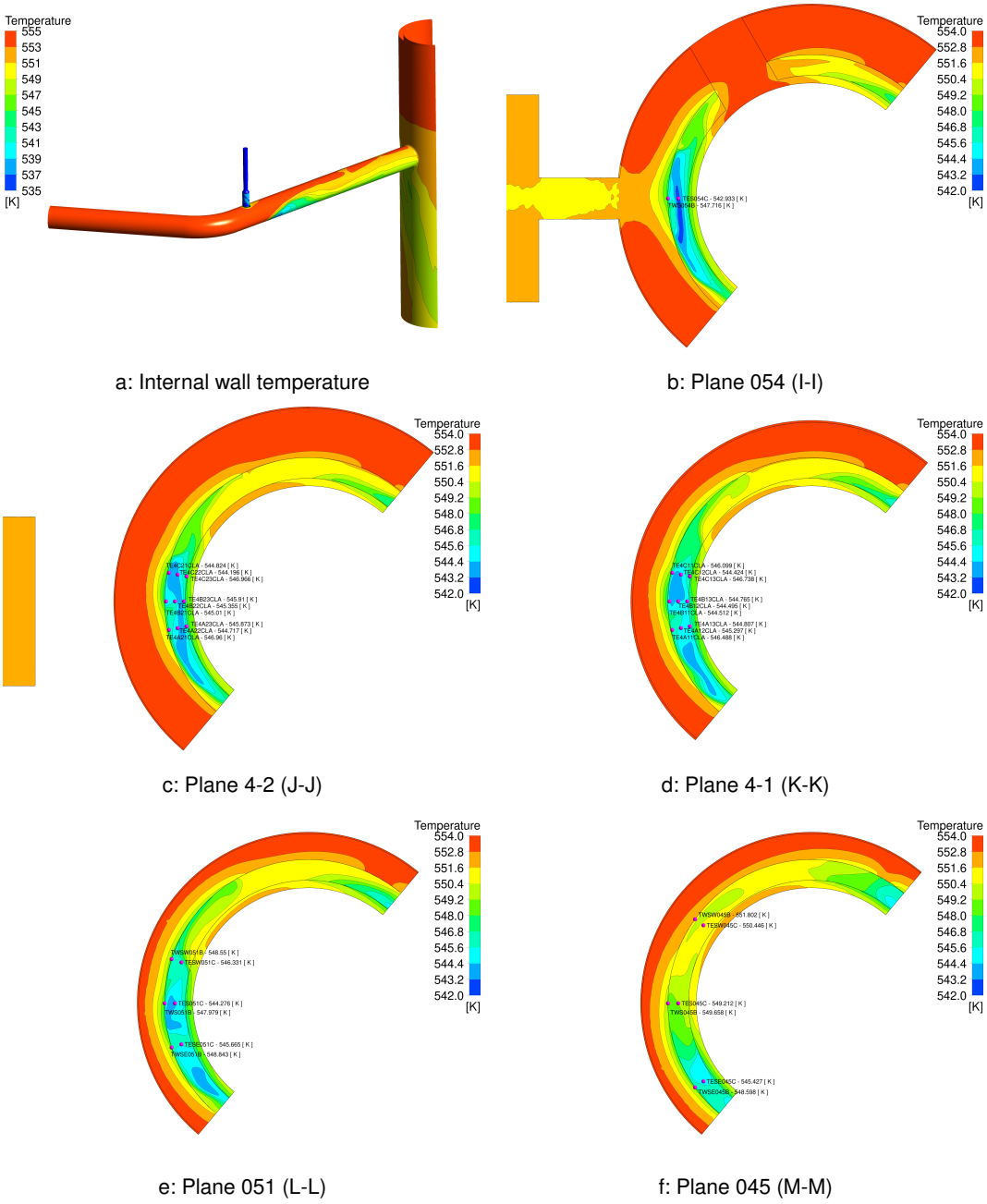

a: Internal wall temperature

b: Plane 054 (I-I)

c: Plane 4-2 (J-J)

d: Plane 4-1 (K-K)

e: Plane 051 (L-L)

f: Plane 045 (M-M)

Figure 4.18: Temperature (K) contours at t = 90 s on the downcomer planes identified in Figure 2.8.

4.5.1 Transient Fluid Temperatures

The fluid temperatures at all thermocouple locations were monitored during the transient to provide time history data. The CFD temperature predictions have been compared against the Test 1-1 measurements by making them relative to the temperature at t = 0 s i.e. $T - T_0$. This removes the effect of any differences in the results due to offsets in the thermocouple measurements or uncertainty in the CL-A inlet temperature.

The predicted and measured transient data is plotted for the CL-A (Figure 4.19) and downcomer (Figure 4.20) thermocouple locations. For simplicity, only a limited number of thermocouple locations have been included, although the level of agreement is consistent for the remaining thermocouple locations. The locations of the named thermocouples are marked on the contour plots in Figures 2.7 and 2.8.

The CL-A fluid temperatures show large high frequency temperature fluctuations close to the ECCS injection (Planes 080 and 2), which are not picked up by the low frequency thermocouple measurements (reading every 2.5 s). However, the average values are consistent at all locations, and further away from the ECCS injection the fluctuations reduce as the flow stratifies. The results confirm that the predicted level of stratification in the pipe is consistent with the measurements.

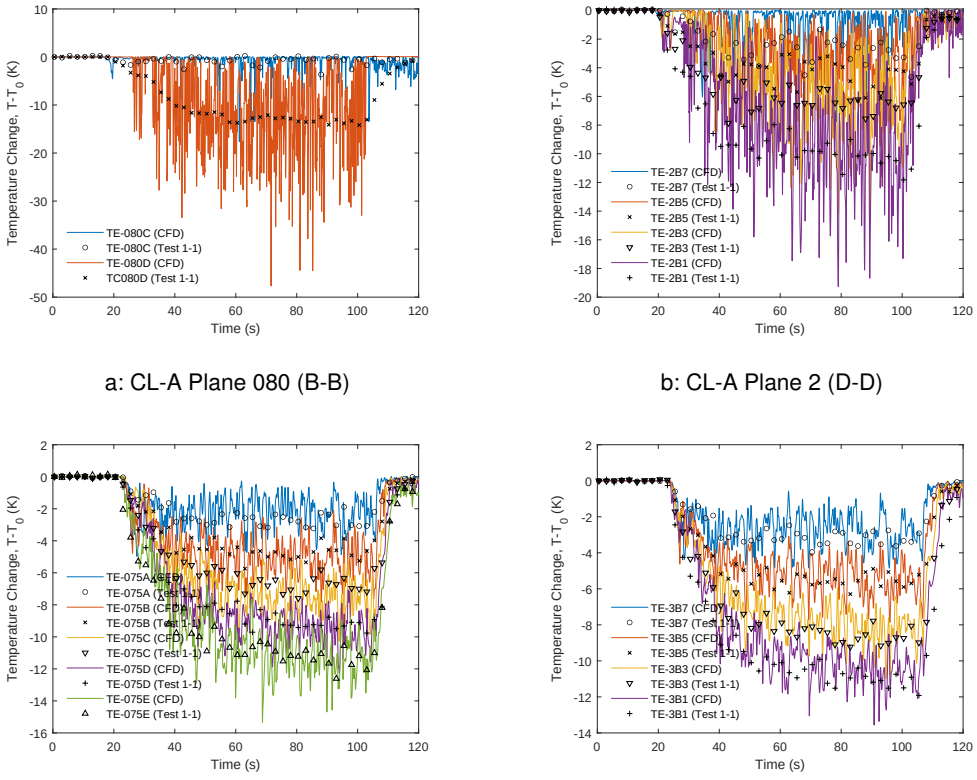

a: CL-A Plane 080 (B-B)

b: CL-A Plane 2 (D-D)

c: CL-A Plane 075 (F-F)

d: CL-A Plane 3 (G-G)

Figure 4.19: CL-A temperature variation at thermocouple locations.

The downcomer fluid temperatures show that the initial temperatures at inlet to the downcomer are consistent (Planes 055 and 054), although are potentially a bit cooler than the measurements.

As the flow travels down the downcomer, the average temperature is consistent with the measurements, but the temperature profile across the downcomer is not predicted in the CFD model. The measured temperatures are cooler at the outer radius of the downcomer than the inner radius, while the CFD predictions are more uniform. This suggests that there is too much mixing in the CFD model and the cold flow should remain more attached to the PV wall. The recent CSNI cold leg mixing benchmark (Orea *et al.*, 2020) highlights how challenging it is for CFD to predict which side of the downcomer the flow attaches to and how it is distributed.

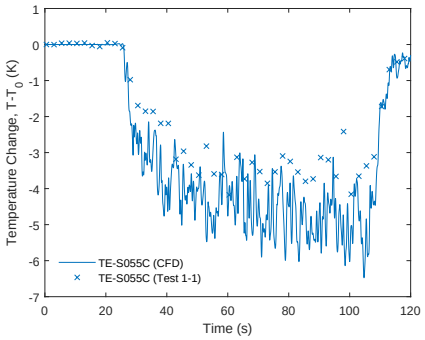

a: Downcomer Plane 055 (H-H)

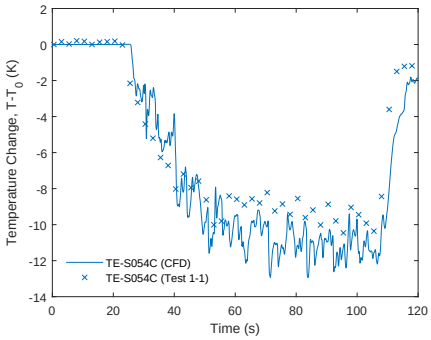

b: Downcomer Plane 054 (I-I)

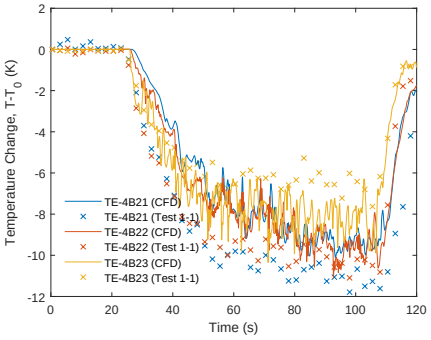

c: Downcomer Plane 4-2B (J-J)

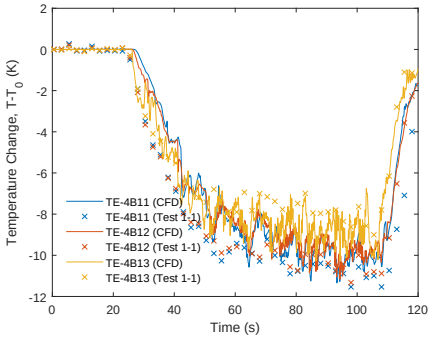

d: Downcomer Plane 4-1B (K-K)

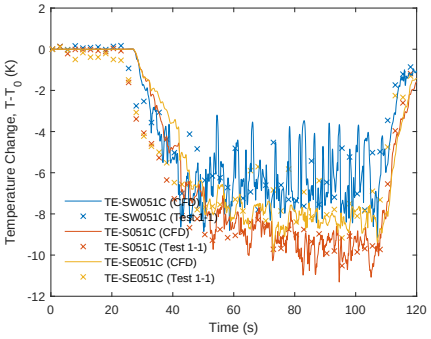

e: Downcomer Plane 051 (L-L)

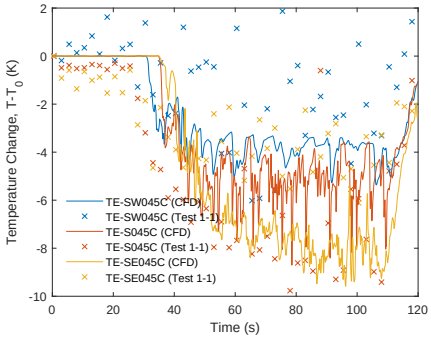

f: Downcomer Plane 045 (M-M)

Figure 4.20: Downcomer temperature variation at thermocouple locations.

4.5.2 Transient Solid Temperatures

The inner wall temperatures at all thermocouple locations were monitored during the transient and have been compared against the Test 1-1 measurements (Figure 4.21), again relative to the temperature at t = 0 s i.e. $T - T_0$.

The predicted CL-A wall temperature at Plane 080 is consistent with the thermocouple, although the prediction is slightly cooler than measured. This shows good agreement, especially considering that it is located in the fluctuating ECCS jet region.

The first thermocouple in the downcomer (Plane 054) is located just below the downcomer junction in the recirculating region predicted by the CFD model. This shows a 5 °C difference between the predicted and measured wall temperatures. This suggests that there is a difference in the recirculating region in the test facility and the cool flow may remain attached and travel down the outer wall of the downcomer. This is discussed in more detail in Section 4.5.3.

The wall temperature measurements further down the downcomer show a consistent trend with the CL-A centre plane thermocouple measurements being noticeably cooler than the off-centre thermocouples. This suggests that the cold fluid remains attached to the outer wall and travels vertically down the downcomer. This is not seen in the CFD model, which predicts increased mixing in the downcomer flow. However, it is often hard to ensure that the thermocouples are in good contact with the surface and so not influenced by the fluid temperature (Volume 2, Section 3.5.2).

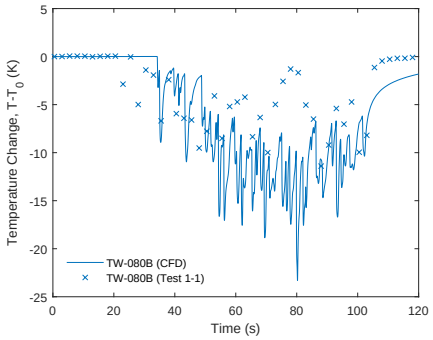

a: CL-A wall temperature Plane 080 (B-B)

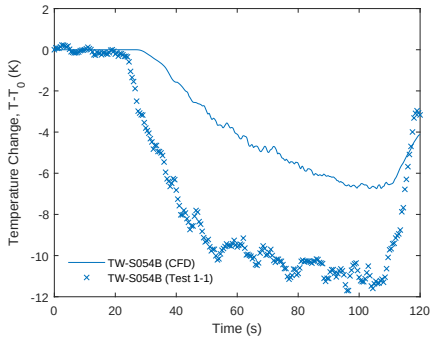

b: Downcomer wall temperature Plane 054 (I-I)

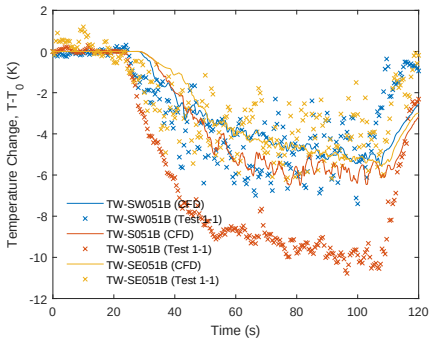

c: Downcomer wall temperature Plane 051 (L-L)

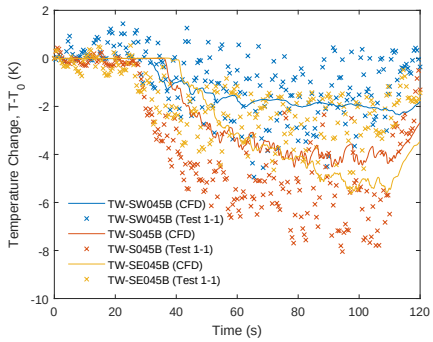

d: Downcomer wall temperature Plane 045 (M-M)

Figure 4.21: Wall temperature variation at thermocouple locations.

4.5.3 Discussion of Validation Results

The validation results have demonstrated that the temperatures in the CL-A pipe are in good agreement with the measurements, but some differences exist in the downcomer temperatures which are greater than the thermocouple measurement uncertainty of ± 2.75 K.

As discussed in Volume 4 (Section 2.1), it is good practice to consider the possible sources of uncertainty in the temperature predictions due to uncertainty in the inlet and initial boundary conditions, material properties and solution approach. It is also in-line with the guidance in Volume 4 to understand and assess the cause of the main observed discrepancies before applying significant efforts to formally quantify the uncertainty in the results.

Further modelling to investigate this discrepancy is beyond the scope of this case study, but initial areas of investigation and uncertainty have been identified:

- The precise geometry of the CL-A / downcomer junction is not clearly described in the system description document (ROSA-V Group, 2003), and the evidence for the presence of a 19 mm fillet is based on an email referenced in Farkas and Tóth (2010). The CFD results indicate that the geometry of this junction is important to the flow profile into the downcomer, and so needs to be clarified.
- The fixture used to mount the new Test 1-1 (Plane 4-2 and 4-1) thermocouples in the downcomer (Figure 4.22) could have a significant impact on the cold flow at the bottom of the CL-A pipe. The side fixtures could create a cold channel along the centre in this critical part of the downcomer, which could affect the flow profile, and hence separation, over the fillet. Details of this geometry should be obtained and the impact on the flow should be investigated.
- The leakage flow into Hot Leg A and up into the upper head has been neglected in the current model. The sensitivity of the temperature predictions and flow profile to this change in flow split should be investigated to understand whether it is significant. In addition, the impact of the periodic and downcomer outlet boundaries on the downcomer flow should be considered.

Figure 4.22: Thermocouple installation in downcomer for Test 1-1 (JAEA, 2008a).

The CFD modelling approach has also been reviewed subsequent to the validation exercise in order to identify areas for improvement:

- The non-conformal mesh at the fluid-solid interface was checked during the solution and is correctly interpolating the solution between the two domains. Although a non-conformal interface is simpler to mesh, issues were found during the solution set up that needed to be resolved. The model required similar levels of mesh resolution on both sides of the interface due to the highly curved nature of the surfaces in order to connect the two domains. Therefore, it is suggested in creating future geometries of this type, that a conformal mesh is used to remove the risk of undetected interpolation issues, in contradiction to the guidance given in the CFX modelling guide (ANSYS, 2020).
- The sensitivity of the results to the mesh has been assessed (Section 4.4.2), although this was primarily focused on the CL-A temperatures. Further work should be undertaken to refine the mesh in the downcomer below the CL-A pipe to assess the sensitivity of the mixing processes in these areas to mesh resolution. In addition, the RSM turbulence model should be re-considered as it did slightly improve the predictions in the downcomer.
- One way to determine whether the separation predicted at the CL-A / downcomer junction is due to inaccuracies in the modelling or uncertainty in the test conditions would be to run a high-fidelity LES solution. This transient model could be solved using steady ECCS flow conditions without the solid components present. These higher fidelity results would provide increased confidence in the RANS turbulence model predictions and determine whether a URANS modelling approach is appropriate.

At this stage in the analysis, it is also worth understanding the impact of the uncertainty in the wall temperature predictions on the thermal stresses in the PV, and hence potential impact on the structural integrity of the component. Since this is the ultimate purpose of the analysis process, this can be used to determine the accuracy / level of uncertainty that is acceptable in the temperature predictions.

5 Application of Results

The overall aim of this case study has been to demonstrate the role of multiple analysis techniques at different levels of fidelity to the study of complex thermal hydraulics behaviour that cannot be adequately represented using a single technique. This has been achieved using the example of a PTS assessment, combining system code and CFD analysis during a SBLOCA scenario.

As highlighted in Section 1.3, this case study forms only a small part of the significant, multi-disciplinary analysis sequence that would be required to establish the PTS risk as part of the development of a new reactor design, such as an SMR.

This case study only considers the initial development and validation process of the system code and CFD analysis approach to predict the transient temperature variation in the cold leg and RPV. The CFD validation study has demonstrated the following benefits of using CFD analysis within a multi-disciplinary analysis process:

- The CFD analysis results confirm that the temperature variation in the CL-A and PV components is highly asymmetric due to the buoyancy-driven stratification in the cold leg. This cannot be resolved or quantified in a system code analysis.
- A CHT approach can be used to resolve the detailed transient temperature variation in the solid, which can be interpolated onto a FEA model as part of the structural integrity assessment.
- A two minute transient can be solved in two days using a URANS approach, which means that the initial part of an SBLOCA scenario relevant to PTS is practical to perform using CFD as part of a design process.
- Although the ECCS flow is inherently unsteady, the pressure drop and flow profile under normal operation could be assessed and optimised using steady-state analysis, which would significantly reduce the timescales associated with the concept design process.
- The geometry of CL-A / downcomer junction can have a significant impact on the level of mixing and location of the cold plume in the downcomer. Therefore, the geometry and flow profile need to be understood to a high level of confidence under a range of potential scenarios.

The CFD validation results also demonstrate the complexity and difficulty involved in modelling and validating ECCS injection and cold leg mixing due to both uncertainty in the experimental setup and the accuracy of the modelling approach. The complexity associated with modelling this type of flow is further demonstrated in the results of the recent cold leg mixing CSNI CFD benchmark (Orea *et al.*, 2020).

5.1 Next Steps

Once the discrepancies in the ROSA Test 1-1 downcomer temperatures have been understood and resolved, the accuracy of the CFD predictions could be assessed using uncertainty quantification (Volume 4). This would more formally complete the development and validation of the CFD analysis methodology and enable it to be applied for Best Estimate Plus Uncertainty (BEPU) assessments of reactor design geometry and conditions.

The system code, CFD and structural integrity analyses then need to be coupled together. This coupling process should be verified and validated to ensure that no errors are introduced into the coupled analysis process.

In the future, the CFD validation exercise could be extended to include two-phase flow conditions in the CL-A pipe and downcomer. This would then enable the analysis sequence to be applied over the full range of SBLOCA scenarios associated with PTS. The issues associated with two-phase PTS events and the phenomena involved in them are discussed in detailed in CSNI (2014).

6 References

Angeli P E (2021) Wall-Resolved Large Eddy Simulations of the Transient Turbulent Fluid Mixing in a Closed System Replicating a Pressurized Thermal Shock. *Flow, Turbulence and Combustion*, dx.doi.org/10.1007/s10494-021-00272-z.

ANSYS (2020) CFX-Solver Modeling Guide, Release 2020 R1.

Bajorek S M, Bernard M, Gingrich C, Hoxie C L, Ireland A, Kelly J, Mahaffy J, Murray C, et al. (2015) Development, Validation and Assessment of the TRACE Thermal-Hydraulics Systems Code. In *Proceedings of 16th International Topical Meeting on Nuclear Reactor Thermal Hydraulics (NURETH-16)*.

Basse N T (2019) Turbulence Intensity Scaling: A Fugue. *Fluids*, 4(4), 180, dx.doi.org/10.3390/fluids4040180.

Bessette D E, Arcieri W, Fletcher C D, Beaton R (2005) Thermal Hydraulic Evaluation of Pressurized Thermal Shock. NUREG-1809, U.S. Nuclear Regulatory Commission.

Boumaza M, Moretti F, Dizene R (2014) Numerical Simulation of Flow and Mixing in ROCOM Facility Using Uniform and Non-Uniform Inlet Flow Velocity Profiles. *Nuclear Engineering and Design*, 280, 362–371, dx.doi.org/10.1016/j.nucengdes.2014.10.018.

Boyd C (2008) Pressurized Thermal Shock, PTS. In *Proceedings of THICKET 2008*.

Cremer I, Mutz A, Trewin R, Grams S (2019) Two-Phase Pressurized Thermal Shock Analysis with CFD Including the Effects of Free-Surface Condensation. *Nuclear Engineering and Design*, 355, 110282, dx.doi.org/10.1016/j.nucengdes.2019.110282.

CSNI (1989) Thermohydraulics of Emergency Core Cooling in Light Water Reactors: A State of the Art Report. NEA/CSNI-161, OECD NEA Committee on the Safety of Nuclear Installations.

CSNI (1994) User Effects on the Transient System Code Calculations. NEA/CSNI/R(94)35, OECD NEA Committee on the Safety of Nuclear Installations.

CSNI (1996) CSNI Integral Test Facility Validation Matrix for the Assessment of Thermal-Hydraulic Codes for LWR LOCA and Transients. NEA/CSNI/R(1996)17, OECD NEA Committee on the Safety of Nuclear Installations.

CSNI (1998) Good Practices for User Effect Reduction. NEA/CSNI/R(1998)22, OECD NEA Committee on the Safety of Nuclear Installations.

CSNI (2007) International Standard Problem ISP-47 on Containment Thermal Hydraulics: Final Report. NEA/CSNI/R(2007)10, OECD NEA Committee on the Safety of Nuclear Installations.

CSNI (2011a) BEMUSE Phase VI Report: Status Report on the Area, Classification of the Methods, Conclusions and Recommendations. NEA/CSNI/R(2011)4, OECD NEA Committee on the Safety of Nuclear Installations.

References

CSNI (2011b) Report of the OECD/NEA - Vattenfall T-Junction Benchmark Exercise. NEA/CSNI/R(2011)5, OECD NEA Committee on the Safety of Nuclear Installations.

CSNI (2013) Final Integration Report of OECD/NEA ROSA Project 2005-2009. NEA/CSNI/R(2013)1, OECD NEA Committee on the Safety of Nuclear Installations.

CSNI (2014) Extension of CFD Codes Application to Two-Phase Flow Safety Problems - Phase 3. NEA/CSNI/R(2014)13, OECD NEA Committee on the Safety of Nuclear Installations.

CSNI (2017) Post-BEMUSE Reflood Model Input Uncertainty Methods (PREMIUM) Benchmark Final Report. NEA/CSNI/R(2016)18, OECD NEA Committee on the Safety of Nuclear Installations.

Farkas T, Tóth I (2010) Fluent Analysis of a ROSA Cold Leg Stratification Test. *Nuclear Engineering and Design*, 240(9), 2169–2175, dx.doi.org/10.1016/j.nucengdes.2009.11.025.

Gallardo S, Abella V, Verdú G, Querol A (2012) NRC: Assessment of TRACE 5.0 Against ROSA Test 3-1, Cold Leg SBLOCA. NUREG/IA-0413, U.S. Nuclear Regulatory Commission.

Gallardo S, Querol A, Lorduy M, Verdú G (2019) Simulation of ROSA-2 Test-2 Experiment: Application to Nuclear Power Plant. NUREG/IA-0511, U.S. Nuclear Regulatory Commission.

Hosseini S M, Yuki K, Hashizume H (2008) Classification of Turbulent Jets in a T-Junction Area with a 90-Deg Bend Upstream. *International Journal of Heat and Mass Transfer*, 51(9-10), 2444–2454, dx.doi.org/10.1016/j.ijheatmasstransfer.2007.08.024.

IAEA (2008) Best Estimate Safety Analysis for Nuclear Power Plants: Uncertainty Evaluation. Safety Reports Series No. 52, International Atomic Energy Agency.

IAEA (2010) Pressurized Thermal Shock in Nuclear Power Plants: Good Practices for Assessment. IAEA-TECDOC-1627, International Atomic Energy Agency.

INL (2018) RELAP5-3D Code Manual Volume V: User's Guidelines. INL-EXT-98-00834, Idaho National Laboratory.

JAEA (2008a) Final Data Report of OECD/NEA ROSA Project Test 1-1, ECCS Water Injection under Natural Circulation Condition. Thermohydraulic Safety Research Group, Japan Atomic Energy Agency.

JAEA (2008b) Final Data Report of OECD/NEA ROSA Project Test 1-2, 1% Hot-Leg Break LOCA Experiment with HPI. Thermohydraulic Safety Research Group, Japan Atomic Energy Agency.

Julbe A, Muñoz-Cobo J, Escrivá A, Romero A (2012) NRC: Analysis with TRACE Code of ROSA Test 1.1: ECCS Water Injection Under Natural Circulation Condition. NUREG/IA-0419, U.S. Nuclear Regulatory Commission.

Lai J K, Merzari E, Hassan Y A, Fischer P, Marin O (2020) Verification and Validation of Large Eddy Simulation with Nek5000 for Cold Leg Mixing Benchmark. *Nuclear Engineering and Design*, 358, 110427, dx.doi.org/10.1016/j.nucengdes.2019.110427.

Lee G H (2018) Review of Audit Calculation Activities on the Applicability of CFD Software to Nuclear Safety Problems. *MATEC Web of Conferences*, 240, 05016, dx.doi.org/10.1051/matecconf/201824005016.

References

Munoz-Cobo J, Romero A, Chiva S (2013) NRC: Analysis with TRACE Code of ROSA Test 1.2: Small LOCA in the Hot-Leg with HPI and Accumulator Actuation. NUREG/IA-0420, U.S. Nuclear Regulatory Commission.

Orea D, Vaghetto R, Nguyen T, Hassan Y (2020) Experimental Measurements of Flow Mixing in Cold Leg of a Pressurized Water Reactor. *Annals of Nuclear Energy*, 140, 107137, dx.doi.org/10.1016/j.anucene.2019.107137.

Ortiz M G, Ghan L S (1992) Uncertainty Analysis of Minimum Vessel Liquid Inventory during a Small-Break LOCA in a B W Plant: An Application of the CSAU Methodology Using the RELAP5/MOD3 Computer Code. NUREG/CR-5818, U.S. Nuclear Regulatory Commission, dx.doi.org/10.2172/6771672.

Petruzzi A, D'Auria F (2008) Thermal-Hydraulic System Codes in Nulcear Reactor Safety and Qualification Procedures. *Science and Technology of Nuclear Installations*, 2008, 1–16, dx.doi.org/10.1155/2008/460795.

Queral C, Gonzalez-Cadelo J, Jimenez G, Villalba E, Perez J (2014) NRC: Simulation of LSTF Upper Head Break (OECD/NEA ROSA Test 6.1) with TRACE Code. Application to a PWR NPP Model. NUREG/IA-0426, U.S. Nuclear Regulatory Commission.

ROSA-V Group (2003) ROSA-V Large Scale Test Facility (LSTF) System Description for the Third and Fourth Simulated Fuel Assemblies. JAERI-Tech–2003-037, Japan Atomic Energy Research Institute.

Scheuerer M, Weis J (2012) Transient Computational Fluid Dynamics Analysis of Emergency Core Cooling Injection at Natural Circulation Conditions. *Nuclear Engineering and Design*, 253, 343–350, dx.doi.org/10.1016/j.nucengdes.2011.08.063.

Takeda T (2018) ROSA/LSTF Test and RELAP5 Code Analyses on PWR 1% Vessel Upper Head Small-Break LOCA with Accident Management Measure Based on Core Exit Temperature. *Nuclear Engineering and Technology*, 50(8), 1412–1420, dx.doi.org/10.1016/j.net.2018.08.004.

Takeda T, Wada Y, Sibamoto Y (2021) Major Outcomes through Recent ROSA/LSTF Experiments and Future Plans. *World Journal of Nuclear Science and Technology*, 11(01), 17–42, dx.doi.org/10.4236/wjnst.2021.111002.

Tunstall R, Laurence D, Prosser R, Skillen A (2016a) Benchmarking LES with Wall-Functions and RANS for Fatigue Problems in Thermal–Hydraulics Systems. *Nuclear Engineering and Design*, 308, 170–181, dx.doi.org/10.1016/j.nucengdes.2016.08.022.

Tunstall R, Laurence D, Prosser R, Skillen A (2016b) Large Eddy Simulation of a T-Junction with Upstream Elbow: The Role of Dean Vortices in Thermal Fatigue. *Applied Thermal Engineering*, 107, 672–680, dx.doi.org/10.1016/j.applthermaleng.2016.07.011.

Turner J S (1973) Buoyancy Effects in Fluids. Cambridge University Press, dx.doi.org/10.1017/CBO9780511608827.

US NRC (1989) Quantifying Reactor Safety Margins Application of Code Scaling, Applicability, and Uncertainty Evaluation Methodology to a Large-Break, Loss-of-Coolant Accident. NUREG/CR-5249 Rev. No. 4, U.S. Nuclear Regulatory Commission.

References

US NRC (2007) Technical Basis for Revision of the Pressurized Thermal Shock (PTS) Screening Limit in the PTS Rule (10 CFR 50.61). NUREG- 1806, U.S. Nuclear Regulatory Commission.

Wagner W, Cooper J R, Dittmann A, Kijima J, Kretzschmar H J, Kruse A, Mareš R, Oguchi K, et al. (2000) The IAPWS Industrial Formulation 1997 for the Thermodynamic Properties of Water and Steam. *Journal of Engineering for Gas Turbines and Power*, 122(1), 150–184, dx.doi.org/10.1115/1.483186.

Zhang L, Yang V (2017) Flow Dynamics and Mixing of a Transverse Jet in Crossflow—Part I: Steady Crossflow. *Journal of Engineering for Gas Turbines and Power*, 139(8), 082601, dx.doi.org/10.1115/1.4035808.

7 Nomenclature

Latin Symbols

A	Area, m^2
At	Atwood number ($At = (\rho_1 - \rho_2)/(\rho_1 + \rho_2)$)
Bi	Biot number ($Bi = hL/k_s$)
c_p, c_v	Specific heat at constant pressure or volume, $\mathrm{J\,kg^{-1}\,K^{-1}}$
d or D	Diameter ($D_h = 4A_{cs}/p_{cs}$ for hydraulic diameter), m
f	Darcy-Weisbach friction factor
Fo	Fourier number ($Fo = \alpha_s t/L^2$)
Gr	Grashof number ($Gr = gL^3\Delta\rho/\nu^2\rho = gL^3\beta\Delta T/\nu^2$, using the Boussinesq approximation $\Delta\rho/\rho \approx -\beta\Delta T$, where ΔT is often taken as $T_w - T_{s,\infty}$)
g	Acceleration due to gravity, $\mathrm{m\,s^{-2}}$
h	Specific enthalpy, $\mathrm{J\,kg^{-1}}$, Heat Transfer Coefficient (HTC), $\mathrm{W\,m^{-2}\,K^{-1}}$ or height, m
I	Radiative intensity, $\mathrm{W\,m^{-2}\,sr^{-1}}$ or $\mathrm{W\,m^{-2}\,sr^{-1}\,\mu m^{-1}}$ for a spectral density, where sr (steradian) is solid angle
J	Radiosity, $\mathrm{W\,m^{-2}}$
k	Thermal conductivity, $\mathrm{W\,m^{-1}\,K^{-1}}$
L	Length or wall thickness, m
M	Molar mass of a species, $\mathrm{kg\,kmol^{-1}}$
Ma	Mach number ($Ma = U/a$, where a is the speed of sound)
n	Refractive index
Nu	Nusselt Number ($Nu = hL/k_f$)
p	Perimeter, m
P	Pressure (P_s = static pressure, P_T = total pressure), $\mathrm{N\,m^{-2}}$ or Pa
Pe	Péclet number ($Pe = RePr$)
Pr	Prandtl number ($Pr = c_p\mu/k_f$)
q	Heat flux (rate of heat transfer per unit area, $q = Q/A$), $\mathrm{W\,m^{-2}}$
Q	Rate of heat transfer, W
r	Radius, m
R	Gas constant (for a particular gas, $R = \tilde{R}/M$), $\mathrm{J\,kg^{-1}\,K^{-1}}$
$\tilde{R}$	Universal gas constant, $8314.5\,\mathrm{J\,kmol^{-1}\,K^{-1}}$
R_{th}	Thermal resistance, $\mathrm{K\,W^{-1}}$
Ra	Rayleigh number ($Ra = GrPr$)
Re	Reynolds number ($Re = \rho UL/\mu$, or for an internal flow $Re = WD_h/A_{cs}\mu$)
Ri	Richardson number ($Ri = Gr/Re^2$)
Sr	Strouhal number ($Sr = fL/U$, where f is frequency)

St	Stanton number ($St = Nu/RePr$)
t	Time, s
T	Temperature (T_s = static temperature, T_T = total temperature), K
u_τ	Wall friction velocity ($u_\tau = \sqrt{\overline{\tau_w}/\rho}$), $\mathrm{m\,s^{-1}}$
U	Velocity, $\mathrm{m\,s^{-1}}$ or thermal transmittance, $\mathrm{W\,m^{-2}\,K^{-1}}$
v	Specific volume, $\mathrm{m^3\,kg^{-1}}$
V	Volume, $\mathrm{m^3}$
W	Mass flow rate, $\mathrm{kg\,s^{-1}}$
y	Wall distance, m
y^+	Non-dimensional wall distance ($y^+ = y u_\tau/\nu$)

Greek Symbols

α	Thermal diffusivity ($\alpha = k/\rho c_p$), $\mathrm{m^2\,s^{-1}}$
β	Volumetric thermal expansion coefficient ($\beta = -(1/\rho)(\partial\rho/\partial T)$), $\mathrm{K^{-1}}$
γ	Ratio of specific heats ($\gamma = c_p/c_v$)
ϵ	Emissivity or surface roughness height, m
κ	Absorption coefficient, $\mathrm{m^{-1}}$
λ	Wavelength, m
μ	Viscosity, $\mathrm{kg\,m^{-1}\,s^{-1}}$
ν	Kinematic viscosity and momentum diffusivity ($\nu = \mu/\rho$), $\mathrm{m^2\,s^{-1}}$
ρ	Density, $\mathrm{kg\,m^{-3}}$
σ	Stefan Boltzmann constant, $5.67 \times 10^{-8}\,\mathrm{W\,m^{-2}\,K^{-4}}$
τ	Shear stress, $\mathrm{N\,m^{-2}}$
ϕ	Porosity or void fraction

Subscripts and Modifications

b	Bulk (mass-averaged) quantity
cs	Cross-sectional quantity
f	Quantity relating to a fluid
i	Quantity relating to a particular species
T	Total (stagnation) quantity
t	Turbulent quantity
s	Static quantity or quantity relating to a solid
w	Quantity relating to a wall or surface
∞	Quantity far from a wall or in free-stream
$\overline{\square}$	Average quantity
$\tilde{\square}$	Molar quantity
$\square'$	Varying quantity

8 Abbreviations

AIS	Accumulator Injection System
BEPU	Best Estimate Plus Uncertainty
CAD	Computer Aided Design
CAMP	Code Applications and Maintenance Program
CFD	Computational Fluid Dynamics
CFL	Courant-Friedrichs Lewy
CHT	Conjugate Heat Transfer
CL-A	Cold Leg of Loop A
CL-B	Cold Leg of Loop B
CSNI	Committee on the Safety of Nuclear Installations
ECCS	Emergency Core Cooling System
FCH	First Cell Height
FEA	Finite Element Analysis
FOM	Figure of Merit
HPIS	High Pressure Injection System
HTC	Heat Transfer Coefficient
IAPWS	International Association for the Properties of Water and Steam
IET	Integral Effect Test
ISI	In-Service Inspection
JAEA	Japan Atomic Energy Agency
LBLOCA	Large Break Loss-Of-Coolant Accident
LES	Large Eddy Simulation
LOCA	Loss-Of-Coolant Accident
LPIS	Low Pressure Injection System
LSTF	Large Scale Test Facility
LWR	Light Water Reactor
MCP	Main Coolant Pump
NEA	Nuclear Energy Agency
NPP	Nuclear Power Plant
NTH	Nuclear Thermal Hydraulics
OECD	Organisation for Economic Co-operation and Development
PIRT	Phenomena Identification and Ranking Table
PTS	Pressurised Thermal Shock
PV	Pressure Vessel
PWR	Pressurised Water Reactor
RANS	Reynolds-Averaged Navier-Stokes
RMS	Root Mean Square
ROSA	Rig-of-Safety Assessment
RPV	Reactor Pressure Vessel
RSM	Reynolds Stress Model

Abbreviations

SBLOCA	Small Break Loss-Of-Coolant Accident
SET	Separate Effect Test
SG	Steam Generator
SMR	Small Modular Reactor
SST	Shear Stress Transport
URANS	Unsteady Reynolds-Averaged Navier-Stokes
US NRC	United States Nuclear Regulatory Commission
V&V	Verification and Validation

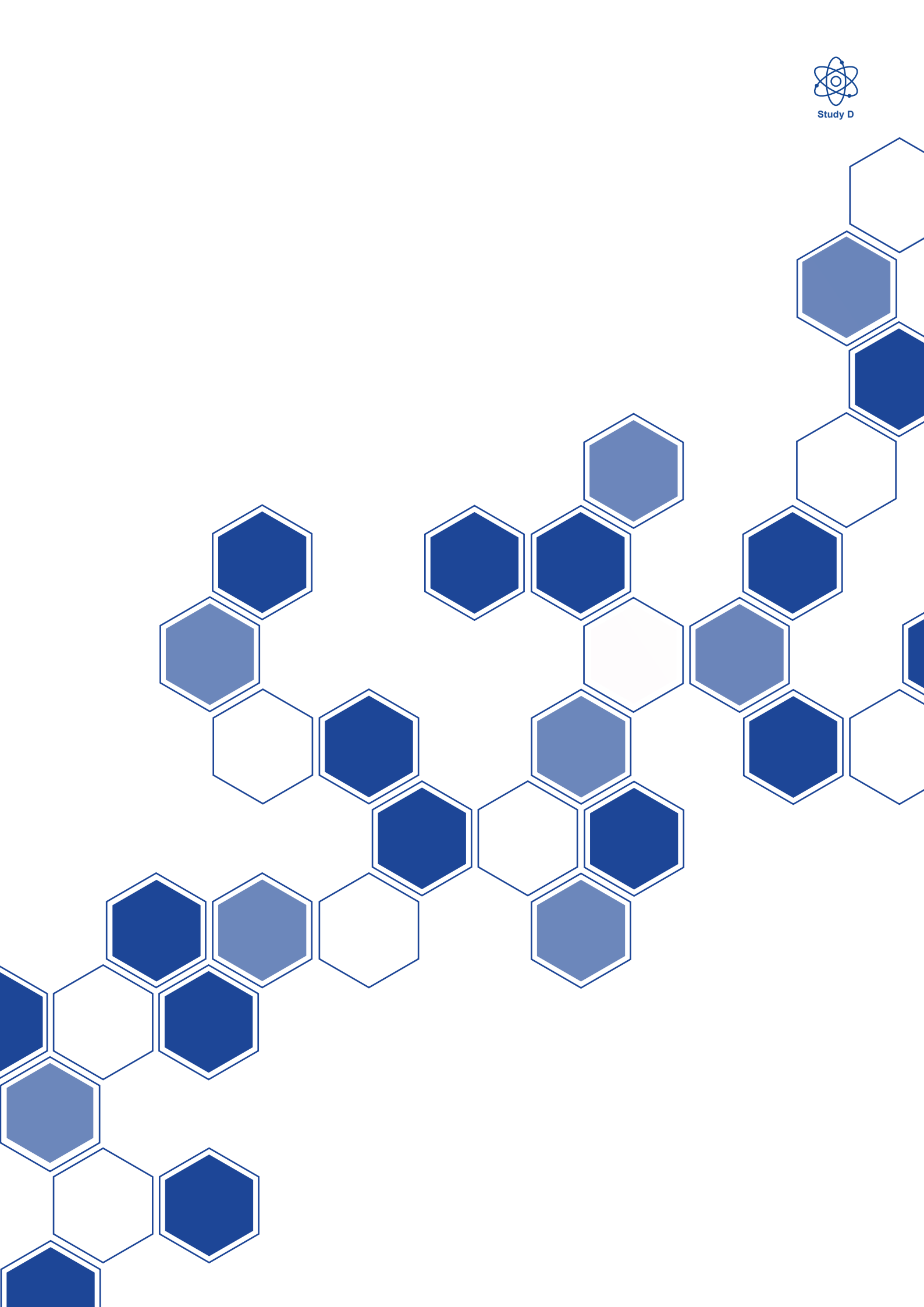
Study D